# The use of an interphase to improve the transverse properties of unidirectional glass fibre reinforced polymer composites

Ellis, Keith

*Award date:*
1990

*Awarding institution:*
University of Bath

The use of an interphase to improve the
transverse properties of unidirectional
glass fibre reinforced polymer composites

Submitted by Keith Ellis
for the degree of PhD
of the University of Bath
January 1990







ProQuest LLC
789 East Eisenhower Parkway
P.O. Box 1346
Ann Arbor, MI 48106-1346

*TO SUZANNE*

ABSTRACT

The aim of the project was to improve the transverse mechanical properties of unidirectional glass fibre reinforced plastics (G.R.P.). In addition it was intended that the longitudinal mechanical properties should not be significantly degraded as a result of the transverse improvement.

The scientific and commercial literature were consulted to determine the most feasible means of improving the transverse properties. Four possible methods were identified , the most promising of which was interfacial modification.

Interfacial modification involves the introduction of a third material ( "the interphase" ) at the interface between the fibre and the matrix. For this project the interphase material was selected to be compliant or rubbery in nature.

The Kies model for predicting the magnification of strain in the resin between fibres was extended to include an interphase. The model was developed for two modes of applied stress. The first was pure tension acting transverse to the fibre axis. The second was shear in the plane transverse to the fibre axis.

A novel apparatus was constructed to manufacture composites with a compliant interphase. The apparatus combined a self-regulating coating technique with filament winding to give a continuous production facility.

A range of mechanical tests were performed on composites both with and without an interphase. Presence of an interphase improved the following properties: transverse flexural strength , interlaminar and intralaminar shear strength , and transverse flexu-

ral fracture energy. No improvement was noted for pure transverse tension. These results indicated that the interphase acted beneficially only when the composite was stressed in a predominantly shear mode.

Conclusions from mechanical test results were supported by S.E.M. fractography. Considerable deformation of the interphase was found in composite tested in shear. This deformation was absent in composite tested in tension.

It was postulated that these differences between behaviour in tension and shear were the result of constraint of Poisson's ratio contraction in the compliant interphase. To confirm this , dynamic mechanical testing was used to measure tensile and shear moduli of the interphase material as a function of thickness. Constraint and support were provided by a thin steel substrate. The tensile modulus increased by orders of magnitude the thinner , and hence more constrained , the material became. Near to the interphase thickness used in practice the tensile modulus of the interphase was shown to approach that of the matrix.

In summary , the use of a compliant interphase resulted in significant improvements in mechanical properties of the composite in shear.

# Table of Contents

# 1 INTRODUCTION

The aim of the project was to improve the transverse mechanical properties of unidirectional glass fibre reinforced plastics (G.R.P.). In addition it was intended that the longitudinal mechanical properties should not be significantly degraded as a result of the transverse improvement.

Recent developments in the use of unidirectional G.R.P. In structural automotive components , such as the leaf spring suspension part , have led to the realisation of the importance of their transverse performance. The transverse strength , for example, of a unidirectional composite is likely to be less than 1% of the longitudinal strength. Consequently , relatively small loads applied in the transverse direction can lead to levels of stress sufficient to cause cracking of the matrix and reduction in the overall composite failure strength. By careful design these transverse stresses can be minimised but never entirely eliminated.

Transverse stresses can arise from a number of different sources. The most common source is thought to be from the complex three dimensional loading applied to the components in service. Stresses also arise from the necessity of attaching the component to the main structure. Suppression of anticlastic bending and lateral constraint due to gripping are two significant examples and both are due to Poisson's ratio effects.

Anticlastic bending occurs when a beam of sufficient width to thickness ratio is bent along its length. The Poisson's ratio effect causes the beam to contract when subject to a tensile load and expand when subject to a compressive load.

When bending a beam along its length the outer surface is put into tension and the inner into compression. ( Figure 1 ) Consider a section through the centre of the beam. ( Figure 2a ) Poisson's ratio effects lead to a compressive force across the top surface and tensile force across the lower surface. These forces cause the beam to bend across its width , ( Figure 2b ) , leading to the anticlastic phenomenon. Suppression of this bending by , for example , a stiff plate across the whole width of the beam leads to a transverse tensile load across the top surface.

Lateral constraint is a similar effect as the suppression of anticlastic bending. It occurs for components loaded in tension and gripped across their width at some point. The grip constrains the Poisson's contraction leading to a transverse tensile stress through the whole thickness rather than just on the top surface. ( Figure 3 ).

Having established some of the primary sources of transverse stress the scientific and commercial literature was reviewed to identify possible means for improving transverse strength of unidirectional G.R.P. Five possibilities were established and their relative merits are discussed in the following sub-sections.

## 1.1 Modification of brittle matrix resins by the addition of toughening agents.

The majority of work to date on the toughening of brittle matrix resins has been centred on the use of liquid rubbers which phase separate during cure. ( 1,2,3,4,5,6,7 ). The phase separation leads to the formation of small rubber spheres within the brittle main phase resin. Toughness increases in the order of a few hundred percent have been achieved for the matrix resin alone ( 2 ). However , composite materials utilising the same modified resins achieved increases of only five per cent. Toughening by additions of other polymers may hold more promise.

Improvements in the toughness or ductility of a brittle resin matrix composite were shown when additions of flexible polymers were made to the matrix. ( 8,9,10 ). In particular discussions with leading resin manufacturers indicated that the latest commercial direction for toughening of polyester/vinyl ester matrices is to blend them with urethane type resins.

This area of research is being actively considered as part of a concurrent project at Bath , linked to this work by the same sponsoring organisation. Therefore , no further work is presented here on this subject.

## 1.2 The use of thermoplastic matrices

Thermoplastics are being considered for use in structural composites for a number of reasons. Thermoplastics are tough , fast to process , and can be repaired or reused. However , there are also a number of problems associated with their use , which are primarily the base polymer strength and modulus , and the poor quality of pre-pregs. These problems must be overcome before thermoplastics can be successfully used in structural composites. Pre-preg materials with unidirectional fibre and a thermoplastic matrix are few and far between. The best known and most widely used is carbon fibre reinforced polyetheretherketone ( PEEK ) , marketed as APC2 by ICI. However , this and a number of other aerospace oriented thermoplastic pre-pregs are prohibitively expensive. This is not only because they tend to use carbon fibre rather than glass fibre but also because they use high performance , and consequently high cost , thermoplastics. What is needed for mass produced automotive structural components is a pre-preg utilising glass fibre in a cheap but relatively high performance thermoplastic.

Such pre-pregs are now being manufactured experimentally by ICI. They utilise unidirectional continuous glass fibres with a selection of cheap thermoplastics such as polypropylene , polyethylene terephthalate ( PET ) , and nylon 6,6.

Initial studies by the author on a glass fibre nylon 66 pre-preg ( 11 ) showed good bonding at the interface and acceptable mechanical performance. Industrial processing characteristics and fatigue performance have still to be assessed. This and all future work will be progressed at the industrial sponsors laboratories. Therefore , thermoplastic matrix composites will not form any further part of this report.

## 1.3 The use of discrete interlaminar layers.

The use of a rubbery ply between sheets of carbon fibre pre-preg to improve through thickness toughness and transverse mechanical properties has been previously reported. ( 12 , 13 , 14 ). To date commercial systems have been developed entirely for the aerospace market. Consequently , these systems are not available with glass fibre reinforcement.

The use of a non-woven thermoplastic mesh as a discrete layer in unidirectional fibre composites has also been investigated ( 15 , 16 ). A carbon fibre epoxy composite with a mesh interlayer was shown to increase toughness and delocalise damage ( 15 ). A glass fibre epoxy composite was shown to improve the through thickness compressive fatigue life ( 16 ).

The concept of this work was taken and expanded to investigate the effect of a thermoplastic polyester mesh on the mechanical properties of a G.R.P. laminate ( 17 ). Both unidirectional and cross ply laminates were considered. Initial results indicated possible improvements in shear properties with the mesh placed at the 0/90 interface in cross ply composites. However , the extent of the improvements was considered too small to continue the work at the present time.

## 1.4 Modification of the interface by the use of a fibre coating.

The case of a unidirectional fibre composite is directly analogous to that of a series of cylindrical holes or inclusions in a plate. It has been shown that when such a plate is loaded

transverse to the cylinder axis stress concentrations develop around the cylinder or hole ( 18 , 19 , 20 ). These studies would suggest then that stress concentrations will exist at or near the interface in a unidirectional composite stressed transverse to the fibre axis.

It has been postulated ( 21 - 29 ) that by inserting a third , comparatively thin , phase at the interface ( the so called interphase ) , these stress concentrations might be reduced or eliminated. By considered choice of interphase material and thickness , composite properties such as strength , failure strain , toughness and fatigue life , particularly transverse to the fibres , might be improved.

Two general possibilities exist for the interphase material. It should either be of intermediate modulus to reduce the modulus mismatch between adjacent phases , or it should be of low modulus to allow for large deformations at the interface. Both approaches have been attempted although by far the most popular approach is that of the low modulus interphase.

### 1.4.1 Intermediate modulus interphase.

Kardos , Cheng and Talbot ( 30 ) describe work which examines the effect of an intermediate modulus interphase on short carbon fibre polycarbonate composite. Fibre volume fraction was low and no attempt was made to align the fibres. The interphase was grown around the fibres by a heating technique similar to annealing in metals. The result was a polycarbonate interphase of significantly higher crystallinity , and hence higher modulus , than the matrix. Three point bending tests showed improved strength and modulus.

Aronhime and Marom ( 22 ) developed a model based on concentric cylinders intended to model the response of longitudinal properties to the presence of an interphase. The main conclusion was that to improve longitudinal properties a rigid , or intermediate modulus ,

interphase was required. Preliminary investigations by Aronhime also indicated that improvements in transverse strength would best be achieved with a low modulus , rather than intermediate modulus , interphase.

### 1.4.2 Low modulus interphase.

Initial work ( 23 , 24 , 25 , 28 , 29 , 31 ) , both theoretical and experimental , supports the belief that a compliant interphase can improve transverse properties of unidirectional composite. This work will be considered in more detail in the theoretical and experimental sections. Briefly , however , the work of Lavengood and Michno ( 24 ) and of Tryson and Kardos ( 23 ) is important as it actually involved the testing of composite materials manufactured from coated mono-filament.

It was found ( 24 ) that transverse bending strength could be increased by up to 60% with the use of coated fibre. The failure strain was found to increase by the same amount. The composite was also tested after boiling in water for two hours. Transverse bending strength was down 4% from unboiled values for the coated fibre composites but down 40% for the normal fibre composites. Interlaminar shear strength as measured by short beam shear was increased by 25% with the coated fibre. Fatigue tests , conducted in torsion under maximum stress control , showed increases in fatigue life of at least one order of magnitude.

The choice of a low modulus interphase rather than an intermediate modulus is favoured for the composite system under consideration in this project. Both theory and experiment indicate that a well bonded interphase with shear modulus lower than the matrix will reduce the stress concentration around a single fibre loaded transverse to its axis. A suitable theoretical model will be required to determine the optimum properties of the interphase material.

The low modulus interphase has been shown to increase transverse bending strength and failure strain , interlaminar shear stress and torsional fatigue life. For these reasons the low modulus interphase approach was adopted for use in this project.

# 2 DEVELOPMENT OF A THEORETICAL MODEL TO ILLUSTRATE THE EFFECT OF A THIRD PHASE AT THE INTERFACE

## 2.1 Introduction

It has already been established that fibres introduce stress and strain concentrations into the matrix , resulting in a reduction of the matrix strength. A model is needed which can predict the levels of stress or strain concentration and the effect of introducing a third phase at the interface.

A number of models have been developed which consider a three phase system based on fibre , interphase , and matrix. Many of these models ( 22 , 32 , 33 , 34 , ) consider the effect of an interphase on the longitudinal properties of aligned continuous or discontinuous fibre composites. However , of most relevance to this project are the models of Arridge ( 28 ) and Tirosh ( 31 ) , both of which deal with transverse properties.

### 2.1.1 Work of Tirosh

Tirosh presented the equations of Muskhelishvili ( 20 ) for a plate under plane strain containing an inclusion of radius R ( see figure 4 ). The stresses in the plate at a point $(r,\theta)$ are given by:

$$\sigma_{rr}=\frac{\sigma}{2}\left(1-\gamma\left(\frac{R}{r}\right)^2-\left(1-2\beta\left(\frac{R}{r}\right)^2-3\delta\left(\frac{R}{r}\right)^4\right)\cos 2\theta\right)$$

$$\sigma_{\theta\theta}=\frac{\sigma}{2}\left(1+\gamma\left(\frac{R}{r}\right)^2+\left(1-3\delta\left(\frac{R}{r}\right)^4\right)\cos 2\theta\right)$$

$$\tau_{r\theta}=\frac{\sigma}{2}\left(1+\beta\left(\frac{R}{r}\right)^2+3\delta\left(\frac{R}{r}\right)^4\right)\sin 2\theta$$

where

$$\gamma = \frac{-(k-1)}{2}$$

$$\beta = -\frac{2}{k}$$

$$\delta = \frac{1}{k}$$

$$k = 3 - 4\nu$$

$\sigma_{rr}$ is the radial stress component , $\sigma_{\theta\theta}$ is the circumferential stress component , $\tau_{r\theta}$ is the shear stress component , R is the fibre radius , $\nu$ is the Poisson's ratio and $(r, \theta)$ are position polar coordinates.

Solving these equations shows that cracking is most likely to occur not at the interface but at a small distance of 1.2 R ahead of the interface.

The next stage was to introduce fracture mechanics to determine critical load and hence predict transverse tensile strength. Cracks were examined for four different cases. These were radial cracks at 0° or 90° to the load (Figure 5 a,b) or circumferential cracks at 0° or 90° to the load (Figure 5 c,d).

For radial flaws the stress intensity factor , $K_I$ , was given by:

$$K_I = \left(\frac{\pi l}{2}\right)^{-\frac{1}{2}} \int_R^{R+l} \sigma_{\theta\theta} \left(\frac{r-R}{l-(r-R)}\right)^{\frac{1}{2}} dr$$

where l is the length of flaw ,

and for circumferential flaws at distance r ,

$$K_I = (\pi r \alpha)^{-\frac{1}{2}} \int_{-\alpha}^{\alpha} \sigma_{rr} \left( \frac{\alpha + \theta}{\alpha - \theta} \right)^{\frac{1}{2}} d\theta$$

where $\alpha$ is the crack half angle.

Case (c) (Figure 5) was shown to be the most severe.

Having established that the most likely crack to occur was a circumferential one and that it would occur a short distance into the matrix , Tirosh next considered the effect of toughening that region with a compliant interphase material.

Tirosh used a finite element analysis program which included in its unit cell the fibre , the interphase , the matrix , and the influence of nearby fibres. Including the influence of other fibres is important and is rarely considered in other theoretical models. The main conclusions of this section of the work were:

(i) A thin adhesive layer of lower shear modulus than the matrix improves the transverse strength of the composite.

(ii) $K_I$ is almost insensitive to the crack length. Fracture may therefore occur by simultaneous propagation of many cracks as well as just a single crack.

## 2.1.2 Work of Arridge

Arridge presented the equations of Savin ( 35 ) for the prediction of stress in a plate containing a hole into which two reinforcing rings had been welded (Figure 6 ). By reducing the radius of the hole to zero the inner ring increases its thickness until it becomes a solid disc. At this point a fibre , interphase , matrix model is achieved. Arridge made this assumption and numerically solved the complex equations. It is important to note that Arridge's model does not allow for fibre-fibre interaction.

Arridge modelled the case of a coated steel wire in an epoxy sheet. The shear modulus and Poisson's ratio of the interphase ( coating ) were varied but the thickness was kept constant at 0.1 of the radius of the fibre. Figure 7 shows how the stress concentration factor varies against interphase shear modulus for $\sigma_{rr}$ ( radial stress ) and $\sigma_{\theta\theta}$ ( circumferential stress ).

The results show that to minimise the stress concentration factor for both $\sigma_r$ and $\sigma_{\theta\theta}$ an ideal value of shear modulus is predicted ( the cross-over point ). The value is shown to increase with decreasing Poisson's ratio.

Arridge , in conjunction with Marom , tested his model experimentally. Steel wires , some coated with silicone rubber or flexibilised epoxy , were inserted into holes drilled into sheets of epoxy resin. Results of tensile tests carried out transverse to the wire axis showed two main points of interest. First , insertion of steel wires with no coating resulted in drastic reduction from the " holes only " strength. Second ,insertion of coated wire resulted in slight improvements over the "holes only" strength. The type of interphase material made no significant difference to the transverse tensile strength.

### 2.1.3 Work of Kies

All of the models discussed so far have been stress concentration models. No model has been presented in the literature which examines the effect of an interphase on strain concentration.

Kies ( 36 ) , however , developed a model for the prediction of transverse tensile strain magnification between fibres in a unidirectional composite ( a simple two phase system ). He considered two adjacent lines of load in a transverse section of a unidirectional composite ( Figure 8 ). One line passes through two fibres ( A-B ) and the other through no fibres ( C-D ). If the composite is strained by an amount $\varepsilon_c$ , then the matrix along C-D will also be strained by $\varepsilon_c$. The matrix between the fibres , however , along E-F will be strained by some larger

amount , $\varepsilon_r$ . This is because the fibres are significantly stiffer than the matrix and so deflect less under the applied load. Since the total deflection must be constant the matrix between the fibres must deflect more to make up the difference. Kies showed that this strain magnification , defined as $\frac{\varepsilon_r}{\varepsilon_c}$ , is given by:

$$\frac{\varepsilon_r}{\varepsilon_c} = \frac{2r+s}{s+2r\left(\frac{E_r}{E_g}\right)} \qquad \text{.....1}$$

where r is the fibre radius , s the interfibre spacing , $E_g$ is the fibre transverse modulus , and $E_r$ is the resin modulus.

A similar model can be developed for the case of shear strain magnification , $\frac{\gamma_r}{\gamma_c}$ ( Figure 9 ).

In this case Kies showed $\frac{\gamma_r}{\gamma_c}$ to be given by:

$$\frac{\gamma_r}{\gamma_c} = \frac{1}{\left(G_r I + \frac{s}{2r+s}\right)} \equiv \frac{2r+s}{s+(2r+s)G_r I} \qquad \text{.....2}$$

where

$$I = \int sub0^{\pi over 2} \frac{\cos\theta d\theta}{G_r\left(1+\frac{s}{2r}\right)+G_g\cos\theta}$$

$G_g$ is the fibre shear modulus , and $G_r$ is the resin shear modulus.

As an example , for a glass fibre polymer composite of 50% fibre volume fraction ( see section 2.3 for values used ) the strain magnification factors are:

$$\frac{\varepsilon_r}{\varepsilon_c} = 4.28$$

$$\frac{\gamma_r}{\gamma_c} = 3.86$$

If the volume fraction increases to the point where fibres are practically touching then these values increase to 20 and 17 respectively.

For the purposes of this project a simple model was required capable of illustrating which parameters of the composite most significantly affected the transverse properties. The Kies model is not only simple in concept but also inherently includes fibre-fibre interactions. It was therefore decided to extend the basic Kies models to include an interphase material.

## 2.2 Extended Kies model

The present author extended the basic Kies models to include an interphase. The arguments used and equations obtained are presented separately for the tension and shear models in sections 2.2.1 and 2.2.2 respectively.

### 2.2.1 Tension model

The model is based on a square array of fibres as shown in figure 10. It could in fact also apply to any other arrangement of fibres as the basic unit cell of the model ( figure 11 ) only involves two fibres.

Let

$\delta$ = total elastic deflection transverse to the fibres

$$\delta = \delta_g + \delta_r + \delta_i$$

where

$\delta_g$ = deflection in glass phase

$\delta_r$ = deflection in resin phase

$\delta_i$ = deflection in interphase

The original length l is defined in figure 11 as:

$$l = 2r + 2t + s$$

where r is the fibre radius , t the interphase thickness , and s the resin thickness between fibres.

Now , the total deflection $\delta$ over the original length l is equal to , $\varepsilon_c$ , the average measured strain transverse to the fibres.

Therefore ,

$$\varepsilon_c = \frac{\delta_g + \delta_r + \delta_i}{2r + s + 2t} \qquad \text{.....3}$$

Assuming a common stress $\sigma$ ,

$$\delta_g = 2r\frac{\sigma}{E_g} \qquad \text{.....4}$$

$$\delta_r = s\frac{\sigma}{E_r} \qquad \text{.....5}$$

$$\delta_i = 2t\frac{\sigma}{E_i} \qquad \text{.....6}$$

where $E_g, E_r, E_i$ are the tensile moduli of the glass resin and interphase respectively.

From equations 4 and 5 ,

$$\frac{\delta_g}{\delta_r} = 2r\frac{E_r}{sE_g} \qquad \text{.....7}$$

From equations 5 and 6 ,

$$\frac{\delta_i}{\delta_r} = 2t\frac{E_r}{sE_i} \qquad \text{.....8}$$

Rearrange equations 7 and 8 for $\delta_g$ and $\delta_i$ and substitute in equation 3 giving ,

$$\varepsilon_c = \frac{\delta_r\left(2r\frac{E_r}{(sE_g)}\right) + \delta_r\left(2t\frac{E_r}{(sE_i)}\right) + \delta_r}{2r + 2t + s} \qquad \text{.....9}$$

Now the strain in the resin between fibres , $\varepsilon_r$ , is given by :

$$\varepsilon_r = \frac{\delta_r}{s} \qquad \text{.....10}$$

Rearranging equation 9 for $\delta_r$ and substituting in equation 10 gives ,

$$\varepsilon_r = \frac{\delta_r}{s} = \varepsilon_c \frac{(2r + 2t + s)}{s\left(1 + \left(2r\frac{E_r}{sE_g}\right) + \left(2t\frac{E_r}{sE_i}\right)\right)} \qquad \text{.....11}$$

Then , the tensile strain magnification in the resin is given by :

$$\frac{\varepsilon_r}{\varepsilon_c} = \frac{2r + 2t + s}{s + 2r\frac{E_r}{E_g} + 2t\frac{E_r}{E_i}} \qquad \text{.....12}$$

By a similar argument the tensile strain magnification in the interphase is given by :

$$\frac{\varepsilon_i}{\varepsilon_c} = \frac{2r + 2t + s}{2t + 2r\frac{E_i}{E_g} + s\frac{E_i}{E_r}} \qquad \text{.....13}$$

By varying the input values of equations 12 and 13 the variation in the tensile strain magnifications can be predicted. Initial results using estimated values for these inputs are calculated and presented in section 2.3.

## 2.2.2 Shear model

This model is based on the square fibre array shown in figure 12. The model is based on splitting the model into three blocks ( figure 13 ). The first block contains fibre , interphase and resin. The second block contains interphase and resin. The third block is of resin only.

The model assumes that in these blocks there is a constant deflection for all the phases and determines an average shear modulus for the block. The average shear modulus is determined on a Voigt , or rule of mixtures , basis.

Consider the simplest case of two blocks of different material in shear ( figure 14 ). For a given overall shearing force , P , the shear strains in each block , $\gamma_A$ and $\gamma_B$ are equal and are equal to the overall shear strain $\gamma_{total}$. The total shear stress , $\tau_c$ , is given by :

$$\tau_c = \tau_A V_A + \tau_B V_B \qquad \text{.....14}$$

where $V_A$ and $V_B$ are the volume fractions of each block.

Now , as stated all strains are equal and therefore

$$\tau_A = G_A \gamma_c \qquad \text{.....15}$$

and

$$\tau_B = G_B \gamma_c \qquad \text{.....16}$$

Then ,

$$\tau_c = G_c \gamma_c = \tau_A V_A + \tau_B V_B \qquad \text{.....17}$$

Substituting equations 15 and 16 in 17 and rearranging for $G_c$ gives:

$$G_c = G_A V_A + G_B V_B \qquad \text{.....18}$$

This rule of mixtures principle is used to calculate the average shear modulus for each of the three blocks described earlier ( figure 13 ).

Having established the first principles of the model the equations for the shear magnification can now be developed. The model splits the problem into three blocks ( figure 13 ). Calculations will now be performed for each block in turn.

Assume shear across the fibre-fibre region , block 1 ( Figure 13 ).

Increment of shear displacement , dx ,

$$dx = \tau \frac{dy}{G} \qquad \text{.....19}$$

where

$\tau$ = shear stress

G = average shear modulus in a slab of incremental thickness dy.

The average shear modulus in a slab of thickness dy parallel to the xz plane is ( as established by equation 18 ) :

$$G = \frac{X_g G_g + X_r G_r + X_i G_i}{2r + 2t + s} \qquad \text{.....20}$$

where $X_g, X_r, X_i$ are the areas of glass , resin , and interphase in the unit cell extending unit distance in the direction of the fibres , and $G_g, G_r, G_i$ are the shear moduli of the glass , resin , and interphase.

Then substituting equation 20 in equation 19 gives :

$$dx_1 = \tau dy \frac{(2r + 2t + s)}{X_g G_g + X_r G_r + X_i G_i} \qquad \text{.....21}$$

To simplify the analysis block 2 figure 13 is assumed to have the form shown in figure 15. Then , as for equation 21 ,

$$dx_2 = \tau dy \frac{(2r + 2t + s)}{Y_r G_r + Y_i G_i} \qquad \text{.....22}$$

For block 3 figure 13 there is only resin , and hence

$$dx_3 = \tau \frac{dy}{G_r} \qquad \text{.....23}$$

The total displacement of the unit cell face , F , can then be determined in two stages. First , by adding together all the incremental deflections in each block which basically means integrating equations $dx_1$, $dx_2$ and $dx_3$ for the thickness of each block. Second , by then adding the deflections of the blocks themselves , given that there are two " block 1 " and " block 2 " arrangements and only one " block 3 " arrangement. The equation for total displacement on the unit cell face is then given by :

$$F = 2\int_0^r dx_1 + 2\int_0^t dx_2 + \int_0^s dx_3 \qquad \text{.....24}$$

Then by substituting equations 21 , 22 and 23 in equation 24 ,

$$F = 2\tau \int_0^r dy \frac{(2r + 2t + s)}{X_g G_g + X_r G_r + X_i G_i} + 2\tau \int_0^t dy \frac{(2r + 2t + s)}{Y_r G_r + Y_i G_i} + \tau \int_0^s \frac{dy}{G_r} \qquad \text{.....25}$$

The average ( measured ) shear strain across the unit cell , $\gamma_c$ ,

$$\gamma_c = \frac{F}{2r + 2t + s} \qquad \text{.....26}$$

The shear strain in all incremental slabs in which there is only resin , $\gamma_r$ ,

$$\gamma_r = \frac{\tau}{G_r} \qquad \text{.....27}$$

Then the shear strain magnification factor in the resin can be determined by dividing equation 27 by equation 26 ,

$$\frac{\gamma_r}{\gamma_c} = \left(\frac{\tau}{G_r}\right)\left(\frac{2r + 2t + s}{F}\right) \qquad \text{.....28}$$

Substituting equation 25 in equation 28 gives ,

$$\frac{\gamma_r}{\gamma_c} = \frac{1}{G_r\left(2\int_0^r \frac{dy}{X_g G_g + X_r G_r + X_i G_i} + 2\frac{t}{Y_r G_r + Y_i G_i} + \frac{s}{G_r(2r + 2t + s)}\right)} \qquad \text{.....29}$$

To solve this equation it must be further reduced such that all the components are in terms of r , s , t , $G_g$, $G_r$, or $G_i$. Reducing the equation to such a form gives ,

$$\frac{\gamma_r}{\gamma_c} = \frac{1}{2G_r(I + K) + \left(\frac{s}{2r + 2t + s}\right)} \qquad \text{.....30}$$

where I and K are given by

$$I = \int_0^r \frac{dy}{X_g G_g + X_r G_r + X_i G_i} \qquad \text{.....31}$$

$$K = \frac{t}{Y_r G_r + Y_i G_i} \qquad \text{.....32}$$

To solve I and K , the geometrical terms $X_g, X_r, X_i, Y_r$

and $Y_i$ must be expressed in terms of r , s , and t.

In polar coordinates ( refer to figures 16 and 17 ) ,

$$y = r \sin\theta$$

and therefore ,

$$dy = r \cos\theta d\theta \qquad \text{.....33}$$

Using equation 33 to convert equation 31 to polar coordinates gives ,

$$I = \int_0^{\frac{\pi}{2}} \frac{r \cos\theta d\theta}{X_g G_g + x_r G_r + X_i G_i} \qquad \text{.....34}$$

Now from figure 17 ,

$$y = r \sin\theta = (r + t) \sin\alpha \qquad \text{.....35}$$

Rearranging 35 gives ,

$$\sin\alpha = \frac{r \sin\theta}{r + t}$$

and then ,

$$\alpha = \sin^{-1}\left(\frac{r \sin\theta}{r + t}\right) \qquad \text{.....36}$$

Now ,

$$\frac{X_g}{2} = r \cos\theta$$

and therefore ,

$$X_g = 2r\cos\theta \qquad .....37$$

Also from figure 17 ,

$$\frac{X_g + X_i}{2} = (r+t)\cos\alpha$$

From equation 37 ,

$$\frac{X_i}{2} = (r+t)\cos\alpha - r\cos\theta \qquad .....38$$

Substituting equation 36 in equation 38 and rearranging gives ,

$$X_i = 2\left((r+t)\cos\left(\sin^{-1}\left(\frac{r\sin\theta}{r+t}\right)\right) - r\cos\theta\right) \qquad .....39$$

With $X_g$ and $X_i$ defined in equations 37 and 39 $X_r$ is given by :

$$X_r = (2r + 2t + s) - (X_g + X_i) \qquad .....40$$

With $X_g, X_r, X_i$ in terms of r , t and s the function I can be solved for a given set of variables.

To solve K there is no need to rearrange in polar coordinates because to make the analysis simple block 2 was assumed to take the form shown in figure 15. From figure 16 $Y_i$ is shown to be equal to the value of $X_i$ when $\theta = 90°$. Thus from equation 39 ,

$$Y_i = 2(r+t)\cos\left(\sin^{-1}\left(\frac{r}{r+t}\right)\right) \qquad .....41$$

and from consideration of figure 15 ,

$$Y_r = (2r + 2t + s) - 2Y_i \qquad \text{.....42}$$

Again , with $Y_r$ and $Y_i$ in terms of r , t and s the function K can be solved ( refer section 2.4 ).

Equation 30 can be solved then in conjunction with equations 32 and 34 to predict the level of shear strain magnification for a given set of variables. Initial results are presented in section 2.3.

Unfortunately , it is not possible to determine a shear strain magnification for the interphase because there are no areas where a slab of interphase only exists.

## 2.3 Initial results

Computer programs were written in Turbo Basic to calculate the following quantities:

(i) Tensile strain magnification factor in the resin.

(ii) Tensile strain magnification factor in the interphase.

(iii) Shear strain magnification factor in the resin.

The programs ( presented in Appendix A ) allowed for any of six variables to be ranged between a minimum and maximum figure so that trends could be seen in the results. The initial variables and the mean values assigned to them , consistent with a structural glass fibre - vinyl ester composite , are shown below:

Fibre radius ( r ) , 6 $\mu m$

Interphase thickness ( t ) , 0.2 $\mu m$

Fibre volume fraction ( V ) , 0.5

Fibre Young's modulus ($E_f$) , 76 GPa or Fibre shear modulus ($G_f$) , 25 GPa

Matrix Young's modulus ($E_r$) , 3 GPa or Matrix shear modulus ($G_m$) , 1 GPa

Interphase Young's modulus ($E_i$) , 0.1 GPa or Interphase shear modulus ($G_i$) , 0.03 GPa

The value of inter fibre spacing , minus twice the interphase thickness , is needed for the calculations and has previously been referred to as " s ". This value is calculated from the fibre volume fraction and fibre radius according to the equation ( a modification of the well known version presented in Hull ( 53 ) ):

$$s = r\left(\left(\frac{\pi}{V_f}\right)^{\frac{1}{2}} - 2\right) - 2t$$

The equation assumes a square array for the fibres. The square array is inherent in the model for shear strain magnification.

Fibre modulus was assumed to remain constant but the remaining five variables were ranged plus and minus 50% around their mean values to determine their influence on the calculated quantities.

The results are summarised in figures 18 , 19 and 20. It must be stressed that these results are for values which are expected to be representative of the composite but are not necessarily the " real values ". Bearing this in mind some general trends can be observed from the figures.

### 2.3.1 Transverse tension models

( 1 ) The tensile strain magnification factor in the resin ( tsmfr ) is reduced from 4.3 ( refer section 2.1.3 ) to approximately 1 by the introduction of an interphase.
This is really to be expected as the values for the interphase thickness and modulus were originally chosen to give a tensile strain magnification factor of 1.
( 2 ) The corresponding tensile strain magnification factor in the interphase ( tsmfi ) is approximately 30.
This infers that the strain to failure of the interphase must be large to prevent premature failure of the composite in the interphase.
( 3 ) Variations in all inputs other than fibre volume fraction cause significant changes in the values of tsmfr and tsmfi.

### 2.3.2 Transverse shear model

( 1 ) The shear strain magnification factor in the resin ( ssmfr ) is reduced from 3.86 ( refer section 2.1.3 ) to 3.69 by the introduction of an interphase.
( 2 ) Only variations in fibre volume fraction cause any significant changes in the value of ssmfr.

## 2.4 Conclusions drawn from the initial results of the models

The conclusions of sections 2.3.1 and 2.3.2 show that it is important to know accurate values for all the inputs if accurate values are to be calculated for tsmfr , tsmfi , and ssmfr. Determining accurate " in-situ " values for the variables identified in section 2.3 is not an easy matter , particularly for the interphase where the material is present in minute quantities. Accurate determination of the variables and the special techniques which were developed for those purposes are the subject of subsequent sections of this report ( refer to sections 5 , 6 and 7 ).

# 3 EXPERIMENTAL

## 3.1 Introduction

Characterisation and control of each of the three phases of the composite material is crucial for the success of the project. The material of each phase must be selected and combined to form a composite with improved transverse performance. The use of glass fibre roving is predetermined by the original requirements of the project but the surface treatment of the fibre , the fibre coating ( interphase ) , and the matrix resin are areas of consideration for the project. Also the technique of application of the coating material and the manufacture of the final composite must be considered. In terms of this project the most important area is the selection and application of the coating material.

### 3.1.1 Selection and application of interphase material

Selection of the interphase material is likely to be heavily dependant upon the route chosen for its application. It has been established from the theoretical modelling that the material will be rubbery in nature , that is it will have a low modulus and a high strain to failure. Discussion of the choice of interphase material will therefore be left until the application route has been established.

Four main techniques have been discussed in the literature for the application of coatings to fibres. Briefly these are electropolymerisation ( 26 , 38 , 39 , 40 ) , plasma grafting ( 41 ) , dip coating with viscosity control ( 23 , 24 , 25 , 42 ) and dip coating with surface charge control ( 43 ).

Electropolymerisation is used exclusively for coating carbon fibre. This is because it relies on the fibres acting as one of the electrodes in an electrochemical cell. The coating material

monomer is suspended in solution as the electrolyte and upon application of an electric current is deposited onto the carbon fibres. Unfortunately , glass fibres are non-conductive and so this technique is not suitable for coating them.

Plasma grafting can be used with any substrate material. When a glow discharge of a pure organic vapour is created or when an organic vapour is introduced into a glow discharge of an inert gas such as Argon , the deposition of a highly crosslinked polymer film onto an exposed substrate is observed. Thickness of the coating can be controlled by the monomer flow rate , plasma power level and time of deposition. The technique can be successfully used on fibre rovings.

Dip coating of fibres by running them through a bath in which the coating material is dissolved can be used for all types of fibre. The coating material is generally consolidated by subsequently passing the roving through a drying tower where the suspension medium is driven off. Control of coating thickness relies on the viscosity of the coating solution and the speed at which the fibre passes through the bath. The technique has been used successfully but careful control is necessary to maintain a constant coating thickness.

Peiffer and Nielsen developed a technique for dip coating chopped discontinuous fibres which was not dependant upon coating solution viscosity. First , they adjusted the surface charge of the glass fibre using a colloidal alumina such that it was opposite to the charge on the individual particles of a polymer latex. Second , they dipped the charge reversed fibres into the latex whereupon static attraction and repulsion naturally formed a single particle layer on the fibres. Third , the fibres were removed and the coating dried. The advantages of this technique over viscosity control are :

(i) Fibre speed and viscosity would not need to be monitored and carefully controlled. Indeed the fibre speed would not even have to be constant to maintain a uniform coating thickness. This would allow for the use of non-cylindrical mandrels in a continuous coating / filament

winding process.

(ii) The charged latex particles used for coating are typically suspended in water not a noxious solvent and therefore safety hazards are reduced.

Discussion of the application technique chosen for this project follows in section 3.4.1.

## 3.2 Selection of materials

There were three areas of material selection which had to be decided for the project. These were matrix resin , interphase material , and fibre surface treatment ( silane coupling agent ).

### 3.2.1 Matrix resin

The primary requirements of the matrix resin were as follows :

(i) Heat distortion temperature ( 1.8 MPa ) > 125 - 130 °C

(ii) Good environmental resistance

(iii) Low cost , approximately two pounds per kilogramme.

(iv) Low viscosity for ease of processing by filament winding.

There are a number of thermosetting polymers which satisfy these requirements to varying degrees but the resin finally chosen was a vinyl ester. Vinyl esters generally have good environmental resistance , suitably high glass transition temperatures , easy processing characteristics and low to medium prices. To facilitate filament winding an inhibitor was added to the chosen grade to extend the pot life from 30 minutes to 3-4 hours. The details of the matrix resin system used are :

VINYL ESTER RESIN : Dow Chemicals Derakane 470-36

Chemical name : Epoxy novolac vinyl ester

Parts by weight : 100

ACCELERATOR : 1% Cobalt Octoate in Styrene

Parts by weight : 3

CATALYST : 50% Methyl Ethyl Ketone Peroxide in Styrene

Parts by weight : 1.5

INHIBITOR : Acetyl Acetone

Parts by weight : 0.125 ( 10 drops from a small pipette )

The recommended cure schedule was 24 hours at room temperature followed by 3 hours at 80 °C. The glass transition temperature for this and a number of other cure schedules was determined and the results are presented in section 3.3.1. The mechanical properties of the resin when cured as for the composite were determined and are presented in section 3.3.2.

### 3.2.2 Interphase material

The requirements of the interphase material were that it should be in latex form and the modulus of the cured polymer should be around 0.1 GPa. In fact a modulus slightly lower than this would also be considered to allow for some subsequent increase in modulus due to constraint. The strain to failure of the cured polymer should also be in excess of 100%.

The chosen material was an acrylic polymer latex , Hycar 26084 , manufactured by B.F.Goodrich. The particle size of the polymer in the latex was , according to the manufacturers data , 0.2 micron and the charge on the surface of the particles was negative.

The glass transition temperature and mechanical properties of the cured acrylic polymer in sheet form were determined and are presented in sections 3.3.1 and 3.3.2.

### 3.2.3 Fibre surface treatment

It was felt that to ensure a good level of bonding and environmental resistance a commercial silane coupling agent should be applied to the surface of the glass fibres. The most important criterion in choosing the silane was that it should not reverse or negate the positive charge of the glass fibre surface ( refer section 3.4 ). Additionally the silane should be compatible with resin so that the control samples where no interphase is present will be well bonded to the fibres. Compatibility with the interphase material is also desirable as an additional source of bonding ( that is chemical bonding in addition to the ionic bonding due to attraction of oppositely charged species , refer section 3.4 ).

The silane selected for the glass was ( gamma-Methacryloxypropyltrimethoxy silane ) produced commercially by Union Carbide Chemicals as A 174. Initially the silane was applied separately to the virgin glass fibre roving. Chopped lengths of this fibre were then dipped in the latex to ensure that the charge was correct and that the silane did not cause gross coagulation of the polymer particles. For comparison purposes a silane with a negative charge was also tested in this way. It was found that the negatively charged silane did indeed give rise to gross coagulation of the polymer particles on the fibre surface whereas the A 174 silane used for the project showed no coagulation.

Adhesion tests were also performed to confirm the improved level of bonding when using the A 174 silane coupling agent. Results are presented in section 3.3.3.

## 3.3 Characterisation of selected materials

The resin and the interphase material were characterised using Differential Scanning Calorimetry ( DSC ) and tensile testing of bulk samples. The levels of bonding between the phases were determined using a fibre roving lap shear test. These techniques and results are discussed in more detail in the following sections.

### 3.3.1 Characterisation by Differential Scanning Calorimetry

When thermosetting resins cure they produce heat. This process is called the cure exotherm. Often a thermoset does not fully cure during its initial curing schedule and is subsequently subjected to a further period of heating known as a post cure. Any production of heat during this curing period is called the residual cure exotherm. The degree of residual cure exotherm measured in differential scanning calorimetry is therefore an indication of the degree of initial cure. Figure 21 (a) shows how this exotherm is displayed on a DSC scan. In addition to the residual cure exotherm , the glass transition temperature ( Tg ) can also be determined. This is shown by a distinct drop in the baseline ( refer figure 21 (b) ). These points are well illustrated in a DSC scan on a sample of uninhibited Derakane 470-36 cured for 24 hours at room temperature followed by a post cure of 10 minutes at 100 °C ( figure 22 ).

DSC studies were made on the matrix resin to ensure that no significant changes had occured in the cured resin properties by the using an inhibitor. In figure 23 DSC scans are shown for inhibited Derakane 470-36 cured 24 hours at room temperature and then post cured 1 or 6 hours at 80 °C and 1 or 6 hours at 120 °C. These post cures span the recommended post cure of 3 hours at 80 °C. The first point to note is that the heat flow is very small indicating that generally the samples are well cured. Second only curve (a) displays any residual cure

exotherm and even then it is very small. Finally an unknown transition at approximately 125 °C is masking the glass transition. ( A reproduction of figure 22 in figure 24 shows how easily a shifted residual cure exotherm can mask the glass transition ).

As a result of this analysis it was decided to use the recommended cure schedule of 24 hours at room temperature followed by 3 hours at 80 °C.

A DSC scan on a sample of acrylic sheet dried then post cured 3 hours at 80 °C , to simulate the composite cure , is shown in figure 25. No residual cure exotherm is noticeable , indicating a fully cured sample , and a glass transition temperature of approximately 8 °C is apparent.

### 3.3.2 Characterisation of tensile mechanical properties

Plates of resin were cast and cured for 24 hours at room temperature followed by 3 hours at 80 °C. Sheets of acrylic polymer were prepared by drying of the latex followed by curing for 3 hours at 80 °C. Dogbone shaped samples of vinyl ester and acrylic were cut from the sheets and tested in tension in an Instron 1195 test machine. The tensile load deflection curves were analysed and the strength , failure strain and Young's modulus were calculated. Results are presented in Table 1.

### 3.3.3 Adhesion testing

A simple lap shear test utilising the fibre roving as the adherend was used to assess the relative level of bonding for uncoated fibre , A 174 coated fibre , and then both these fibres coated with acrylic. The bond between the rovings was made with the matrix resin using an overlap length of approximately five millimetres ( figure 26 ). The ends of each tow were simply gripped in an Instron 1122 and the failure load recorded. The bonded area was measured before testing under a binocular microscope. Results are presented in Table 2.

The results show that use of the silane coupling agent as a pre-treatment for the acrylic coating improves the bond strength ( 4 vs. 3 in Table 2 ). The use of an acrylic coating either with or without pre-treatment also improves the bond strength ( 3 and 4 vs. 1 in Table 2 ). The maximum bond strength is achieved using the silane coupling agent only. Introducing the acrylic coating reduces bond strength ( 3 and 4 vs. 2 in Table 2 ) but this may be due to a lower shear strength in the acrylic rather than a failure at the interface. Overall then the results confirm that the use of A 174 silane coupling agent on the fibre is beneficial.

## 3.4 Interphase application and composite preparation

In the following sections the techniques and apparatus used in this project for both applying the interphase and for manufacturing the final composite material are presented.

### 3.4.1 Interphase application

The technique selected was an extension of the concept developed by Peiffer and Nielsen ( 43 ) such that a continuous fibre roving could be passed through a latex bath ( figure 27 ), the polymeric particles being attracted to the fibres by electrostatic forces on the surface ( figure 28 ). The fibre roving then passed through drying towers to remove the water in which the polymer particles were suspended. Finally the fibre passed through a matrix resin bath and onto a flat plate mandrel ( see section 3.4.2 ). Using a single process for application of the interphase and manufacture of the final composite plate ensured that minimum damage occurred to the coated fibre. The advantages of this technique over other techniques is the relatively simple , low cost equipment needed and the lack of strict process control necessary to ensure a constant and uniform coating thickness.

Using this technique and the latex selected in section 3.2.2 an acrylic coating approximately 0.2 micron thickness can be applied to the glass fibre roving in a continuous process. Peiffer

and Nielsen ( 43 ) showed that the thickness could be increased in 0.2 micron steps by using a colloidal alumina to restore the positive charge on the coated glass fibre. For the purposes of this project a single layer only will be used to establish the principles of the interphase concept but future studies might consider the possibility of varying the coating thickness in this way.

### 3.4.2 Production of composite plates

The general production route for the composite plates was as follows ( refer figure 27 ) :

(i) The fibre roving unwound internally from a cheese of glass fibre commercially coated with A 174 silane coupling agent.

(ii) The roving passed through an acrylic latex bath and then through drying towers to remove the water and form an acrylic film around the fibres.

(iii) From the towers the roving passed into a bath of matrix resin. As the fibre left the resin bath it passed through pinch rollers which both aided the wetting of the fibres by the matrix resin and removed any excess resin from the roving.

(iv) Finally the roving was wound around a flat plate mandrel. The speed of rotation of the mandrel was carefully matched against the linear speed of the guiding eye to ensure that rovings were wound leaving no space between them.

(v) Once sufficient passes of the plate had been made to give the required final plate thickness the fibre was cut and the mandrel removed. The fibre/resin winding was then compressed between two plates such that the final thickness was controlled ( see figure 29 ).

(vi) The plates were left to cure for 24 hours at room temperature in the press and then removed. The cured composite was then slit along the edges of the mandrel to give two composite plates. Excess resin was removed from the edges of the plates which were then post cured in an oven for 3 hours at 80 °C.

A number of specific problems were encountered during perfection of the technique and these will be dealt with one point at a time.

(a) Initial surface quality of the composite plates was poor due to two reasons. First the width of the roving tended to vary quite significantly because it twisted as it unwound from the cheese. Therefore spaces between subsequent roving winds occurred when the speeds were matched for the untwisted roving width. Second the surface of the plate produced a duller and inferior quality surface to that of the release film ( mylar ) used between the upper surface and the compression plates. These problems were overcome by adjusting the speeds such that the roving spacing on each wind matched the minimum observed roving width , and by using a piece of release film secured to the mandrel surface by a thin layer of Vaseline. This second solution also significantly improved the ease of removal of the cured plates from the mandrel.

(b) Problems were encountered early on in managing to fully dry the fibre after it had passed through the latex bath. This was solved in two ways. First , by slowing down the speed of rotation of the mandrel and hence the speed at which the fibre passed through the drying towers. Second , by adding a further drying tower to the system ( refer figure 30 ).

(c) The first plates which were made after the drying problem had been solved showed a white "marbling" ( refer figure 31 ) in their cross section and excessive voidage ( refer figure 32 ). This was thought to be a result of an excess of acrylic polymer around the outside of the roving. The excess showed up as the white marbling and " sealed in " air leading to the voidage. This view is supported by figure 33 which shows a close up of a marbled area. The fibres stand proud of the surface indicating that the medium they are in is softer than the other areas of matrix. This is obviously the case for the acrylic versus the vinyl ester.
Having established where the problem lay the cause and solution had to be found. The cause was felt to be that the roving passed immediately into a vertical drying tower after it had

emerged from the latex bath. Excess latex therefore ran down the outside of the roving , gradually drying as it did so. This process lead to a build up of acrylic around the outside of the roving. To overcome this , scraping off of the excess acrylic, washing of the fibre , and a reduction in the concentration of the as received latex were proposed and combinations of these tried. Both optical microscopy of cross sections and the short beam shear test ( 44 ) were used to monitor progress. Table 3 summarises the results which show that the problem was finally overcome by using a latex diluted 1 - 99 ( as received - distilled water ) , a scraper , and a distilled water wash before drying. This improved the short beam shear strength from 65.7 MPa to 76.2 MPa compared to 68.8 MPa for the uncoated composite.

The final production apparatus is shown in figure 34.

# 4 MECHANICAL TESTING

## 4.1 Introduction

The main thrust of the project was to improve the transverse mechanical properties of unidirectional continuous glass fibre composites. It is therefore necessary to review the types of tests and results gained from previous work which were instrumental in selecting suitable tests for this project. The mechanical properties can be split into two general groups. First , there are those properties which characterise the response of the material to loads applied at relatively low speeds ( static testing ). Second , there are those properties which characterise the response of the material to loads applied at high speeds ( dynamic testing ). The properties of concern within each of these groups are detailed in the following sections.

### 4.1.1 Static testing

(a) Mechanical properties

In a unidirectional composite material ( figure 35 ) the response to loads applied in the longitudinal direction is dominated by the properties of the fibres. However , the response to loads applied in the transverse or shear directions are dominated by the matrix and the interface , or in the case of this project the interphase. The three properties which characterise the mechanical response of the material are the modulus , the strength , and the strain to failure. Measurement of these properties in the transverse direction can be carried out either in pure tension ( figure 36 ) or in flexure ( figure 37 ).

Shear properties are generally determined by two means. The first is the short beam shear test. Longitudinal samples are loaded in bending but with a small span to depth ratio such that the highest stress generated is an interlaminar shear stress at the centre of the specimen

( figure 38 ). The resulting failure strength is termed the interlaminar shear strength. This author agrees with other workers ( 45 ) , however , in regarding the short beam shear test as an indicator of the level of bonding rather than a test which accurately measures the inter-laminar shear strength of a composite. For that reason results for this test are presented in this report as the short beam shear strength rather than the interlaminar shear strength. The second shear test is the off-axis test. Classically the off-axis angle is taken to be 10°. The paper by Chamis ( 46 ) which proposes this angle , however , reveals that it was calculated for a carbon-epoxy composite and that for a glass-epoxy composite the angle should be 15° ( figure 39 ). The shear strength which is calculated from this test is the intralaminar , rather than the interlaminar , shear strength. This value of shear strength is more representative of the true shear strength and so is quoted as the intralaminar shear strength.

Some of these properties were determined by previous workers for composite materials containing a low modulus interphase.

Lavengood and Michno ( 24 ) coated commercially silaned glass fibres with a flexibilised epoxy resin prior to filament winding epoxy matrix composite plates. Reference composite utilising the fibre in its commercially silaned state only was also manufactured. Transverse bending strength and strain to failure was determined for each composite material both dry and after a two hour boil. The coated fibre composite showed improvements in strength over the reference of 66% dry and 200% wet. Failure strain dry increased by 60% for the coated fibre composite. Short beam shear strength also increased , measured dry , by at least 40%.

Tryson and Kardos ( 23 ) give results for transverse tensile strength in the same system which are exactly the same as those of Lavengood and Michno. Although Tryson acknowledges the work of Lavengood he does not make clear that the results he quotes in his paper are actually those of Lavengood. Furthermore , in expressing the results as transverse tensile strength he is misquoting Lavengood who , as stated , performed bend tests. The equivalent

tensile strength from a bend test is well known to be much higher than the directly measured tensile strength , even in homogeneous materials. The discrepancy might well be more important in the systems considered here because when tested in bending the sample is subject to shear stresses , as well as tensile and indeed compressive stresses , and the coating may respond differently in shear than in pure tension.

Peiffer and Nielsen ( 43 ) quote results for composites made using glass fibres coated with an acrylic polymer in a matrix of epoxy resin. The fibres , however are chopped into short lengths , are in a random orientation , and are present in very low volume fractions ( maximum of 20% ). Measured against a control using silane coated fibres no significant differences were found for tensile modulus and strain to failure while tensile strength was actually found to decrease by 40%. These results can not really be compared against the unidirectional high volume fraction composites used for this project , however , as the fibre arrangement and volume fraction is so different.

Three papers ( 26 , 38 , 47 ) on coated carbon fibre epoxy matrix composites all indicate a reduction in the short beam shear strength when using a compliant coating material. Subramanian ( 38 ) , however , determined in a later paper that the short beam shear strength need not be reduced if the interphase material is carefully chosen to give a good level of bonding or interaction with the matrix resin.

For work where comparable results exist then , encouraging levels of improvement in transverse and shear properties have been discovered.

(b) Toughness

Toughness can be determined " statically " from double cantilever beam tests ( figure 40 ) and from area under the curve of transverse stress-strain response , or dynamically from impact testing. The former two tests are described in this section and the latter in section 4.1.2..

Classic fracture mechanics ( 48 ) utilises the double cantilever beam test to measure the fracture toughness , $G_{1C}$ , for the controlled growth of a crack. This technique is adopted for measuring the interlaminar fracture toughness of a composite material using the arrangement shown in figure 40. Another test which has been used ( 45 , 49 , 50 ) to measure the toughness of a composite at low strain rates is a simple measurement of the area under the stress-strain curve. This area is an indication of the energy absorbing capability of the material under test. No work has been carried out using either test for composite utilising a compliant interphase. However , work has been carried out to investigate the transverse toughness of unidirectional composites ( 45 , 49 , 50 ).

Marom and co-workers ( 49 , 50 ) investigated the transverse fracture toughness of unidirectional glass fibre epoxy composites. They used four point bending of notched specimens and approximated $\gamma_{Icomposite}$ , the fracture surface energy of initiation. They also determined $\gamma_{Fcomposite}$ , the total fracture surface energy , by measuring the area under the stress-strain curve. Values of $\gamma_{Fcomposite}$ varied with c/d ratio ( c = depth of cut , d = depth of specimen ) and final results were the values extrapolated to c/d = 1. The terms $\gamma_{Icomposite}$ and $\gamma_{Fcomposite}$ were further split as follows:

$$\gamma_{Icomposite} = \gamma_{Imatrix} A_m + \gamma_{Iinterface} A_m$$

and

$$\gamma_{Fcomposite} = \gamma_{Ffibre} A_f + \gamma_{Fmatrix} A_m + \gamma_{Finterface} A_i$$

where $A_x$ is the respective fraction of the fracture surface.

They showed that $\gamma_{Icomposite}$ decreased rapidly with increasing volume fraction. At $V_f = 0.906$ , the theoretical maximum for a hexagonal array , the fibres are touching and cracks can pass through the composite entirely along the interface. Therefore at $V_f = 0.906$ , $\gamma_{Icomposite} = \gamma_{Iinterface}$. By extrapolation of experimental results this value was found to be 0.015 KJ/$m^2$.This author believes that by introducing an interphase material strongly bonded and capable of high energy absorption $\gamma_{Iinterface}$ could be significantly increased leading to an overall increase in the measured toughness.

In his work on measuring the area under the stress-strain curve of a transverse tensile test Newaz ( 45 ) showed that this method of fracture toughness determination could be used to show the difference in bond quality between two composites. When using an epoxy matrix with glass fibre the fracture energy was 68 KJ/$m^3$ and the surface of the fibres after fracture showed much adhering resin. However , when using a vinyl ester resin matrix the fracture energy dropped to 40 KJ/$m^3$ and the surfaces of the fibres after fracture were practically clean.

Determination of the fracture energy by measuring the area under the stress-strain curve appears to be of use , particularly when comparison between two materials is sought. It is also economical of material as stress-strain curves must be derived anyway to determine the mechanical properties.

### 4.1.2 Dynamic testing

(a) Fatigue

Newaz ( 51 ) compared two brittle polymer matrix unidirectional glass fibre composites in a four point bending fatigue. One matrix had a higher strain to failure but both had a similar

strength and modulus. Fatigue was performed under deflection control for two reasons ; (i) it allowed for decreased tendency towards hysteretic heating since the load generally decreases with increasing fatigue life , (ii) the damage or cracks do not grow in an uncontrolled manner as can happen in load controlled testing. Also , creep fatigue interaction is minimised. At low deflection levels splitting , longitudinal fibre debonding , was the dominant failure mechanism in both composites , and was attributed to transverse stresses generated during gripping of the specimens ( figure 3 ). It was found that the higher strain to failure matrix gave a longer fatigue life. This is because initiation of fibre matrix debonding was delayed when compared to the lower strain to failure matrix composite.

Shih and Ebert ( 52 ) studied the effect of the quality of adhesion at the fibre matrix interface on four point bending fatigue life for unidirectional glass fibre composites. Numerous matrices and coupling agents were assessed but the only combination used throughout the investigation was an epoxy matrix with an aminoethyl-aminopropyl-trimethoxy silane coupling agent ( AAPS ). This composite provided an excellent bond during static wet and dry tests and was compared to an epoxy matrix composite that utilised no coupling agent. Short beam shear testing was found to be a more sensitive indicator of interfacial degradation than longitudinal flexural strength. Fatigue testing was deflection controlled. The composite with higher interfacial strength was found to possess a longer fatigue life. This was shown to be because the strong interface delayed the onset of fibre ridging ( debonded fibres becoming raised at the surface ) and longitudinal matrix cracking.

Investigating fatigue of unidirectional glass epoxy composites transverse to the fibres Newaz ( 53 ) and Agarwal and Joneja ( 54 ) observed some quite different results. Newaz conducted tensile fatigue under strain control and noted that stiffness remained unchanged over the whole life of the composite , failure being catastrophic. Agarwal and Joneja , however , conducted cantilever bending fatigue tests under deflection control and noted distinct drops

in stiffness over the fatigue life of the specimen , starting with a large drop ( 70% ) between 0.1% and 5% of the overall fatigue life. This drop was found to correspond with failure of the fibre matrix bond at the surface , near to where the samples were gripped. In fact , reconsiling the difference between these two sets of results is not that difficult. In the bending fatigue tests tensile failure at the surface was the first failure to occur and dropped the stiffness by 70%. In tensile fatigue this same tensile failure would result in catastrophic failure of the specimen because the whole of the specimen rather than just the surface was in tension. Thus if the fatigue life for the two tests were compared on the basis of failure occuring at the first sign of tensile failure the results would be much more comparable.

Both longitudinal and transverse fatigue tests have indicated that for two matrix systems of comparable tensile strength and modulus the one with the higher strain to failure will give a longer fatigue life. Also a longer fatigue life can be expected for a composite with a high interfacial bond strength. This author therefore believes that by introducing a strongly bonded high strain to failure interphase the fatigue life could be significantly improved.

The only work to date which considers the fatigue performance of a compliant interphase composite material ( 24 ) supports this view. Lavengood conducted torsional fatigue tests on a glass epoxy composite which utilised a flexibilised epoxy interphase. He showed that the torsional fatigue life could be improved from that of an uncoated fibre composite by at least one order of magnitude.

(b) Impact toughness

All of the work to date ( 26 , 38 , 43 , 47 ) which has assessed the toughness improvements to be had by introducing a compliant interphase has measured the impact toughness rather than the static toughness. Both Charpy and Izod impact testing was carried out with improvements noted of between 30% and 40%. As for mechanical property measurement

Peiffer and Nielsen ( 43 ) noted a slight reduction in impact toughness for the interphase composite. Both Bell and Chang ( 26 ) and Ying ( 47 ) noted an improvement in impact toughness but with a corresponding drop in short beam shear strength as mentioned earlier. This corresponds with the classical view that higher toughness is achieved with lower interfacial bond strength and hence greater fibre pull out. Subramanian ( 38 ) , however , achieved an increase in both impact toughness and short beam shear strength. It is postulated by this author that this was achieved by taking advantage of a different energy absorption mechanism. By ensuring a good bond between fibre and matrix the short beam shear strength is high and the high energy absorbing capability of the interphase material is fully realised.

The work described in these sections indicates that a strongly bonded compliant interphase material should give rise to significant improvements in composite performance , particularly in off-axis properties. The tests selected to characterise the composites manufactured in this project are discussed in detail in the following section.

## 4.2 Selection of testing techniques

A number of test techniques were selected to determine properties of the composite material manufactured in this project. Most of the techniques used determine the static properties of the material.

### 4.2.1 Static test techniques

(a) Transverse tensile / transverse bending

These tests were used to determine the transverse strength , modulus and strain to failure in tension and flexure. Test samples were cut from plates of interphase and control composite such that the fibre axis ran at 90° to the length of the sample ( figure 41 ). In tension the ends of the sample were gripped and loaded at 1 mm/minute in an Instron 1195 test machine using

a Wallace non-contacting extensometer to measure the extension. In bending the samples were loaded in three point bending at 1 mm/minute in an Instron 1122. The span to depth ratio used was 20:1. Centre deflection was measured using a linear variable differential transformer ( LVDT ) calibrated against a known displacement ( figure 42 ).

In tension the failure stress is simply calculated as the failure load divided by the cross sectional area. Failure strain is the failure deflection divided by the original sample length. Modulus is the slope of the elastic portion of the stress-strain curve.

In flexure the strength , failure strain and modulus are given by the following equations:

$$\sigma_{max} = \frac{1.5 p_f s}{w t^2}$$

$$\varepsilon_f = \frac{12 \Delta_f t}{s^2}$$

$$E_f = \frac{s^3 m}{4 w t^3}$$

where $P_f$ is the failure load , s is the supporting span , w is the width , t is the thickness , $\Delta_f$ is the failure deflection and m is the slope of the load deflection curve in the elastic region.

(b) 15° off-axis shear test

This test was used to determine the intralaminar shear strength according to the work of Chamis ( 46 ). Samples were cut from the composite plates at an angle of 15° to the fibre axis ( figure 43 ). Care must be taken in selecting a suitable length and width that the distance between the grip regions exceeds the angled fibre length. This ensures that failure will not be affected by stresses in the gripping region.

The samples were then gripped in an Instron 1195 and tested in tension to failure. Failure load was recorded and the shear stress calculated according to the equation ( 46 ) :

$$\tau_{12} = 0.5\sigma_{xx} \sin 2\theta$$

where $\sigma_{xx}$ was the applied tensile stress and the angle $\theta$ was equal to 15°.

(c) Short beam shear test / longitudinal flexural test

These two tests are presented together because both are carried out in three point bending on samples cut with the fibres running along the axis of the sample ( longitudinally ). The difference between the tests , however , is the span to depth ratio used. For the shear test the span to depth ratio is kept to 5:1 whilst for the longitudinal flexural test the span to depth ratio is 20:1. The smaller span to depth ratio maximises the shear stress in the sample and the larger span to depth ratio maximises the surface tensile stress in the sample.

The short beam shear strength can be calculated according to the equation:

$$S.B.S.S. = \frac{0.75P_f}{w}t$$

The longitudinal flexural properties can be calculated using the same equations as given in (a) above.

(d) Toughness

The interlaminar double cantilever beam ( DCB ) test ( figure 40 ) was used to measure the toughness of the composite materials.

Figure 44 shows the sample used for the DCB test. A folded piece of aluminium was moulded into the composite plate at one end to enable an interlaminar crack to be easily initiated. Load was applied to the sample by gripping the hinges ( figure 40 ) in an Instron 1195 and pulling

in tension at 1 mm/minute. A pre-crack was used to ensure that measurements were made for the growth of a natural crack through the material. Load was applied to drive the crack in a controlled manner the length of the specimen ( form $a_0$ to $a_1$ in figure 44 ). A typical load-deflection curve for this type of test is given in figure 45. The critical fracture surface energy , $G_{1C}$ , is determined using the equation ( 55 ) :

$$G_{1C} = \frac{A}{w(a_1 - a_0)} \qquad KJ/msuper2$$

## 4.2.2 Dynamic test techniques

(a) Fatigue

Fatigue testing was carried out in three point bending with longitudinal samples ( fibre axis aligned with the span ). This was done for a number of reasons. First , longitudinal testing was of most interest to the industrial sponsors and as time constraints would not allow for any prolonged course of fatigue testing only one fibre orientation could be chosen. Second , the very small loads required for testing these materials transverse to the fibres could not be properly controlled on any of the available fatigue testing machines. Finally , by testing fairly wide samples in the longitudinal direction anticlastic bending is induced which leads to longitudinal splitting or transverse failure of the sample. This failure is not catastrophic but yields additional information on the relative resistance to transverse cracking of the two materials.

It was therefore decided that longitudinal three point bending fatigue would be used at an R ratio of 0.1 ( that is the ratio of minimum applied stress to maximum applied stress is kept constant at 0.1 ). The support span was 50 millimetres. Failure was defined as a 5% drop in

modulus. The number of cycles to failure was recorded for each of three specimens of each material. The stress levels used for the test were approximately 70% , 60% , 53% , and 44% of the static failure stress.

(b) Impact toughness

No results were generated for impact toughness in this project although this would be an area for further work.

## 4.3 Results

### 4.3.1 Static testing

(a) Transverse tensile testing

Results are presented in Table 4 for transverse tensile tests on coated and uncoated fibre composites. Straight sided test samples led to too many failures within the grips of the test machine. To overcome this problem waisted or "dog-bone" samples were used. Subsequent results were more consistent and it is these which are quoted in Table 4.

The results were compared , coated to uncoated , to see if the coating had affected the measured properties. Values were then compared for significant differences Using the student "t" test ( Appendix B ) , no significant differences were found between coated and uncoated fibre composites.

(b) Transverse bending tests

Results are presented for the transverse bending tests in Table 5. Comparing the results by "t" test indicates a significant difference between the results for uncoated and coated fibre

composite strength. Modulus and strain to failure show no significant difference. Transverse bending strength was shown to increase by approximately 21% when using the interphase material.

(c) Shear strength

Results are presented in Table 6 for the 15° off-axis test and the short beam shear test. Comparison by the "t" test shows significant differences in both cases. The 15° off-axis shear strength was shown to increase by approximately 17% when using the interphase material. The short beam shear strength was shown to increase by approximately 5%.

(d) Longitudinal bend test

When testing samples in longitudinal bending suppression of anticlastic bending results in transverse tensile stress at the top surface. The mechanism for this effect was discussed in section 1. The transverse tensile stress leads to longitudinal splitting of the composite at a stress considerably lower than the failure stress. This stress was defined as the longitudinal splitting threshold stress. Results are presented in Table 7 for the threshold stress and the failure stress. The results show no improvement in the failure stress when using an interphase. However , the longitudinal splitting threshold stress increases by 35% when using an interphase.

(e) Toughness

The results for double cantilever beam testing are presented in Table 8. The results show no significant difference when using an interphase.

### 4.3.2 Fatigue testing

The fatigue results are presented in Table 9 and show the number of cycles to failure at four stress levels for both the coated and uncoated fibre composite. This data is plotted as a standard stress against log cycles to failure in figure 46. The graph shows that no significant differences exist in the fatigue life of the two materials.

### 4.3.3 Summary of results

In none of the tests which were performed on the two materials was there any reduction in properties due to the use of the interphase material. Table 10 summarises the areas where significant increases were found. It is clear from this table that all properties which have shown an improvement are either shear or shear related properties. These results give the first indication that the interphase coating is only having any significant effect on properties when the loading regime is primarily one of shear.

# 5 MICROSCOPY

Microscopy was used in two main areas in the project. First , it was used to determine the range of fibre diameter and distribution actually present in the composite materials manufactured. Second , it was used to examine samples of coated fibre before it was used in the composite , and subsequently to examine the surfaces of fractured test pieces and cross sections of the composites.

## 5.1 Fibre diameter and distribution

Samples of each type of composite were taken and mounted in resin such that a polished section through the fibres could be prepared. The sections were then polished using progressively finer Carborundum papers and finished using diamond paste. To enhance the contrast between fibre and matrix resin the sections were then exposed to hydrofluoric acid vapour for approximately twenty seconds. The cross sections were then viewed in a Zeiss optical microscope in reflected light. Figures 47 and 48 show optical micrographs for the two composites. A standard grid was also photographed at the same magnification to provide a calibration reference for determining the fibre diameter.

Only one micrograph was used to determine the range of fibre diameter because the same fibre was used in both composites. The measurements were taken from the enlarged negative using a set of digital calipers. One hundred fibres were measured and their average and standard deviation determined.

The average fibre diameter was found to be 17$\mu m$ with a standard deviation of 1.1 $\mu m$ . The estimated error in the measurement and conversion using the calibration reference was plus or minus 2.4%.

Accurate determination of the fibre distribution is not so easy. Ideally a range of the inter-fibre spacings observed over a large area is required. However , from figures 47 and 48 it is obvious that many fibre are touching , or appear to be at that magnification. Deciding which inter-fibre spacings to measure for determining the average would greatly affect the result. The model assumes that the load is applied along the axis from fibre centre to fibre centre. Unless the fibres are in a perfect square array , which obviously they are not , the axis of load for most fibres would not intersect the fibre centres. This only serves to further complicate the measurements.

For the purposes of this project an average inter-fibre spacing was used as the baseline. It was calculated in the computer programs ( Appendix A ) from the fibre volume fraction previously measured by burn off technique to be approximately 60% for both composites. Higher "local" fibre volume fractions were also considered to give smaller inter-fibre spacings and hence simulate the touching fibre case. For further discussion see section 8.

## 5.2 Scanning electron microscopy

(a) Fracture surfaces

Fractured test pieces from the mechanical test work detailed in section 4 were examined in a scanning electron microscope ( SEM ). It was intended to compare the surfaces for any differences due to the coating or the stress mode which caused the failure.

Two types of test piece were examined , transverse tensile failure and intralaminar shear failure , for both coated and uncoated fibre composites. The surfaces were mounted on aluminium planchettes and gold coated to avoid charging up of the specimen by the electron beam. The samples were then placed in a JEOL T330 SEM. The surfaces were examined and representative photographs are shown in figures 49 - 53.

No significant differences were found in the appearance of the fracture surfaces when comparing the failure mode alone. However , significant differences were noted between coated and uncoated fibre composites in both modes of failure. Figures 49 and 50 show the typical appearance of a fibre after fracture in transverse tension for the uncoated and coated composite respectively. The surface of the uncoated fibre is relatively clean whilst the surface of the coated fibre is covered in a "scaly" deposit. It is postulated that this "scaly" deposit is the remains of the ripped acrylic coating material. This view is confirmed when considering figures 51 and 52. They show the grooves left in the resin when fibres were ripped out in the intralaminar shear test. The uncoated fibre composite ( fig. 51 ) shows a smooth groove whilst the coated fibre composite ( fig. 52 ) shows some damage within the groove. A close up of this damaged area ( figure 53 ) shows a section of thin ripped material which is thought to be the acrylic coating.

It is difficult from the observations made to make definite conclusions about the failure mode of the interphase itself. However , from the information available it would appear possible that the "scaly" failure observed in tension is more brittle in nature whilst the "ripped" failure observed in shear is one of high deformation. More work is needed in this area to define confirm the existence and appearance of the interphase and its failure modes.

(b) Fibre surfaces

Samples of coated and uncoated fibre roving were cut from the production apparatus , teased apart , and mounted on aluminium planchettes. The samples were then gold coated and placed in a JEOL T330 SEM. Photographs of the fibres are shown in figures 54 and 55. The surface of the coated fibre appears to have numerous smooth "hills and valleys" while the uncoated fibre appears to be fairly free of surface relief. Otherwise there is no significant difference between them.

(c) Composite cross sections

The composite cross sections used in section 5.1 were gold coated and examined in a JEOL T330 SEM. The main emphasis of the examination was to see if the fibres which appeared to, be touching at low magnification could be resolved at much higher magnifications. Figures 56 and 57 show typical photographs of inter-fibre spacings for coated and uncoated fibre composite respectively. The photographs show that spacings are resolvable at high magnification , although measuring these spacings for a large enough sample of fibres would prove extremely time consuming. Also , it is not clear without further work which fibre spacings are relevant to the determination of maximum strain and which are not. Therefore , it is not possible to determine which spacings need to be measured.

Another feature of the photographs , however , is the easily discernible ring which exists around each fibre. The rings are discernible on both coated and uncoated fibre , although the thickness of the ring may be slightly different for each. Approximate measurements of the thickness of this ring indicate it to be 0.1 micron. It is possible that this might be direct evidence of the interphase. It is also possible that it might simply be damage to the outer region of the glass caused by the etching process. This question remains unresolved at the present time.

# 6 DETERMINATION OF COATING GEOMETRY AND THICKNESS

## 6.1 Introduction

It was stated in the theoretical section that for the models to have any reality in their predicted values the inputs into the models must be as true to reality as possible. This means determining the thickness of the interphase as it will be in the composite. A number of techniques were envisaged whereby this might be achieved. First , by taking a cross section through the composite containing an interphase and simply viewing it under the scanning electron microscope. Second , mounting single fibres and measuring their diameters with and without the coating. Third , using an x-ray analysis technique in the electron probe microanalyser.

The first technique was unsuccessful because when sectioned glass fibres are viewed end on , as they are in a cross section through a composite , they charge up. The charge , caused by the electron beam , causes a halo to form around the circumference of the fibre. The dimensions of this halo were approximately 0.4 micron. As the coating thickness is expected to be in the region of 0.2 micron the technique seemed to offer little hope of accurately measuring the coating thickness.

The second technique was adopted when the first proved unsuccessful. It was decided that measuring the thickness of the coating on single fibres should still give a good representation of the interphase thickness as the coating was not expected to merge with the matrix but remain as a separate phase. It was intended to mount single coated fibres , measure their diameter at given points on a reference grid , and then burn off the coating. The clean fibres would then be remeasured at the same points. The second diameter measured subtracted from the first diameter measured would then give twice the coating thickness. A number of problems were encountered in attempting to perform these measurements. The fibres had to be coated with gold before they were viewed in the SEM to avoid excessive charging up.

Consequently it was not possible to be sure that during the burning off process all the gold coating had been removed along with the acrylic coating. It was also very difficult to ensure that the fibres were being measured at exactly the same point once they were replaced in the SEM after burn off. The final technique of x-ray analysis became known at this point and all further studies using direct measurement were abandoned in its favour.

## 6.2 X-ray analysis technique

A technique to determine the coating thickness of metals on metal substrates ( 56 ) was applied by this author to the case of very thin polymeric coatings on glass fibres. The principles of the technique can be explained in a number of simple steps:

(a) When an electron beam strikes a material one of the results of the interaction is the production of an x-ray from the sample. The x-ray will be characteristic of the element from which it was generated and the intensity of the x-rays produced will be characteristic of the amount of element within the interaction volume of the electron beam. Thus , when an electron beam strikes the coated glass fibre , x-rays will be produced from the interaction volume ( figure 58 ). The only element present in the coating which is not present in the glass is carbon. A typical spectra from the electron probe microanalyser ( EPMA ) is shown in figure 59 for a coated and uncoated fibre. Note the much higher carbon peak intensity for the coated fibre spectra. By monitoring the carbon peak intensity information regarding the coating only can be discerned.

(b) The technique needs a comparison for the measurements of carbon peak intensity from the coated fibre. This is supplied by using a standard of acrylic thick enough that the beam will not be able to penetrate it.

(c) When the energy of the electron beam is very high it will penetrate through the coating and into the fibre ( figure 60 $E_1$ ). As the energy is reduced the penetrates less and less into the glass fibre until at some critical beam energy ( $E_C$ figure 60 ) the beam just penetrates to the depth of the coating and no more. The intensity of the carbon peak from the coating ( $I_C$ ) is compared to the intensity of the carbon peak from the standard ( $I_S$ ) for a number of different beam voltages. At the critical beam voltage $E_C$ the ratio $\frac{I_C}{I_S}$ is equal to one.

For this case the coating is so thin and the elements so light that the actual value of $E_C$ must be derived by extrapolating a plot of intensity ratio against beam voltage. This is because a beam of sufficiently low energy to not penetrate through into the glass cannot be generated by the machine.

(d) Once the critical voltage has been determined by experimentation it can be used in the equations of Sewell and Love ( 56 ) to calculate the penetration depth of the beam into the coating material. This penetration depth then corresponds directly to the coating thickness.

The experimental procedure adopted for making the measurements necessary to determine the critical beam voltage was as follows:

(i) Single glass fibres were extracted from rovings which were either the as received commercially silaned glass only or the as received glass plus the acrylic coating. The fibres were carefully mounted on level metal supports and secured with silver dag. Then the fibres were gold coated to prevent excessive charging under the electron beam. Both fibres were coated at the same time to ensure that the same thickness of gold was applied to both.

(ii) A standard of acrylic material thick in comparison to the coatings , approximately 1 millimetre , was mounted on the same support as the fibres and received the same gold coating treatment.

(iii) The samples were placed in an electron probe microanalyser and the analyser set to monitor the carbon peak intensity. Measurements of intensity were then taken at 12 micron intervals over a 750 micron length of each fibre. These measurements were taken using a beam voltage of 10 KeV , 7 KeV , 4KeV , and 2 KeV. An intensity reading for the standard was also taken at each beam voltage.

## 6.3 Results

The intensities , as determined by the number of counts recorded in a ten second period , are presented in Table 11. It is difficult to determine whether or not any of these points represent a piece of contamination just by viewing the figures in the table. Therefore , the results were plotted out on graphs of position along fibre against measured intensity and examples are given in figures 61 and 62 . Points which were judged to be from regions of contamination are ringed on each graph. The only graph which presented a major problem in determining whether points were from contaminated regions or not was the graph for the coated fibre measured at 10 KeV ( figure 61 ). This graph appears to show two distinct plateaus. Two possible explanations exist for the plateaus. First , they may represent two regions one in which the coating is present , the other in which it is not. Second , they may represent two regions where the coating is present but where a step occurs in the coating thickness. This might occur if the coating was pulled out in one region as the fibre was extracted from the roving. Further investigation of this type of feature is required before any definite conclusions can be reached. For the purposes of the immediate investigation , however , an average value was taken for all the points. In any case , as will be seen , the value at 10 KeV does not have a significant effect on the prediction of the critical beam voltage.

The selected points were averaged and are presented with their standard deviation in Table 12. Also presented in Table 12 are the beam currents recorded during the measurement of

each point. Before true comparisons can be drawn between the readings they must all be normalised to the same beam current. Results normalised to a beam current of $3 \times 10^{-8}$ A are presented in Table 13.

The first point to note from the results is that as expected the intensity from the standard drops off linearly ( figure 63 ) as the beam voltage decreases.

The second point to note is that in general the intensity from the coating drops with decreasing beam voltage. Also the intensity from the coated fibre is greater than the intensity from the uncoated fibre at all voltages except the lowest. If there is truly a thicker layer of polymer on the coated fibre then it is expected that the intensity should be greater than for the uncoated fibre. For the purposes of the analysis only the coated fibre results will be considered from this point on. Obviously this is not an ideal situation and further measurements need to be taken to improve the accuracy of the technique.

To estimate the value of the critical beam voltage $E_C$ it is necessary to calculate the ratio of the coated fibre intensity ($I_C$ ) to the standard intensity ( $I_S$ ) at each beam voltage. The results of these calculations are presented in Table 14. A straight line relationship is obtained for the ratio $\frac{I_S}{I_C}$ and this graph is plotted in figure 64. The equation for the line of best fit through the points is given by:

$$E = 1.219 + 0.258\left(\frac{I_S}{I_C}\right) \qquad \text{.....43}$$

where E is the beam voltage.

The critical beam voltage is determined at $\frac{I_s}{I_c} = 1$ . Substituting this value into 43 gives $E_C$ =

1.48 KeV. This value is used in the equations of Sewell and Love ( 56 ) to predict the coating thickness as follows:

The coating density thickness , $\rho t$ , is given by :

$$\rho t = \rho z(2.68 + 4.4\exp(-0.724U)) \qquad \text{.....44}$$

where $\rho z$ is the mean depth of x-ray generation and U is the ratio $\frac{E_C}{E_x}$. The mean depth of x-ray generation is given by :

$$\rho z = \rho s_m \frac{(0.49269 - 1.0987\mu + 0.78557\mu^2)\ln U}{0.70256 - 1.09865\mu + 1.0046\mu^2 + \ln U} \qquad \text{.....45}$$

where $\mu$ is the backscatter coefficient , and $\rho s_m$ is the electron range. The electron range is given by :

$$\rho s_m = AZ^{-1}(7.87 \times 10^{-6} J^{0.5} E_C^{1.5} + 7.35 \times 10^{-7} E_C^2) \qquad \text{.....46}$$

where A is the mean atomic weight , Z is the mean atomic number , and J is the mean ionisation potential.

For this case the following information is known:

A = 7.2 g , Z = 3.6 , J = 0.0135 Z , $E_C$ = 1.48 KeV ,

Therefore from equation 46 , $\rho s_m = 9.46751 \times 10^{-6}$

For the carbon $K\alpha$ x-ray line , the excitation energy $E_x$ equals 0.282 KeV. Therefore U = 5.248 . $\mu = 0.09$.

thus , from equation 45 , $\rho z = 2.768 \times 10^{-6}$ and from equation 44 $\rho t = 7.689 \times 10^{-6}$.

Given that the density of the acrylic , $\rho$ , equals 1.2 g/cc the thickness of the coating then equals $6.41 \times 10^{-6}$ centimetres , which equals 0.064 micron.

This coating thickness is somewhat lower than the minimum expected thickness of 0.2 micron. However the only reason for expecting a minimum thickness of 0.2 micron was that the manufacturers literature had stated that this was the size of the latex particles. It was therefore decided to measure the size of the particles independently. Latex particles were mounted on a copper grid which had been coated with a polymer film and then a layer of carbon. The grid was suitable for use in a transmission electron microscope. The particles were stained with a uranium salt to give contrast and viewed in the TEM. Figure 65 shows a photograph of a typical selection of latex particles. The size of the particles was measured and the average found to be 0.14 micron.

So , the latex particles are still found to be somewhat larger in diameter than the coating thickness. It is quite possible however that the thickness of the particles could be a good deal less than their measured diameter. Consider figure 66. This figure shows how the surface wetting characteristics of the particle on the substrate will affect the ratio of the diameter to thickness. It is pointless to further examine the latex samples on the grid to determine the degree of flattening of the particle because this will not be the same as for a particle on the glass surface. It is sufficient to realise that the figure for the coating thickness generated from the x-ray measurements is credible in light of the measured particle diameter.

It must be stated again , however , that these results are subject to large variations and that the measurements are taken from a relatively small portion of fibre. Variations could come from a number of sources not least of which is the natural tendancy for carbon to contaminate surfaces in the SEM. Further work might consider the possibility of doping the interphase with a heavy element which would make analysis of the coating thickness less susceptible to contaminants.

# 7 DYNAMIC MECHANICAL ANALYSIS

Dynamic mechanical analysis was used to assess the effect of constraint and thickness on the interphase modulus , and also to investigate the differences between the coated and uncoated fibre composite.

## 7.1 Effect of thickness and constraint on the interphase modulus

### 7.1.1 Introduction

It was thought that the modulus of the compliant interphase material was unlikely to remain at its "bulk" value ( that is thick and unconstrained ) when it was used as a thin constrained layer in the composite system. Techniques for measuring the degree of change were needed. The shear modulus could be measured directly in a Polymer Laboratories dynamic mechanical analysis machine using a shear clamping arrangement. This is discussed in more detail in section 7.1.2. Measurement of the constrained tensile modulus was not as straight forward.

Previous work by Wetton ( 57 ) has shown that the tensile modulus of a polymeric coating on a stiff substrate can be measured using dynamic mechanical analysis. Wetton was more concerned with determining the "bulk" modulus of the coating without having to remove it from the substrate. Wetton found that as the thickness of the coating decreased the modulus increased. This was thought to be due to constraint and Wetton determined a minimum thickness of film that could be measured before constraint significantly affected the modulus. For this project , however , it was this very affect of constraint on modulus which needed to be investigated. In a separate paper ( 58 ) Wetton presented an equation for determining the modulus of a coating on a substrate. The substrate was coated on both sides and was tested in single cantilever bending. The equation was:

$$(kE')_{composite} = E_s' b\left(\frac{t_s}{l}\right)^3 + E_c' b\left(\left(\frac{t_s + 2t_c}{l}\right)^3 - \left(\frac{t_s}{l}\right)^3\right) \qquad .....47$$

where $(kE')_{composite}$ is the measured stiffness of the "composite" ( coating plus substrate ) beam , $E_s'$ and $t_s$ are the substrate modulus and thickness , $E_c'$ and $t_c$ are the coating modulus and thickness , b is the beam width , and l is the mean free length of vibration of the beam ( see figure 67 ).

## 7.1.2 Experimental technique

(a) Tensile modulus

From equation 47 it is obvious that the minimum coating thickness that can be measured by this technique will be a function of the minimum substrate thickness. Therefore , it was important to try to use the thinnest steel substrate that the machine was capable of measuring.

The minimum substrate thickness will be controlled by the lowest stiffness which the dynamic mechanical analyser can measure. For the Polymer Laboratories machine fitted with a power head the lowest measurable stiffness is quoted as 300 N/m ( 59 ). Selecting steel as the substrate material and using equation 48 the minimum thickness for the substrate can be calculated as follows:

$$(kE')_{substrate} = E_s' b\left(\frac{t_s}{l}\right)^3 \qquad .....48$$

$$kE' = 300N/m = E_s b\left(\frac{t_s}{l}\right)^3$$

Now $E_s = 2.1 \times 10^{11}$ and so ,

$$b\left(\frac{t_s}{l}\right)^3 = 1.43 \times 10^{-9} m$$

Using a beam width of 10 mm and a free length of 1 mm to give the stiffest beam possible , gives a minimum substrate thickness of 0.0053 millimetres.

The most readily available material with which to start experimentation was shim steel. The thinnest shim steel available was 0.05 mm. This material was selected as the substrate but a suitable width and free length had then to be determined. Both the aspect ratio of the beam and the overall free length were varied and the modulus of the steel substrate measured ( Table 15 ). The results of Table 15 are plotted in figure 68. It was found that the absolute free length was of more importance than the aspect ratio in measuring an accurate modulus. An accurate value for the steel substrate , 210 GPa , was measured using a geometry which resulted in a beam with the lowest stiffness the machine was capable of measuring. Thus , the geometry selected for subsequent testing was a free length of 9 mm and a beam width of 10 mm. Using these figures in equation 48 predicts a minimum substrate thickness of 0.047 millimetres.

The next stage was to coat pieces of the shim steel with the acrylic polymer. Layers were added one at a time by dipping the steel into the latex and then drying it off with a hot air blower. Samples were prepared which had the following number of layers of acrylic ; 1 , 2 , 4 , 5 , 10 , 20 , 35 , 50. Before use the coated beams were cured for 3 hours at 80 °C. The coating thickness was determined by measuring the total beam thickness , subtracting the substrate thickness , and then dividing by two.

Each coated beam was measured three times , regripping to a constant torque setting each time , to determine the accuracy of each result. This was particularly important for the free

length varied slightly from the intended nine millimetres each time and had to be accurately measured. A frequency of vibration of 1 Hz was used with a peak to peak deflection of 32 micron. All measurements were made at room temperature.

(b) Shear modulus

As stated, the shear modulus of the acrylic was measured in the Polymer Laboratories dynamic mechanical analysis machine using a shear clamping arrangement ( figure 69 ). The acrylic was tested in shear at room temperature and at 1 Hz frequency with a peak to peak deflection of 32 micron. Time constraints led to initial studies only being carried out. These initial studies determined the modulus for three thicknesses of acrylic ; 0.05 mm , 0.36 mm , and 0.63 mm.

### 7.1.3 Results

(a) Tensile modulus

The measured results were in terms of the beam stiffness and are presented in Table 16. The coating modulus for each of the measurements was then calculated according to equation 47 and the results are presented in Table 17. The log values for coating thickness and modulus are plotted in figure 70. Also plotted on figure 70 is the thick, unconstrained value of modulus for the acrylic polymer measured by dynamic mechanical analysis.

The values of modulus calculated for the interphase by this technique should not be considered as absolute , particularly in view of the variations noted previously for the substrate modulus. However , the results of this analysis show quite clearly that the modulus of the acrylic increases significantly as the thickness decreases. The modulus value at 55 micron is already

comparable with the modulus of the vinyl ester resin. It is not clear from the curve if a maximum has been reached for the modulus of the acrylic or whether significant increases will occur as the thickness reduces further to the sub micron levels present in the composite.

It is unlikely that values of coating modulus could be determined at thicknesses less than those already measured. This is because the measured stiffness for the 55 micron coating thickness ( Table 16 ) is very close to the stiffness value measured for the substrate only , although it is shown by Student "t" test to still be significantly different. Once these stiffness measurements become indistinguishable from one another the coating modulus can no longer be calculated.

(b) Shear modulus

The results of the shear studies are presented in Table 18 and plotted in figure 70. Again , the values should not be regarded as absolute particularly as the geometry was not pre-determined for a material of known and similar modulus. These initial studies show , however , that the shear modulus is not affected by reduction in thickness in the same way as tensile modulus. In fact , far from there being an increase in modulus as the thickness decreases the modulus actually decreases as well. This different response to shear and tensile forces , particularly when very thin and constrained , is reflected by the mechanical properties measured in section 4.

## 7.2 Analysis of coated and uncoated fibre composites

### 7.2.1 Introduction

It was decided to investigate the dynamic response of the coated fibre and uncoated fibre composites over a range of temperature. This was for two main reasons. First and foremost was to ensure that the inclusion of a compliant interphase did not significantly affect the

stiffness of the composite in the predicted temperature range of use ( -40°C to +130°C ). Second , previous studies ( 25 , 60 ) have shown that the presence of the interphase can be confirmed using dynamic mechanical analysis.

A sample of each type of composite was cut from the composite plate such that three point bending transverse to the fibres could be performed. Gerard ( 25 ) found that the interphase could only be detected using very low frequencies of vibration ( 0.03 Hz ). The Polymer Laboratories machine allows the storage modulus , loss modulus and damping ( tan δ ) to be determined at a range of frequencies while scanning from low to high temperature. For this project the temperature was scanned from -50°C to +150°C at frequencies of 0.3 Hz , 1 Hz , 3 Hz , 10 Hz , and 30 Hz.

### 7.2.2 Results

Figures 71 - 74 show the measurements of storage modulus and tan δ made for the coated and uncoated fibre composites over the temperature range - 50 °C to +150 °C. There is no detectable difference between either of the materials. This means that whilst the technique was not able to show the presence of the interphase material , it was able to confirm that the interphase material does not reduce the transverse modulus over the temperature range of interest.

The value of the storage modulus at room temperature should correspond closely to the transverse bending modulus measured in the mechanical testing section. The value measured for the storage modulus was 14 GPa while the value measured by mechanical testing was approximately 15 GPa. Although the result for the storage modulus must be treated with some degree of scepticism following the results on measurement of the modulus of steel the dynamic and statically measured results appear to agree well. For further discussion of transverse modulus see section 8.2.

# 8 DISCUSSION

## 8.1 Predictions of strain magnification models

### 8.1.1 Predictions based on original parameters

The results of the initial predictions of the extended Kies model using values of t , r etc. listed in section 2.3 , are presented in figures 18 , 19 and 20. They show how variations of 50% either side of the estimated value for the parameters of fibre volume fraction , fibre radius , interphase thickness , fibre modulus , matrix modulus and interphase modulus affect the strain magnification factors.

The tensile model ( figures 18 and 19 ) predicts variations in the strain magnification factors which are as one would intuitively expect except for the fibre volume fraction. This parameter is shown to have little effect on the predicted strain magnification factor even when varied over a significantly large range ( 0.25 to 0.75 ). The basic Kies model shows marked dependence of the strain magnification factor on fibre volume fraction. This discrepancy prompted a critical examination of the extended model.Refering to equation 12 , the interphase thickness , t , was set at zero. The strain magnification then reduced to the Kies model , as required. However , further investigation is required into why the introduction of the interphase so drastically reduces the effect of fibre volume fraction on the predicted strain magnification factors.

Consider equation 12 in more detail. Substituting the equation for s on page 23 on rearranging gives :

$$\frac{\varepsilon_r}{\varepsilon_c} = \frac{r\left(\frac{\pi}{V_f}\right)^{0.5}}{r\left(\frac{\pi}{V_f}\right)^{0.5} + 2r\left(\frac{E_r}{E_g} - 1\right) + 2t\left(\frac{E_r}{E_i} - 1\right)} \qquad \text{.....49}$$

To consider the effect of fibre volume fraction and interphase properties only , the original values for all the other parameters can now be substituted into the equation. This gives :

$$\frac{\varepsilon_r}{\varepsilon_c} = \frac{6\left(\frac{\pi}{V_f}\right)^{0.5}}{6\left(\frac{\pi}{V_f}\right)^{0.5} - 11.52 + 0.4\left(\frac{E_r}{E_i} - 1\right)} \qquad .....50$$

For the value of $\frac{E_r}{E_i}$ first assumed , i.e. 30 , this reduces to :

$$\frac{\varepsilon_r}{\varepsilon_c} = \frac{6\left(\frac{\pi}{V_f}\right)^{0.5}}{6\left(\frac{\pi}{V_f}\right)^{0.5} + 0.07}$$

The limits of fibre volume fraction for a square array of fibres are zero and $\frac{\pi}{4}$. The corresponding values for the strain magnification factor in the resin are 1 and 12/12.07 , which is approximately 1. Thus the effect of fibre volume fraction is shown to be negligible over its full range.

The controlling part of equation 49 then is the sum of the second and third terms of the denominator , that is ,

$$2r\left(\frac{E_r}{E_g} - 1\right) + 2t\left(\frac{E_r}{E_i} - 1\right)$$

For small values of $E_i$ , this sun approaches zero , such that $\frac{\varepsilon_r}{\varepsilon_c}$ is independent of $V_f$. As $E_i$ tends to $E_r$ the final term tends to zero making the sum a large negative value and the equation overall reverts to the basic Kies model in which fibre volume fraction effects are significant.

In contrast the shear model shows marked dependence of strain magnification on fibre volume fraction. This is in agreement with the original Kies model. The reason for the agreement lies in the geometry of the model (figure 13). At no point is there a complete shear path in interphase material alone. The fact that shear occurs in , at the least , a combined block of matrix and interphase , means that the high shear modulus of the matrix will dominate.

### 8.1.2 Predictions using measured parameters

(i) Predictions of tensile model

It was stated earlier that for the theoretical models to produce accurate values the inputs must be truly representative of the composite. The input values were determined as accurately as possible using the techniques described in the previous sections. The absolute values so determined need confirmation from further analysis , but are nevertheless more realistic than the original estimated figures. A summary of the measured values is presented below:

Fibre volume fraction = 0.6

Fibre radius = 8.5 micron ±0.85 micron

Interphase thickness = 0.065 micron ± 0.005 micron

Fibre tensile modulus = 76 GPa

Matrix tensile modulus = 3.75 GPa

Interphase tensile modulus ( constrained ) = 1.27 GPa

Using these results strain magnification factors were calculated by computer program ( Appendix A ) , first with no interphase and then with an interphase having the properties

stated above. In tension the strain magnification factor in the resin ( tsmfr ) dropped from 5.91 to 5.69 on introducing the interphase. The corresponding tensile strain magnification factor in the interphase ( tsmfi ) was 16.81 .

Results were also calculated for the case where the fibres are practically touching ( s = 0.21 micron as against s = 4.77 micron for the first case ). This was done by assuming a fibre volume fraction of 0.77. In tension , tsmfr dropped from 17.03 to 15.13 when using the interphase , with tsmfi at 44.67.

Initial estimates for the reduction in the tensile strain magnification factor in the resin ( refer to section 2.3.1 ) showed that the introduction of an interphase could remove the magnification of strain completely. This relied on the interphase retaining its low modulus when thin and constrained. However , it has been shown that this does not occur. The modulus increases significantly under constraint. The tensile model reflects this change in the properties of the interphase material , and predicts a much less significant reduction in the strain magnification in the resin , as $\frac{E_r}{E_i}$ tends towards 1 in equation 50. Similarly the fibre volume fraction has a significant effect on the level of the strain magnification factor.

The model shows then that to significantly improve the transverse tensile properties of the composite , an interphase material must be used which does not lose its compliancy as it becomes thin and constrained.

(ii) Predictions of the shear model

For calculations of the shear strain magnification factors the geometrical values are the same as for (i) above but the modulus of each phase is different. The shear moduli were calculated using the well known relation:

$$G = \frac{E}{2(1+\nu)} \qquad \text{.....51}$$

where ν is the Poisson's ratio. Poisson's ratio for the glass and resin are 0.24 and 0.3 respectively. This technique was not used to calculate the shear modulus of the interphase because it was determined in section 7 by DMA and differs greatly from the relation given in equation 51 due to constraint. To summarise:

Fibre shear modulus = 30.7 GPa

Matrix shear modulus = 1.44 GPa

Interphase shear modulus = 0.00063 GPa

Using a fibre volume fraction of 0.6 , the shear strain magnification factor dropped from 5.18 to 5.07 on introducing an interphase. When the fibre volume fraction was increased to 0.77 the drop on using an interphase was from 12.89 to 12.13.

These results agree with the earlier ones ( refer to section 2.3.2 ) in that the properties of the interphase have little effect on the strain magnification factor. As discussed previously this is because no shear path exists entirely within the interphase material.

The mechanical test results for interlaminar and intralaminar shear strength indicate an improvement in the laminate property on introducing an interphase. This appears at first to be at odds with the shear model , which predicts no improvement on introducing an interphase. However , detailed consideration of the mode of shear in each case can explain the difference. This consideration is dealt with in section 8.2.2.

## 8.2 Mechanical properties of laminates : measured and predicted

### 8.2.1 Transverse modulus

The simple Reuss model for prediction of transverse tensile modulus is ,

$$E = \frac{E_m E_f}{E_f V_m + E_m V_f}$$

Substituting the measured values of fibre volume fraction and matrix modulus ( 0.6 and 3.75 GPa respectively ) , and using 76 GPa for fibre modulus the model predicts a transverse tensile modulus for the composite of 8.7 GPa. Measured values were considerably higher than this. In transverse tension the value was approximately 17.25 GPa , in transverse bending the value was 15 GPa as measured in the Instron and 14 GPa as measured in DMTA. These values were all determined independently of each other. The results are supported by the work of Wells ( 61 ). Wells considered the transverse tensile modulus for a range of composites with wide variations in matrix moduli. Composite systems comparable to those used in this project showed a transverse tensile modulus of approximately 20 GPa. Wells compared his results with a large range of more complex models for the prediction of composite transverse modulus and found that all of the models predicted a low value when the resin modulus was high ( > 1 GPa ). These results are further confirmation of the results observed in this project.

### 8.2.2 Shear strength

As discussed earlier the extended Kies model predicts no improvements in shear properties from the use of a low modulus interphase. Mechanical tests, however , showed a marked improvement in the interlaminar and intralaminar shear strengths. This can be understood by reference to figure 75. The values of shear strength measured by the short beam bend test

and the 15° off axis test are the "longitudinal" interlaminar shear strength ( $\tau_{21}$ ) and the "longitudinal" intralaminar shear strength ( $\tau_{31}$ ). In these planes there exists an uninterrupted path of interphase material in which shear can occur. This allows the low modulus interphase material to play a dominant role and improve the shear strength. However , the shear planes dealt with in the model are "transverse" interlaminar shear ( $\tau_{12}$ ) and "transverse" intralaminar shear ( $\tau_{13}$ ). Shear along an uninterrupted path of interphase material is not possible in these planes and so no shear strength improvement would be expected. Mechanical shear testing in these planes should confirm these predictions.

## 8.3 Elastic constraints and their effects

### 8.3.1 Constraint effects in tension

Much has been said about constraint and the suppositions that constraint is responsible for an increase in the tensile modulus of the interphase. The concept of constraint , and the reason for its being deleterious in tension but not shear , need further discussion.

In the context of this project constraint refers to the constraint of the Poisson's contractions that would normally occur in a material subjected to a tensile stress. The constraint occurs at the surface of a compliant material when it is bonded to a stiffer material. If the compliant material is relatively thick then these surface constraints do not significantly affect its overall response. However , if the material is thin then the whole material is constrained , leading to a triaxial stress state rather than a simple uniaxial stress state. Under these circumstances the modulus of the material changes from the tensile modulus , E , to the bulk modulus , K. These moduli are related by the equation :

$$K = \frac{E}{3(1-2\nu)} \qquad \text{.....52}$$

For any material with a Poisson's ratio above 0.333 the bulk modulus will be higher than the tensile modulus. In fact , as the Poisson's ratio approaches 0.5 the value of the bulk modulus approaches infinity. Thus , for the "rubbery" interphase material one might expect significant increases in the apparent modulus because for rubbers the Poisson's ratio is generally considered to be 0.5 , or just less than 0.5.

The values from section 7 of constrained , or bulk modulus ( $K = 1.27 \times 10^9$ Pa ) , and unconstrained , or tensile modulus ( $E = 2.88 \times 10^7$ Pa ) , can be used in equation 52 to predict the Poisson's ratio for the acrylic interphase material. The calculated value is 0.496.

It also follows , from equation 52 , that for materials with a Poisson's ratio of less than 0.333 , such as the vinyl ester resin ( $\nu = 0.3$ ) , the bulk modulus will be slightly less than the tensile modulus. Therefore , as the resin becomes thin and constrained , that is as its tensile modulus tends towards its bulk modulus , the apparent value of the modulus will not change significantly. This is because the tensile and bulk moduli of the resin are practically the same , whereas for the acrylic they differ by orders of magnitude. Thus , to use the unconstrained value of tensile modulus in the model , where the resin is actually thin and constrained , should not have led to any significant errors.

### 8.3.2 Constraint effects in shear

If a material is subject to a shear force Poisson's contractions do not arise. Therefore there can be no constraint effects even when the material is thin and bonded to stiff adherends.

The unconstrained values for tensile and shear moduli should be related by equation 51. Using the value for tensile modulus measured for the acrylic alone to represent the unconstrained , infinite thickness ( $E = 2.88 \times 10^7$ Pa ) and using the Poisson's ratio just calculated

( 0.496 ) the shear modulus can be calculated from equation 51 as G = $9.63 \times 10^6$ Pa. The value for shear modulus determined by DMA was $6.89 \times 10^6$ Pa. These values compare very well.

### 8.3.3 Conclusion

Evidence for the effect of constraint on mechanical properties is significant. Results presented in Table 9 show that introduction of an interphase improves properties only when the applied stress is a shear stress or some combination of stresses which include shear stress. Under pure transverse tensile stresses no improvement is observed. This author believes that this improved response to shear stress is a direct result of the fact that no constraint exists in shear. Analysis of the fracture surfaces ( figures 49 to 53 ) tends to support this conclusion since a brittle , or constrained , mode of failure occurred in tension. In shear the failure mode was one which exhibited greater deformation due to the lack of constraint.

In conclusion then it has been shown that the inclusion of a compliant material at the interphase can improve the off-axis properties of a unidirectional glass fibre reinforced thermoset. The geometry of the interphase , and the properties of the interphase material , need to be optimised in order to obtain the maximum benefit from this technique.

## 8.4 Recommendations for further work

### 8.4.1 Immediate work

Recommendations made in this section refer to work which needs to be carried out on the interphase composite system described in this thesis. Five main areas have been identified.

It was proposed in section 8.2 that the resin tensile modulus would not be significantly different when the material was thin and constrained. This proposal needs to be confirmed using the same techniques as were used for the acrylic polymer in section 7.

The x-ray analysis technique described in section 6 relies heavily on the results obtained at a beam voltage of 2 keV. Further measurements need to be made at voltages around this figure to determine the thickness of the coating with greater accuracy. Suggested beam voltages are 1.5 keV , 2 keV , 2.5 keV , and 3 keV. In conjunction with this work further analysis of the latex particle size would be desirable. The possibility of doping the interphase material to allow more accurate identification and consequent improvement in the accuracy of the measured thickness needs to be developed. It was proposed in section 6.3 that the diameter and thickness of the latex particle would not be the same because as the particle touched the surface it would flatten to some degree. Studies of this degree of flattening against a silaned glass surface are of interest. Also of interest is how the particles subsequently behave when subjected to heat during cure.

Determination of the inter-fibre spacing in section 5.1 proved to be problematical for two reasons. First , the fibres were apparently touching at least one other fibre and resolution of this spacing was only possible in the SEM which proved very time consuming. Second , one could not define one direction in which to measure the spacing between fibres because they lay in a random array rather than a well defined square or hexagonal array. Further work is required in two areas then. First , it is necessary to define the spacing which must be measured to provide an appropriate input to the model. Second , these spacings must be determined accurately by measurements in the SEM.

It was discussed in section 5.2 that a ring observed around the fibres in cross sections of the laminates ( figures 56 and 57 ) might have been either damage caused to the glass during etching or the interphase material itself. The first step in determining the origins of the ring

would be to examine cross sections of laminates which had not been etched. If the rings were still observed then the evidence for the ring being the interphase material would be much stronger. Direct observation of the thickness of the interphase would be highly desirable.

Further characterisation of the mechanical response of the two composites is required. This would mainly take the form of repeating mechanical tests to improve the level of confidence in them. Confirmation of the predicted lack of improvement in "transverse" shear strengths should be confirmed. It might also be possible to use strain gauges on the 15° off axis test to give the shear strain to failure and the shear modulus. Of particular interest would be the assessment of off axis fatigue properties. Based on previous work by Lavengood ( 24 ) this might best be achieved by measuring the torsional fatigue life of the two materials.

### 8.4.2 Long term work

This section describes the work which needs to be done over a much longer time period to establish an optimum arrangement for the interphase composite. Four main areas of work are envisaged.

First and foremost is the need to evaluate a range of interphase materials and geometries. In particular, materials which have a low modulus and high strain to failure but retain a Poisson's ratio of around 0.33 would be highly desirable. An interphase utilising such a material should not be significantly affected by constraint when subjected to tensile forces. Therefore improvements in both tension and shear properties might be expected.

To complement the optimisation of the interphase , improved techniques for measuring the interphase geometry and modulus would be needed. The techniques might take the form of improvements in the x-ray analysis and dynamic mechanical analysis. Alternatively , new methods such as acoustic attenuation might be developed.

The chemistry of the system is a particularly important area of research for the future. In particular the chemical reactions and bonding occurring between the three phases must be studied to assess their effect on the overall mechanical performance.

Finally , the theoretical models which have been developed to date are simplistic in nature. The models were intended to identify in the first instance which parameters of the composite system were important. The models succeeded in meeting these initial requirements. However , to optimise the interphase material a more refined model will be needed. In particular this model will need to reflect the effect of constraint on the interphase and the corresponding effect on the mechanical performance. The model must also consider fibre fibre interaction. A good understanding of the practical problems which occur in real composites will be invaluable in developing this new theoretical model.

# 9 CONCLUSIONS

1. The aim of the project was to improve the transverse mechanical properties of unidirectional glass fibre reinforced plastic composites. The method selected was to use a compliant fibre coating ( interphase ).

2. A theoretical model was developed which identified the parameters of the system and the importance of determining their in-situ values.

3. In-situ coating thickness was determined using a newly developed x-ray absorption technique.

4. The tensile modulus of the interphase material was shown to increase by orders of magnitude from its bulk value.

5. In-situ shear modulus did not increase because Poisson's contractions do not occur in shear.

6. Apparatus was designed and manufactured for the production of coated fibre composites.

7. In agreement with theory the transverse tensile properties of the composites were not greatly improved by the use of an interphase.

8. In shear in a plane parallel to the fibre axis , transverse mechanical properties showed a significant improvement in the presence of an interphase.

9. The fracture surface appearance of laminates with an interphase corroborated the findings of mechanical testing as to the difference between shear and tensile fracture behaviour.

10. In summary , the interphase material selected for this project resulted in significant improvements in shear dominated properties. No degradation of other mechanical properties was observed.

## 10 Acknowledgements

I would like to thank Mr. M.G. Phillips for his help and guidance , particularly in preparing this thesis. My thanks also go to G.K.N. Technology for their financial and technical support.

## 11 References

1. "Developments in improved crack resistance of thermoset resins and composites" , EH Rowe , 34th Annual Technical Conference (1979) , Reinforced Plastics/Composites Institute , The Society of the Plastics Industry , Section 23-b.

2. "Effects of rubber additions on the fracture toughness of a polyester resin " , PD Tetlow , JF Mandell , FJ McGarry , 34th Annual Technical Conference (1979) , Reinforced Plastics/Composites Institute , The Society of the Plastics Industry , Section 23-F.

3. "Toughened epoxy resins for filament winding" , ZN Sanjana , JH Testa , 30 th National SAMPE Symposium , March 19-21 , 1985 , pp. 1221-1230.

4. "Rubber modified matrices" , RY Ting , In: The role of the polymeric matrix in the processing and structural properties of composite materials , Eds. JC Seferis , L Nicolais , pp.171-188.

5. "Constituent property-composite property relationships in thermoset polymers" , J Diamant , RJ Moulton , In: Tough composite materials , Ed. LF Vosteen et Al , (1984) , NASA-CP-2334 , pp. 159-172.

6. "The effect of cross-link density on the toughening mechanisms of elastomer modified epoxies" , RA Pearson , AE Yee , Ibid , pp. 173-194.

7. "Morphology and dynamic mechanical properties of diglycidylether of bisphenol-A toughened with CTBN" , S Hong et Al , Ibid , pp. 285-294.

8. "The use of urethane rubber/epoxide resin as matrix materials for glass and carbon fibre composites" , H Wells , NL Hancox , 32nd Annual Technical Conference (1977) , Reinforced Plasics/Composites Institute , The society of the Plastics Industry , Section 9C.

9. "Tough resin carbon fibre composites" , T Muraki , A Takeo , M Hirata , SAMPE (European chapter) International Conference (1986) , pp. 163-176.

10. "ETP : Elastomer-toughened polyesters" , J Korb , 39th Annual Technical Conference (1984) , Reinforced Plastics/Composites Institute , The society of the Plastics Industry , Section 8F.

11. Unpublished internal progress report , K Ellis , University of Bath (August 1988).

12. "Toughened interleafed composites" , RE Evans , JE Masters , JL Courter , Advanced Composites Conference , Dearborn , Michigan (1985) pp.249-255.

13. "An improved 270 F performance interleaf system having extremely high impact performance" , KR Hirschbuehler , 30th National SAMPE Symposium (1985) pp. 1335-1345.

14. "Effect of selective adhesive interleaving on interlaminar fracture toughness of graphite/epoxy composite laminates" , O Ishai , H Rosenthal , N Sela , E Drukker , Composites , 19 ,1 , (1988) , pp. 49-54.

15. "Improved toughness of carbon fibre composites via the use of thermoplastic interplies" , B Carroll , 33rd International SAMPE Conference (1988).

16. Private communication , J Giddings , GKN Technology.

17. Unpublished Final Year Project Report , A Sollis (1988) , School of Materials Science University of Bath.

18. Strength of Materials , GH Ryder , (1983) , The Macmillan Press Ltd. , London.

19. JN Goodier , (1933) , Jnl. Appl. Mech. , Trans. ASME , APM-55-7 , 39.

20. "Some basic problems of the mathematical theory of elasticity" , Muskhelishvili , (1963) , P.Noordhoff Ltd. , Groningen , The Netherlands.

21. "Myths and mechanisms : the interface" , JL Kardos , (1984) , Chemtech , 14 , 7 , pp. 430-434.

22. "Elastic properties of fiber-reinforced composites modified with an interlayer" , MT Aronhime , G Marom , (1987) , Unpublished research report submitted to Pioneering Research Laboratory , Du Pont , Wilmington , Delawre.

23. "The use of ductile innerlayers in glass fibre reinforced epoxies" , LD Tryson , JL Kardos , 36th Annual Technical Conference , Reinforced Plastics/Composites Institute , The Society of the Plastics Industry , Section 2E.

24. "The effects of thick innerlayers on the mechanical performance of fibre reinforced composites" , RE Lavengood , MJ Michno Jr. , (1975) , Proc. Div. Tech. Conf. , Engrg. Props. And Structure Div. , Society Plastics Engineers , p. 127.

25. "Characterisation and role of an elastomeric interphase on carbon fibres reinforcing an epoxy matrix" , JF Gerard , (1988) , Polymer Engineering and Science , 28 , 9 , pp. 568-577.

26. "Application of ductile polymeric coatings onto graphite fibres" , JP Bell , J Chang , HW Rhee , R Joseph , (1987) , Polymer Composites , 8 , 1 , pp.46-52.

27. "A review of recent progress in the studies of molecular and microstructure of coupling agents and their functions in composites , coatings and adhesive joints" , H Ishida , (1984) , Polymer Composites , 5 , 2 , pp. 101-123.

28. "The effects of interlayers on the transverse stresses in fibre composites" , RGC Arridge , (1975) , Polymer Engineering and Science , 15 , 10 , pp. 757-760.

29. "Stress concentrations and transverse modes of failure in composites with a soft fibre-matrix interlayer" , G Marom , RGC Arridge , Materials Science and Engineering , 23 , pp. 23-32.

30. "Tailoring the interface in graphite reinforced polycarbonate" , JL Kardos , FS Cheng , TL Tolbert , (1973) , Polymer engineering and Science , 13 , 6 , pp. 455-461.

31. "The role of fibrous reinforcements well bonded or partially bonded on the transverse strength of composite materials" , J Tirosh , E Katz , G Ligschuetz , AS Tetelman , (1979) , Engineering Fracture Mechanics , 72 , pp. 267-277.

32. "The effect of the interface/interphase on fiber composite properties" , MR Piggott , (1987) , Polymer Composites , 8 , 5 , pp. 291-297.

33. "Adhesion efficiency between phases in fibre reinforced polymers by means of the concept of boundary interphase" , GC Papanicolaou , PS Theocaris , GD Spathis , (1980) , Colloid and Polymer Science , 258 , pp. 1231-1237.

34. "A theoretical study on the effect of the interface on composite toughness" , LJ Broutman , BD Agarwal , (1973) , 28th Annual Technical Conference , Reinforced Plastics/Composites Institute , The Society of the Plastics Industry , Section 5B.

35. "Stress concentration around holes" , GN Savin , (1961) , Pergamon Press.

36. "Maximum strains in the resin of fibre glass composites" , JA Kies , (1962) , U.S. Naval Research Laboratory Report NRL 5752.

37. "An introduction to composite materials" , D Hull , (1981) , Cambridge Solid State Science Series , Cambridge University Press , Cambridge.

38. "Electrochemical poymerisation and deposition on carbon fibres" , RV Subramanian , (1980) , Pure and Applied Chemistry , 52 pp. 1929-1937.

39. "Electrodeposition of a polymer interphase in carbon-fiber composites" , RV Subramanian , AS Castro , (1986) , Polymer Composites , 7 , 4 .

40. "Interfacial aspects of polymer coating by electropolymerisation" , RV Subramanian , JJ Jakubowski , FD Williams , (1978) , J. Adhesion , 9 , pp. 185-195.

41. "Plasma grafting of allylamine onto glass fibres" , V Krishnamurthy , IL Kamel , (1988) , 33rd International SAMPE Symposium , pp. 560-570.

42. "Impact resistance of rubber modified carbon fiber composite" , J Kawamoto , FJ McGarry , JF Mandell , Unpublished report, M.I.T.

43. "Preparation and properties of thick interlayer composites" , DG Peiffer , LE Nielsen , (1979) , Journal of Applied Polymer Science , 23 , pp.2253-2264.

44. British standard , BS 2782 (341A)

45. "Comparing performance of unidirectional composites" , GM Newaz , (1984) , Materials Engineering , pp. 21-24.

46. "Ten degrees off axis test for shear properties in fibre composites" , CC Chamis , JH Sinclair , (1977) , Exp. Mech. 17 , 9 , pp.339-346.

47. "Role of fibre matrix interface in carbon fibre-epoxy composite impact toughness" , L Ying , (1983) , 38th Annual Technical Conference , Reinforced Plastics/Composites Institute , The Society of the Plastics Industry ,Section 12F.

48. "Introduction to polymers" , RJ Young , (1981) , Chapman and Hall , London.

49. "Improvements in the transverse properties of composites. Part 1. Fracture surface energy and mechanism of transverse fracture in glass fibre composites" , G Marom , EFT White , (1972) , Journal of Materials Science , 7 , pp. 1299-1307.

50. "Technical note. Some observations on transverse fracture energies of unidirectional composites" , G Marom , I Engelberg , (1976) , Fibre Science and Technology , 9 , pp.63-67.

51. "Influence of matrix material on flexural fatigue performance of unidirectional composites" , GM Newaz , (1985) , Composites Science and Technology , 24 , pp. 199-214.

52. "The effect of the fibre matrix interface on the flexural fatigue performance of unidirectional fiberglass composites" , GC Shih , LJ Ebert , (1987) , Composites Science and Technology , 28 , pp. 137-161.

53. "A quantitative assessment of debonding in unidirectional composites under long-term loading" , GM Newaz , (1985) , Journal of Reinforced Plastics and Composites , 4 , pp. 354-364.

54. "Flexural fatigue properties of unidirectional G.R.P. In the transverse direction" , BD Agarwal , SK Joneja , (1979) , Composites , pp. 28-30.

55. "CRAG test methods for the measurement of the engineering properties of fibre reinforced plastics" , ED. PT Curtis , (1988) , RAE Technical Report 88012.

56. "X-ray studies related to coating thickness measurements" , DA Sewell , ID Hall , G Love , JP Partridge , VD Scott , (1984) , Journal de Physique, 45 , pp. 33-36.

57. "Measurements of properties of coatings of the thickness range 20 microns to 200 A" , RE Wetton , MR Stone , GE Pratt , (1986) , NATAS Conference , San Fransico , Paper 2.

58. "Dynamic mechanical thermal analysis of polymers and related systems" , RE Wetton , (1986) , In : Developments in polymer characterisation , Applied Science Publishers.

59. Polymer Laboratories DMTA II Operator's Manual , Polymer Laboratories , Loughborough , England.

60. "Modification of the dynamic damping behaviour of epoxy/glass fiber composites via fiber coating with functional latices" , B Schlund , M Lambla , (1985) , Polymer Composites , 6 , 4 ,pp. 272-281.

61. "The transverse mechanical behaviour of glass fibre reinforced plastics" , GM Wells , (1987) , PhD thesis , School of Materials Science , University of Bath.

APPENDIX A

(1) TENSILE MODEL

```
GOSUB Assign1
GOSUB Input1
GOSUB Input2
GOSUB Display1
GOSUB Append1
STOP
END

Assign1:
V$(1)="V  "
V$(2)="T  "
V$(3)="R  "
V$(4)="Ef "
V$(5)="Em "
V$(6)="Ei "
RETURN

Input1:
CLS
LOCATE 3,30:PRINT"INPUT DATA"
LOCATE 4,30:PRINT"=========="
LOCATE 6,10:INPUT"VARIABLE 1 (V) ";V(1)
LOCATE 7,10:INPUT"VARIABLE 2 (T) ";V(2)
LOCATE 8,10:INPUT"VARIABLE 3 (R)";V(3)
LOCATE 9,10:INPUT"VARIABLE 4 (Ef)";V(4)
LOCATE 10,10:INPUT"VARIABLE 5 (Em);V(5)
LOCATE 11,10:INPUT"VARIABLE 6 (Ei)";V(6)
RETURN

INPUT2:
PRINT:PRINT:INPUT"       GIVE VARIABLE NO. TO VARY   ";NUMBER%
PRINT:    INPUT"       GIVE RANGE LIMITS (MIN,MAX) ";MIN,MAX
RETURN

DISPLAY1:
CLS
LOCATE 5,30:PRINT"CALCULATED DATA"
LOCATE 6,30:PRINT"==============="
LOCATE 8,5:PRINT V$ (NUMBER%)
LOCATE 8,20:PRINT"SMFI"
LOOCATE 8,37:PRINT"SMFR"
LOCATE 8,55:PRINT"S"
LOCATE 8,65:PRINT"Ect"
LOCNO%=10
RANGESTEP=((MAX-MIN)/10)
FOR N=MIN TO (MAX+MAX/1000) STEP RANGESTEP
V(NUMBER%)=N
INCR LOCNO%
S=V(3)*(((3.14159/V(1)^0.5)-2)-2*V(2)
SMFI=(2*V(3)+2*V(2)+S)/(2*V(2)+2*V(3)*(V(6)/V(4)+S*(V(6)/V(5)))
SMFR=(2*V(3)+2*V(2)+S)/(S+2*V(3)*V(5)/V(4))+2*V(2)*(V(5)/V(6)))
VI=((V(2)*(2*V(3)+V(2)))/(((V(3)^2)/V(1))-(V(3)^2)))*(1-V(1))
VM=1-(VI+V(1))
```

```
X=(V(1)/V(4))+(VM/V(5))+(VI/V(6))
ER=1/X
ECT=ER+(0.2*(EV-ER))

LOCATE LOCNO%,2:PRINT USING "$$.$$$$$"; N
LOCATE LOCNO%,18:PRINT USING "$$.$$$$$"; SMFR
LOCATE LOCNO%,36:PRINT USING "$$.$$$$$"; SMFI
LOCATE LOCNO%,54:PRINT USING "$$.$$$$$"; S
LOCATE LOCNO%,65:PRINT USING "$$.$$$$$"; Ect
NEXT N
RETURN

APPEND1:
PRINT:PRINT
INPUT"      GIVE FILENAME "FILENAME$

OPEN FILENAMES$ FOR APPEND AS $1
RANGESTEP=((MAX-MIN)/10)
FOR N=MIN TO (MAX+MAX/1000) STEP RANGESTEP
V(NUMBER%)=N
INCR LOCNO%
S=V(3)*(((3.14159/V(1)^0.5)-2)-2*V(2)
SMFI=(2*V(3)+2*V(2)+S)/(2*V(2)+2*V(3)*(V(6)/V(4)+S*(V(6)/V(5)))
SMFR=(2*V(3)+2*V(2)+S)/(S+2*V(3)*V(5)/V(4))+2*V(2)*(V(5)/V(6)))
VI=((V(2)*(2*V(3)+V(2)))/(((V(3)^2)/V(1))-(V(3)^2)))*(1-V(1))
VM=1-(VI+V(1))
X=(V(1)/V(4))+(VM/V(5))+(VI/V(6))
ER=1/X
ECT=ER+(0.2*(EV-ER))

WRITE $1,N,SMFR,SMFI,S,Ect
NEXT N
CLOSE
RETURN
```

(2) SHEAR MODEL

```
GOSUB Assign1
GOSUB Input1
GOSUB Input2
GOSUB Display1
GOSUB Append1
STOP
END

Assign1:
V$(1)="V  "
V$(2)="T  "
V$(3)="R  "
V$(4)="Gf "
V$(5)="Gm "
V$(6)="Gi "
RETURN
```

```
Input1:
CLS
LOCATE 3,30:PRINT"INPUT DATA"
LOCATE 4,30:PRINT"==========="
LOCATE 6,10:INPUT"VARIABLE 1 (V) ";V(1)
LOCATE 7,10:INPUT"VARIABLE 2 (T) ";V(2)
LOCATE 8,10:INPUT"VARIABLE 3 (R)";V(3)
LOCATE 9,10:INPUT"VARIABLE 4 (Gf)";V(4)
LOCATE 10,10:INPUT"VARIABLE 5 (Gm);V(5)
LOCATE 11,10:INPUT"VARIABLE 6 (Gi)";V(6)
RETURN

INPUT2:
PRINT:PRINT:INPUT"       GIVE VARIABLE NO. TO VARY   ";NUMBER%
PRINT:    INPUT"       GIVE RANGE LIMITS (MIN,MAX) ";MIN,MAX
RETURN

DISPLAY1:
CLS
LOCATE 5,30:PRINT"CALCULATED DATA"
LOCATE 6,30:PRINT"================"
LOCATE 8,5:PRINT V$ (NUMBER%)
LOCATE 8,20:PRINT"S"
LOOCATE 8,37:PRINT"SSMFR"
LOCATE 8,55:PRINT"I"
LOCATE 8,65:PRINT"K"
LOCNO%=10
RANGESTEP=((MAX-MIN)/10)
FOR N=MIN TO (MAX+MAX/1000) STEP RANGESTEP
V(NUMBER%)=N
INCR LOCNO%

S=(V(3)*(((3.14159/V(1))^0.5)-2))-(2*V(2))
Q=O
FOR P=O TO 1.5707963 STEP 0.15707963
XG=2*V(3)*COS(P)
D=(V(3)*SIN(P))/(V(3)+V(2))
E=D+((D^3)/6)+((D^5)*0.075)+((D^7*0.0446429)+((D^9)*0.0303819)
XI=2*(((V(3)+V(2))*COS(E))-(V(3)*COS(P)))
XR=(2*V(3)+2*V(2)+S)-(XG+XI)
F(Q)=(V(3)*COS(P))/((V(4)*XG)+(V(5)*XR)+(V(6)*XI))
Q=Q+1
NEXT P
I=0.052359877*(F(0)+F(1)*4+F(2)*2+F(3)*4+F(4)*2+
  F(5)*4+F(6)*2+F(7)*4+F(8)*2+F(9)*4+F(10))
L=V(3)/(V(3)+V(2))
Z=L+((L^3)/6)((L^5)*0.075)+((L^7)*0.0446429)=((L^9)*0.0303819)
YI=(V(3)+V(2))*COS(Z)*2
YR=(2*V(3)+2*V(2)+S)-YI
K=V(2)/(YI*V(6)=YR*V(5))
A1=S/(S+2*V(3)+2*V(2))
B1=(2*V(5)*(I+K)+A1
SSMFR=1/B1

LOCATE LOCNO%,2:PRINT USING "$$.$$$$$"; N
LOCATE LOCNO%,18:PRINT USING "$$.$$$$$"; S
LOCATE LOCNO%,36:PRINT USING "$$.$$$$$"; SSMFR
LOCATE LOCNO%,50:PRINT USING "$$.$$$$$"; I
```

```
LOCATE LOCNO%,65:PRINT USING "$$.$$$$$"; K
NEXT N
RETURN

APPEND1:
PRINT:PRINT
INPUT"      GIVE FILENAME "FILENAME$

OPEN FILENAMES$ FOR APPEND AS $1
RANGESTEP=((MAX-MIN)/10)
FOR N=MIN TO (MAX+MAX/1000) STEP RANGESTEP
V(NUMBER%)=N
INCR LOCNO%

S=(V(3)*(((3.14159/V(1))^0.5)-2))-(2*V(2))
Q=O
FOR P=O TO 1.5707963 STEP 0.15707963
XG=2*V(3)*COS(P)
D=(V(3)*SIN(P))/(V(3)+V(2))
E=D+((D^3)/6)+((D^5)*0.075)+((D^7*0.0446429)+((D^9)*0.0303819)
XI=2*(((V(3)+V(2))*COS(E))-(V(3)*COS(P)))
XR=(2*V(3)+2*V(2)+S)-(XG+XI)
F(Q)=(V(3)*COS(P))/((V(4)*XG)+(V(5)*XR)+(V(6)*XI))
Q=Q+1
NEXT P
I=0.052359877*(F(0)+F(1)*4+F(2)*2+F(3)*4+F(4)*2+
  F(5)*4+F(6)*2+F(7)*4+F(8)*2+F(9)*4+F(10))
L=V(3)/(V(3)+V(2))
Z=L+((L^3)/6)((L^5)*0.075)+((L^7)*0.0446429)=((L^9)*0.0303819)
YI=(V(3)+V(2))*COS(Z)*2
YR=(2*V(3)+2*V(2)+S)-YI
K=V(2)/(YI*V(6)=YR*V(5))
A1=S/(S+2*V(3)+2*V(2))
B1=(2*V(5)*(I+K)+A1
SSMFR=1/B1

WRITE $1,N,S,SSMFR,I,K
NEXT N
CLOSE
RETURN
```

APPENDIX B

Student "t" test

If there are two groups of results size $n_1$ and $n_2$, with means $x_1$ and $x_2$, and standard deviations $s_1$ and $s_2$, then "t" is determined using the equation :

$$t = \frac{x_1 - x_2}{s\left(\frac{1}{n_1} + \frac{1}{n_2}\right)^{0.5}}$$

where s is determined from the equation :

$$s = \left(\frac{s_1^2 + s_2^2}{2}\right)^{0.5}$$

The value of t is then compared against the number of degrees of freedom of the system ( given by $(n_1 + n_2) - 2$ ) on tables of probability. From these tables the level of confidence that there is a difference between the two sets of results can be determined.

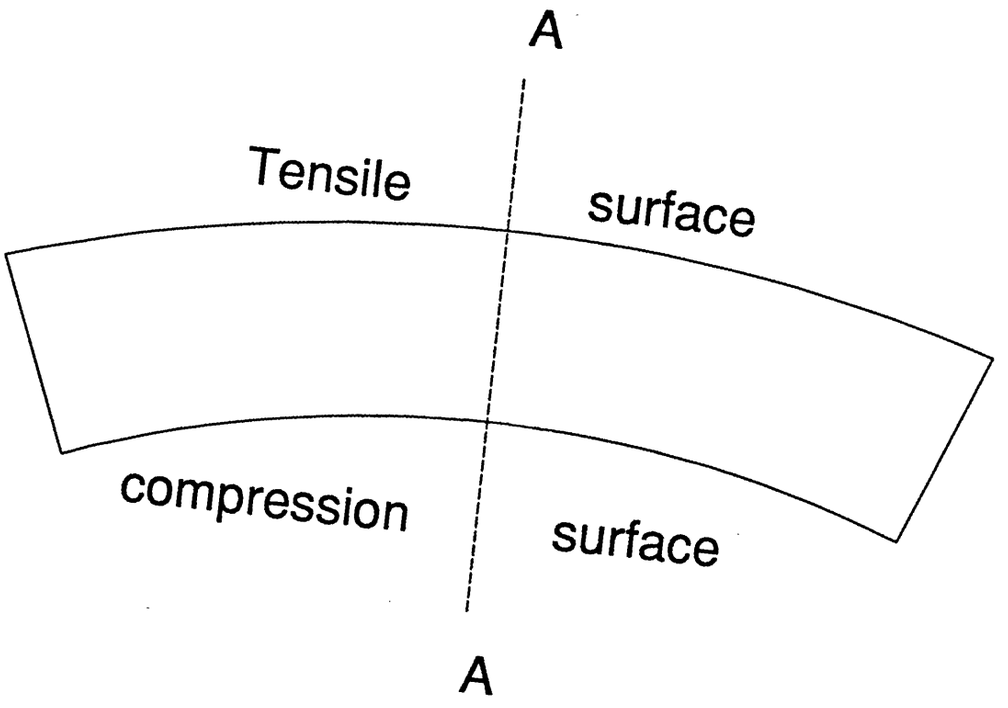


Figure 1. Beam in bending

(a) Forces acting on section A-A

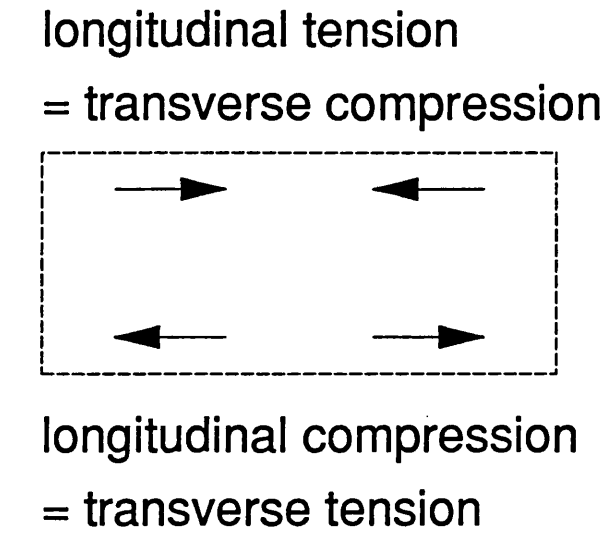


(b) Resulting shape of beam cross section

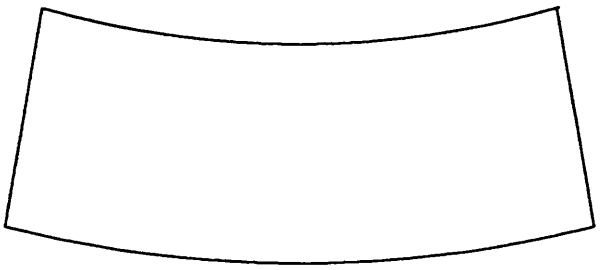

Figure 2. Cross section through beam

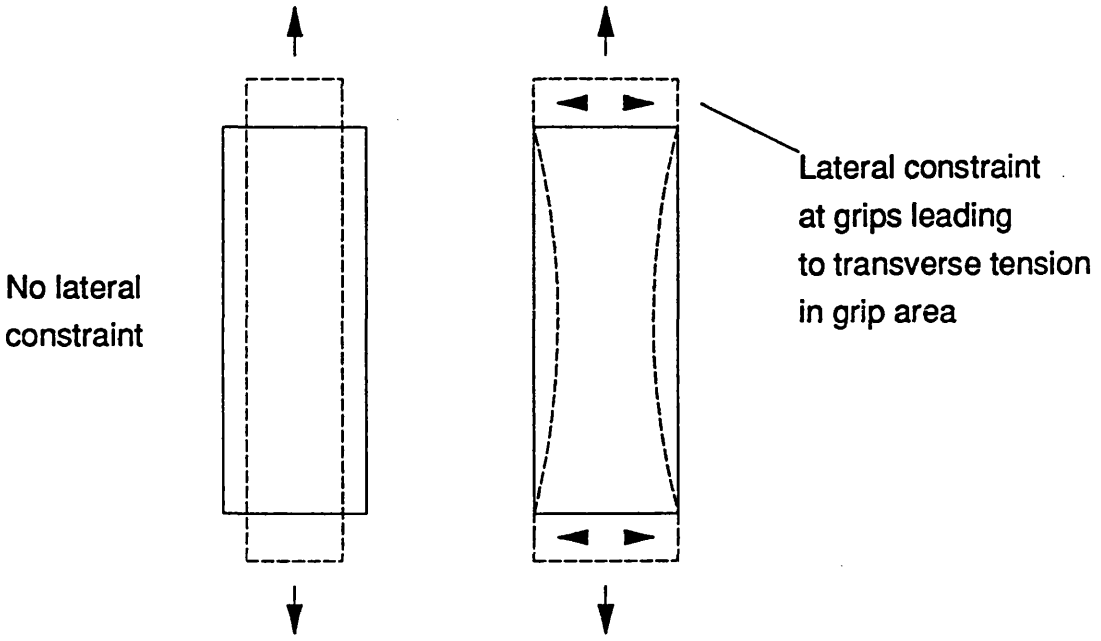


Figure 3. Lateral constraint due to gripping

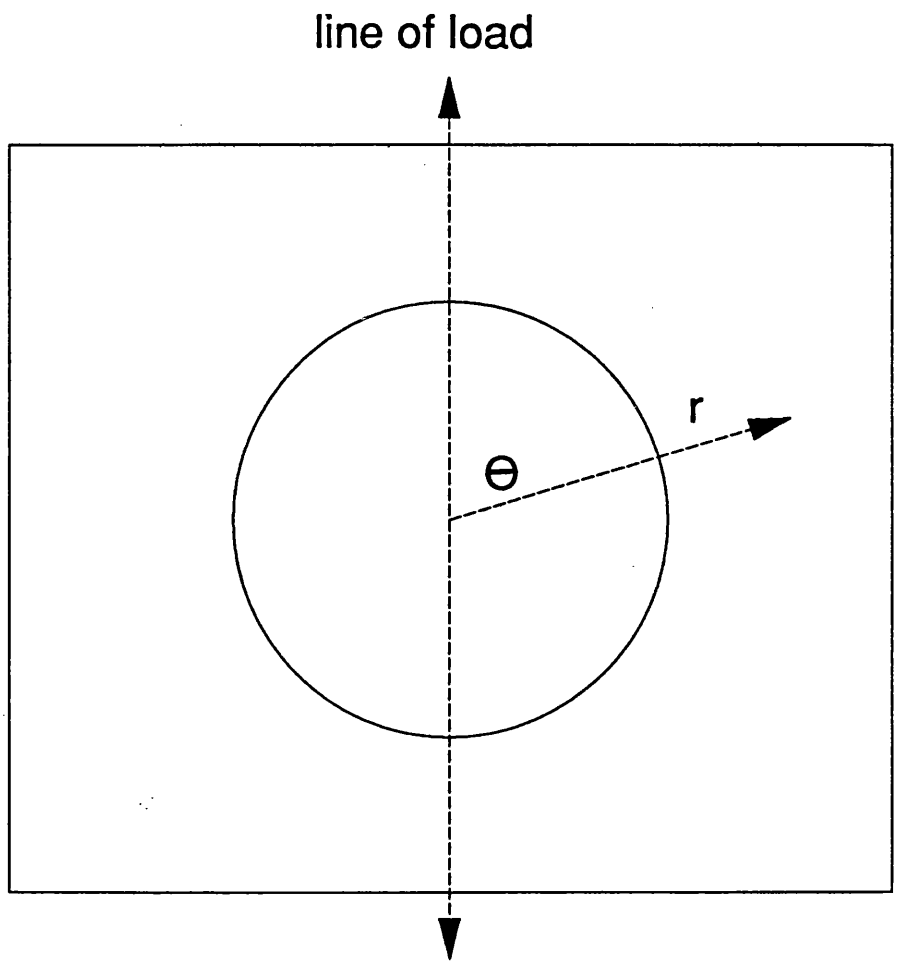


Figure 4. Co-ordinate system for plate with inclusion

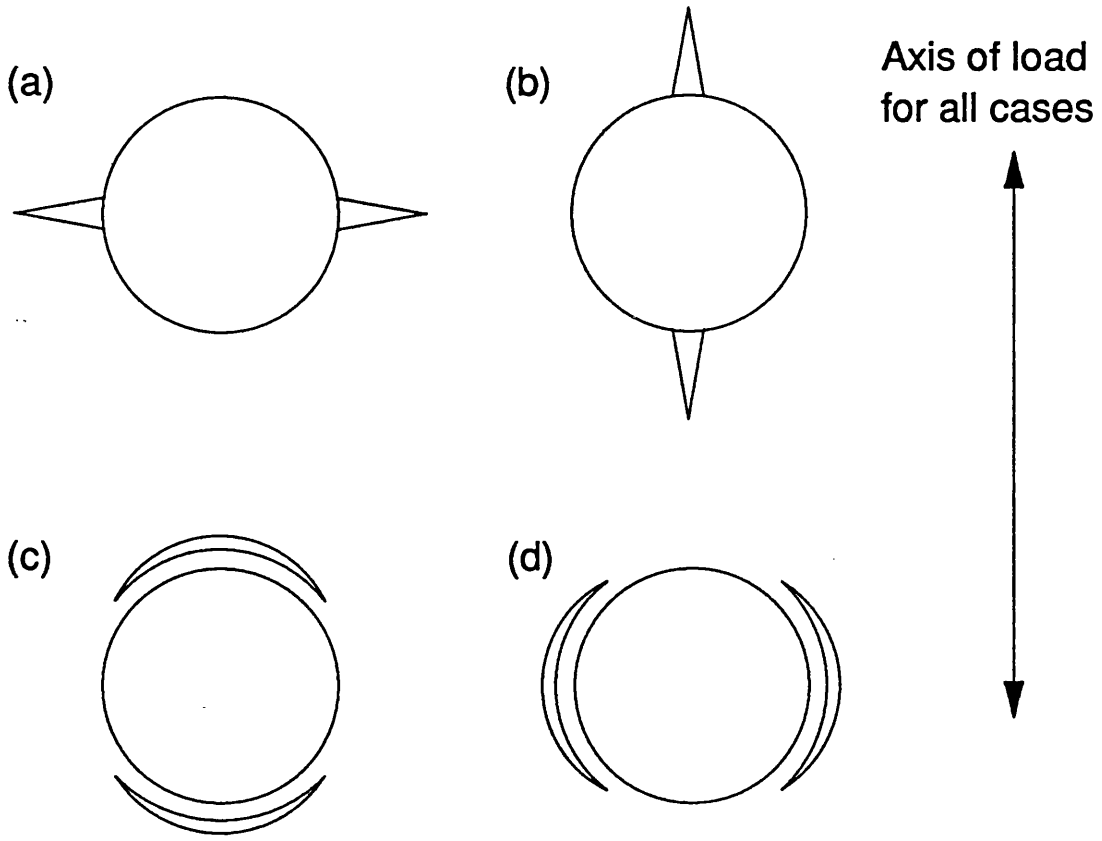


Figure 5. Four possible cases of crack growth around a fibre

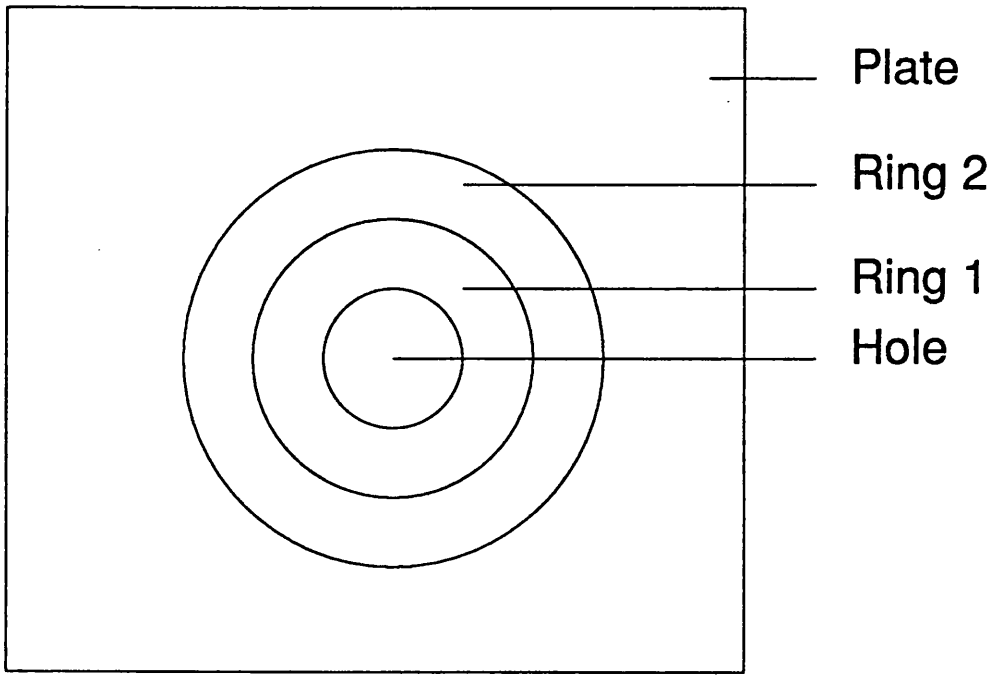


Figure 6. Hole with reinforcing rings

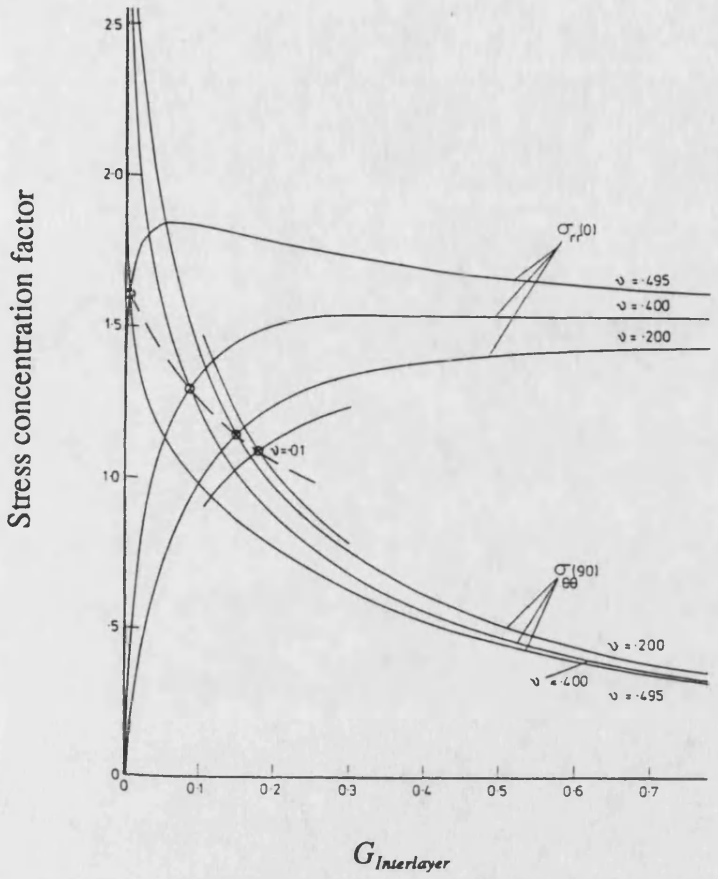


Figure 7. Stress concentration as a function of interlayer modulus

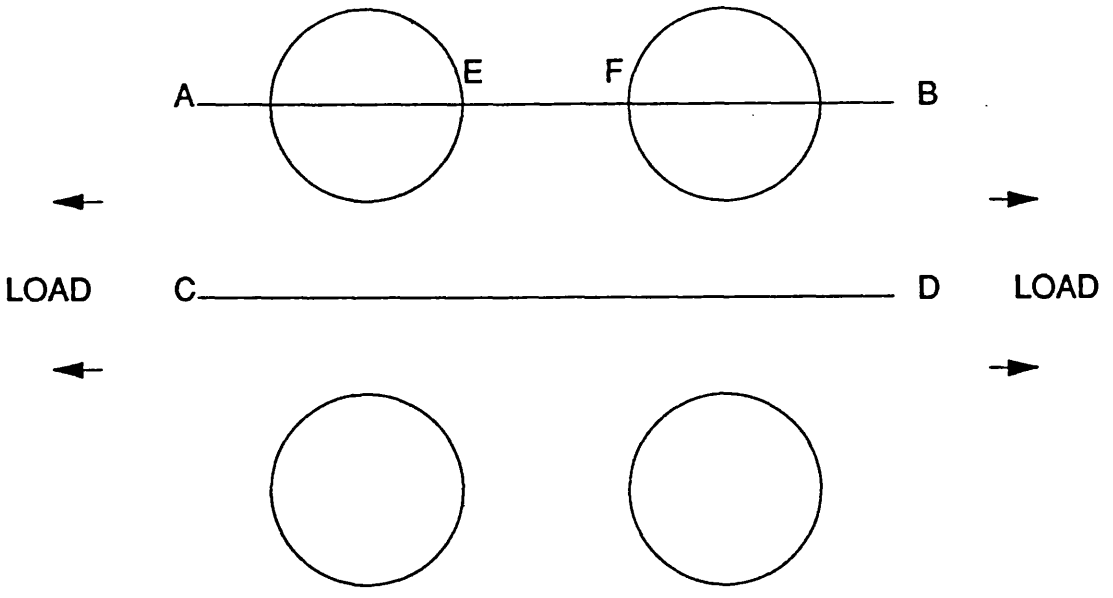


Figure 8. Transverse section through ideal composite

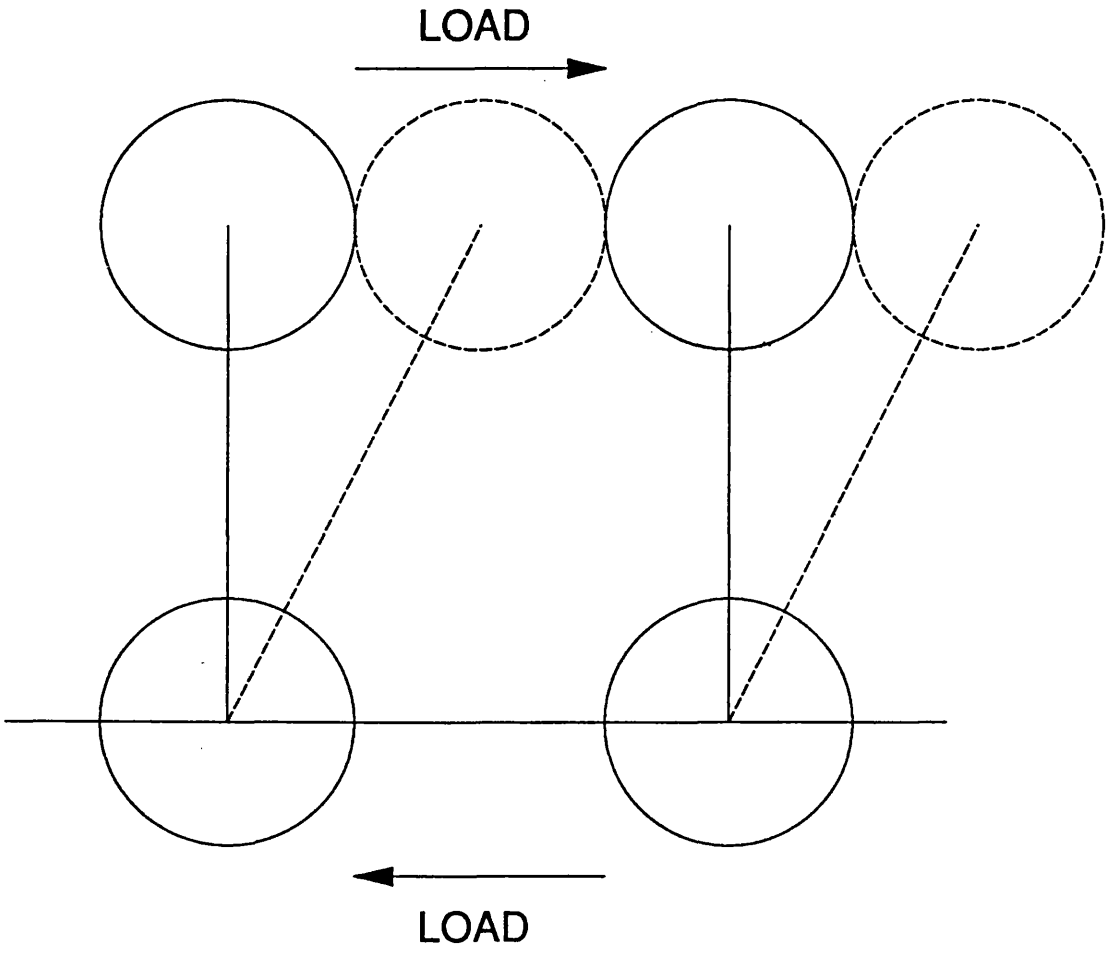


Figure 9. Kies shear model

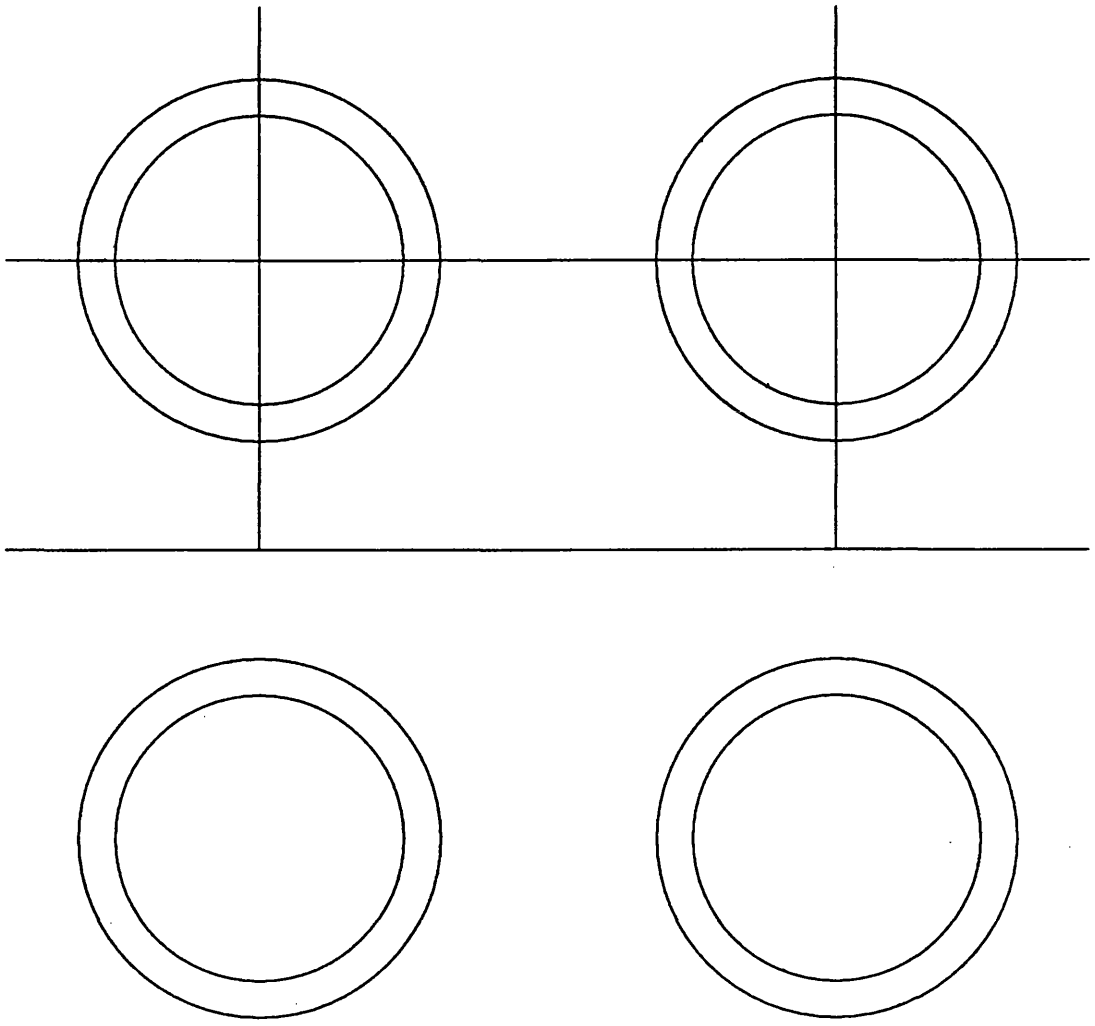

Figure 10. Kies model with added interphase

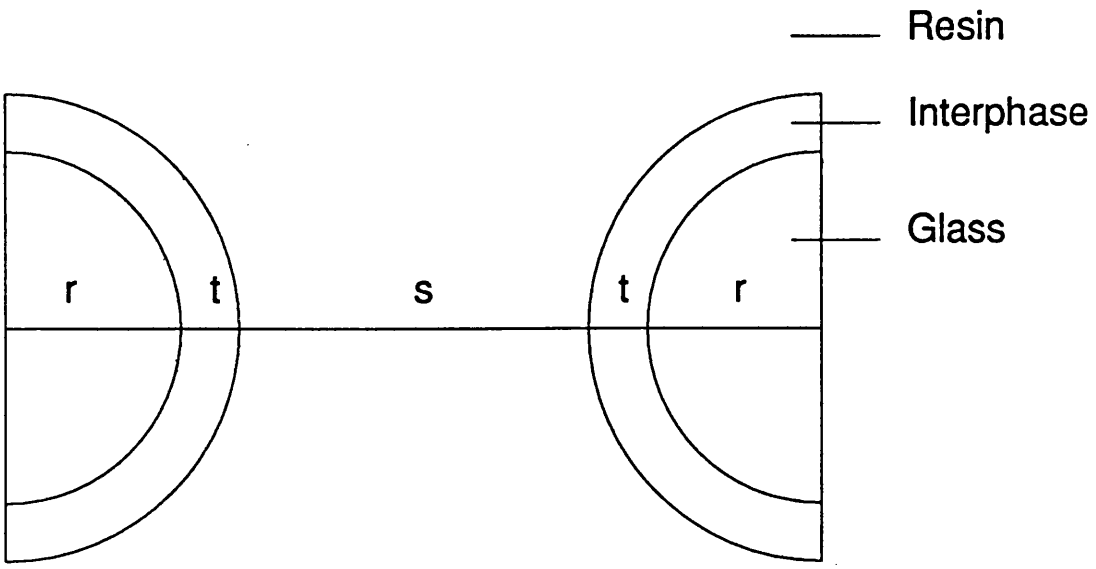


Figure 11. Parameters of extended model

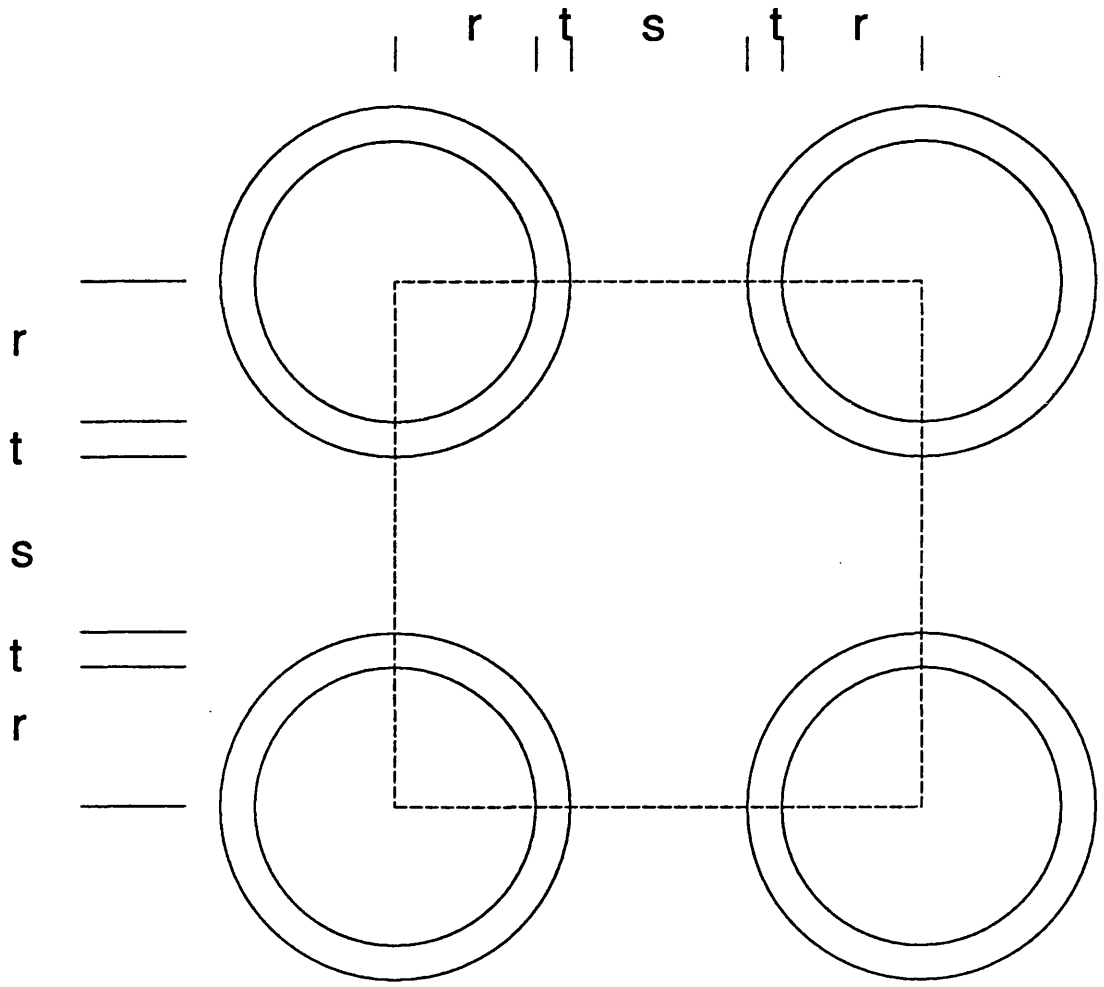


Figure 12. Extended Kies shear model

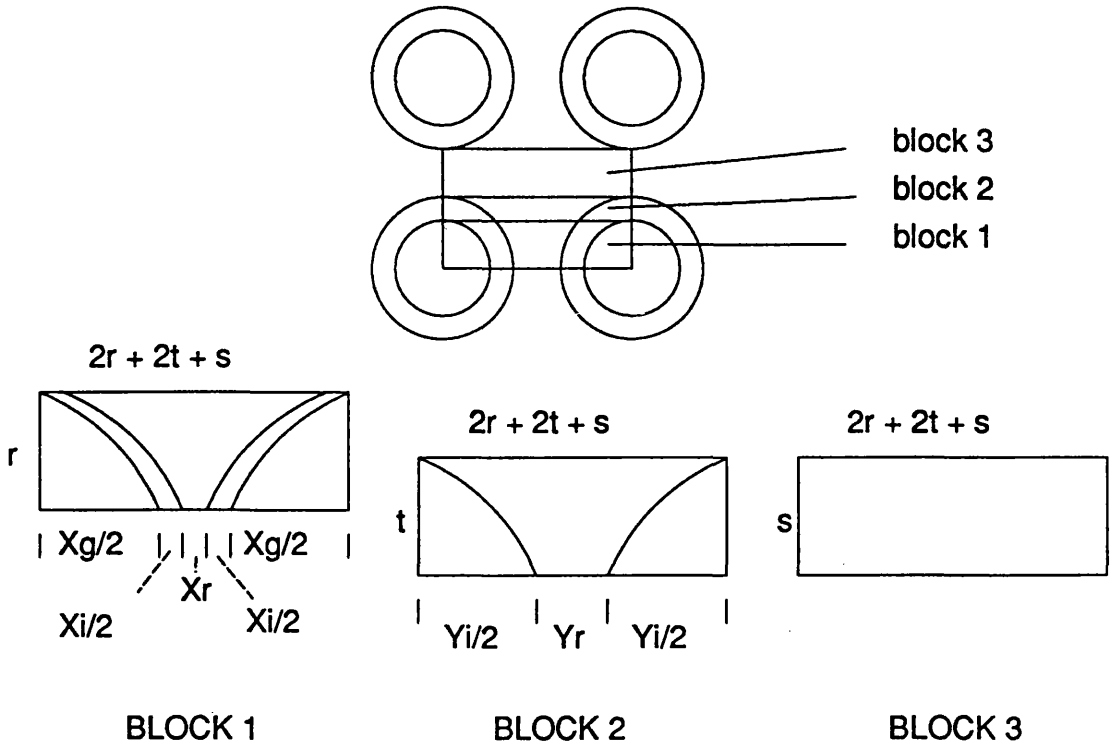


Figure 13. Shear model split into blocks

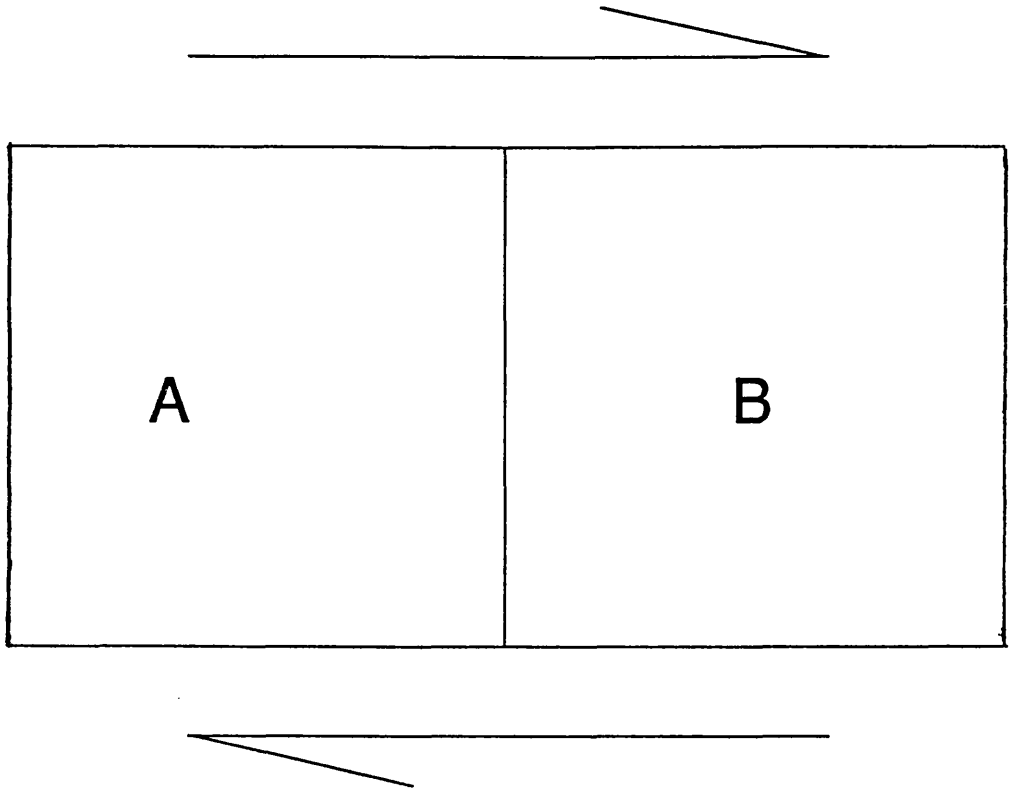


Figure 14. Two blocks in shear

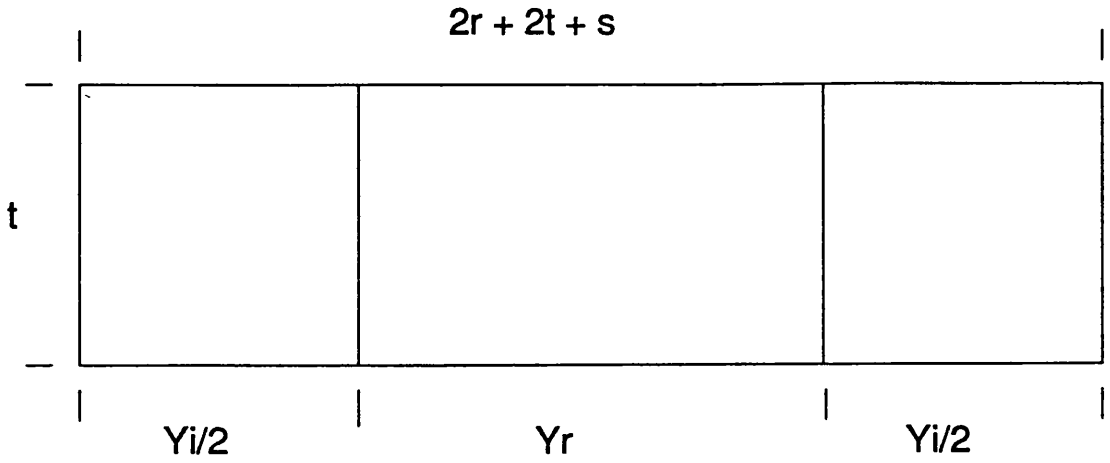


Figure 15. Simplified form of block 2 , shear model

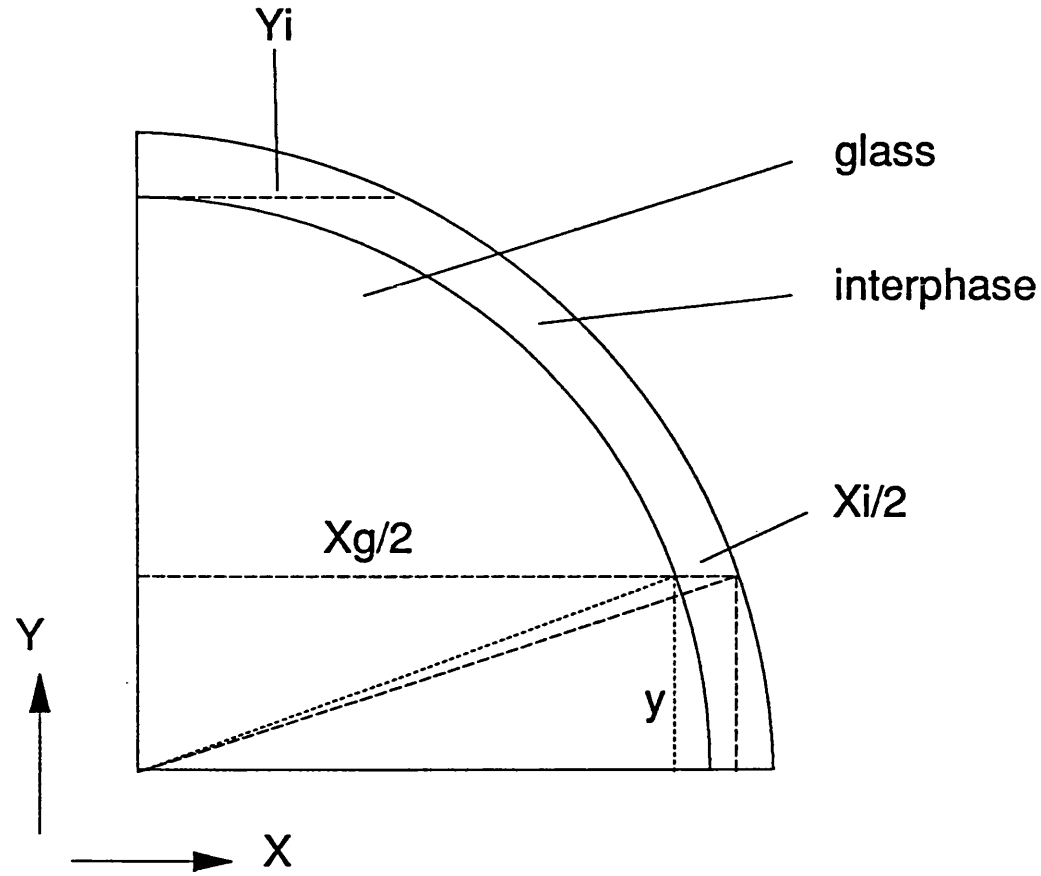


Figure 16. Converting to polar co-ordinates

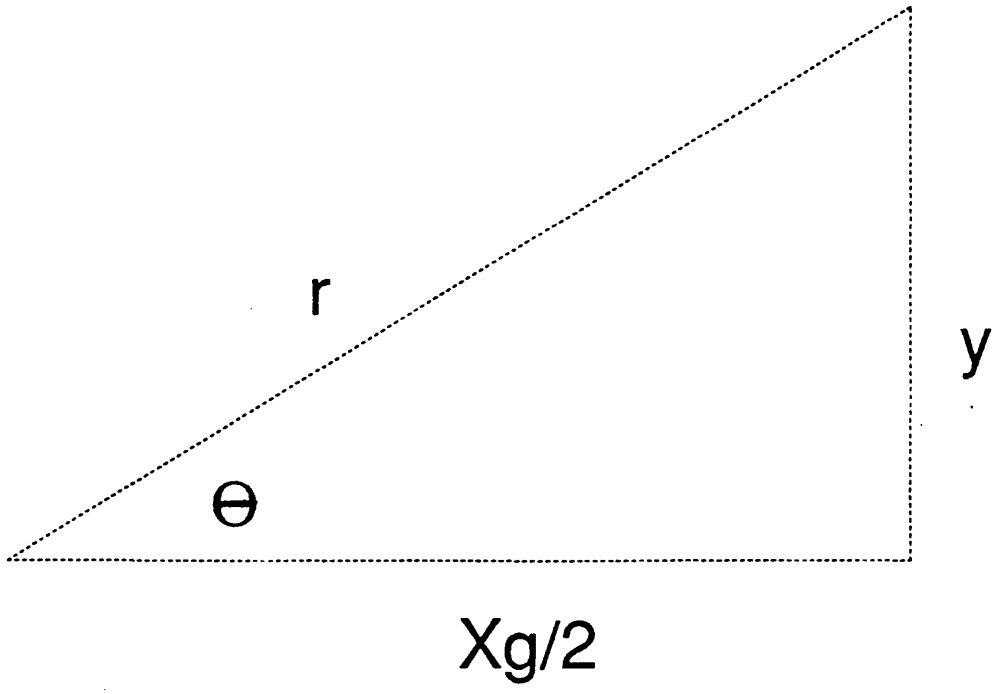


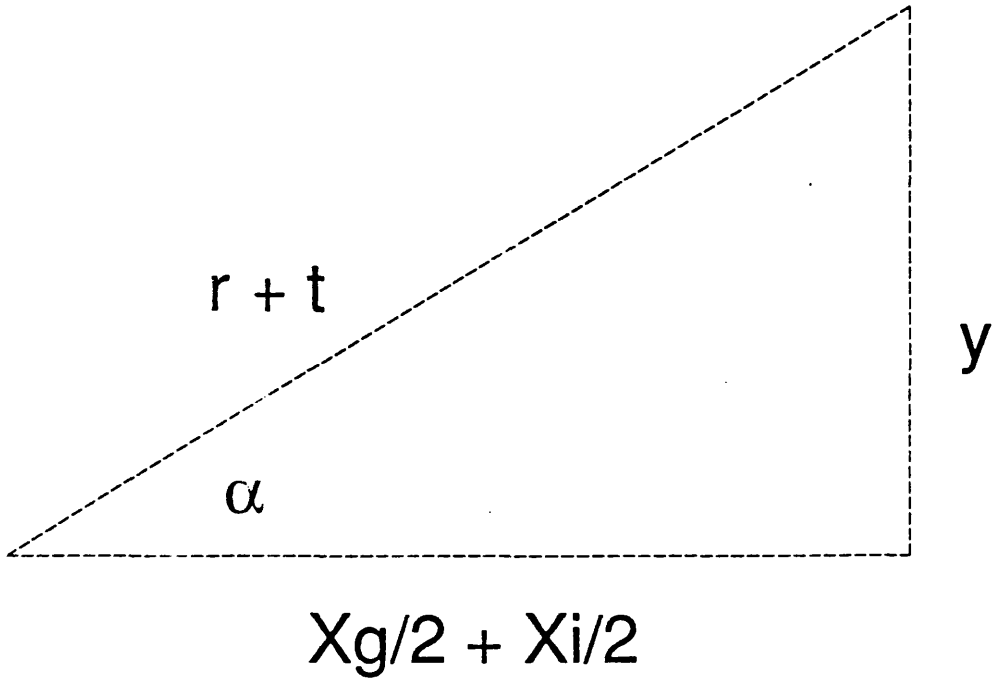


Figure 17. Relation between angles

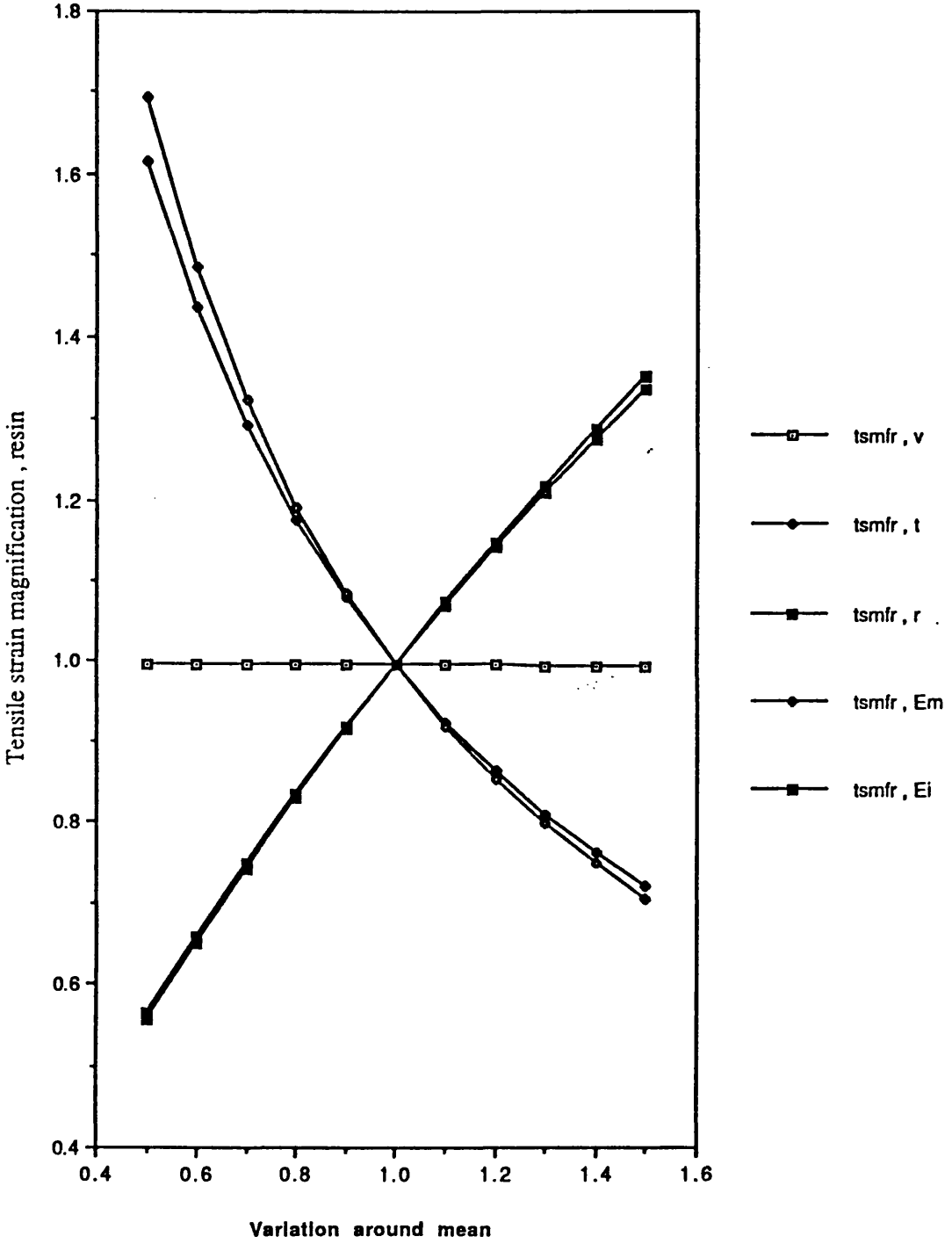


Figure 18. Variations in the tensile strain magnification factor , resin

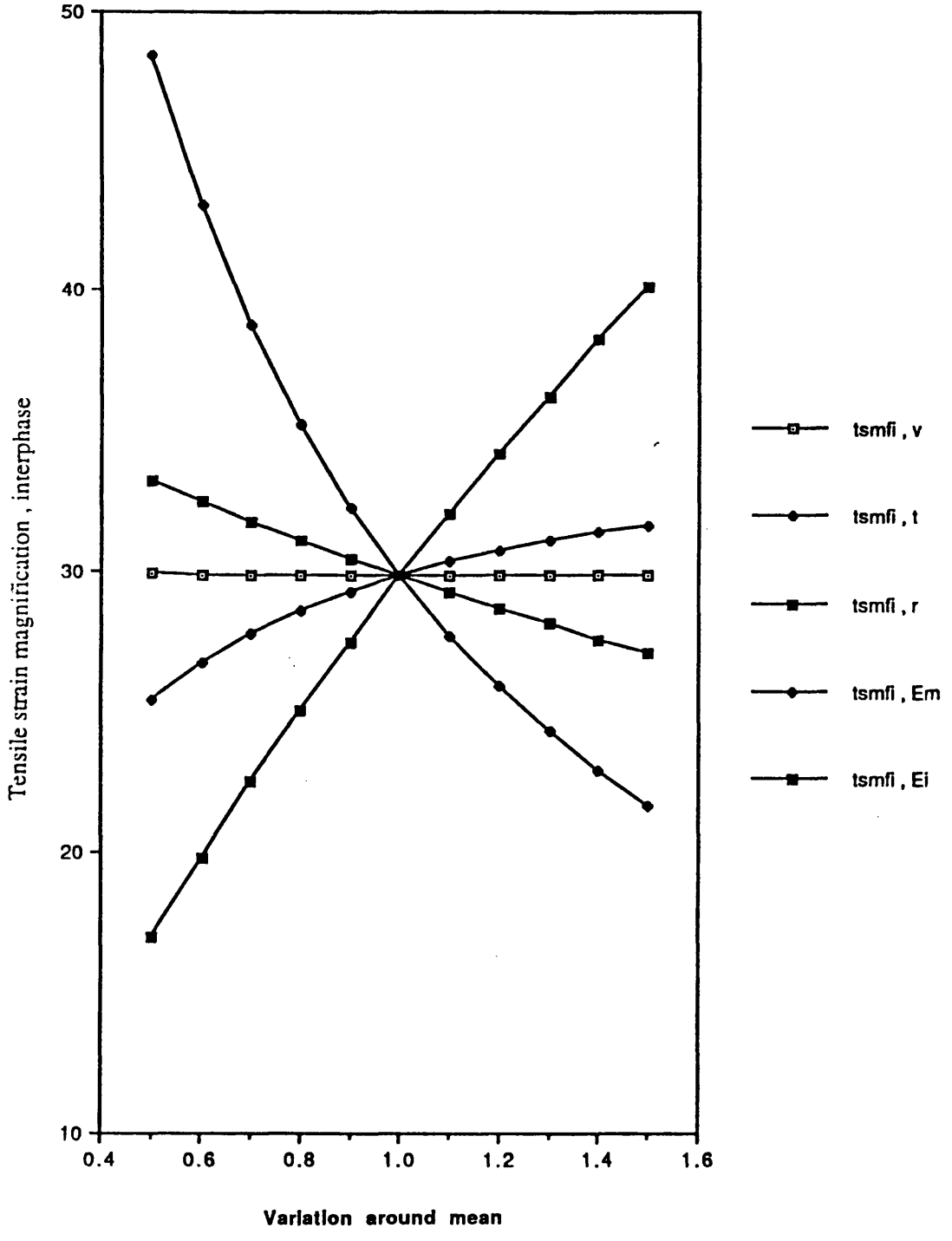


Figure 19. Variations in the tensile strain magnification factor , interphase

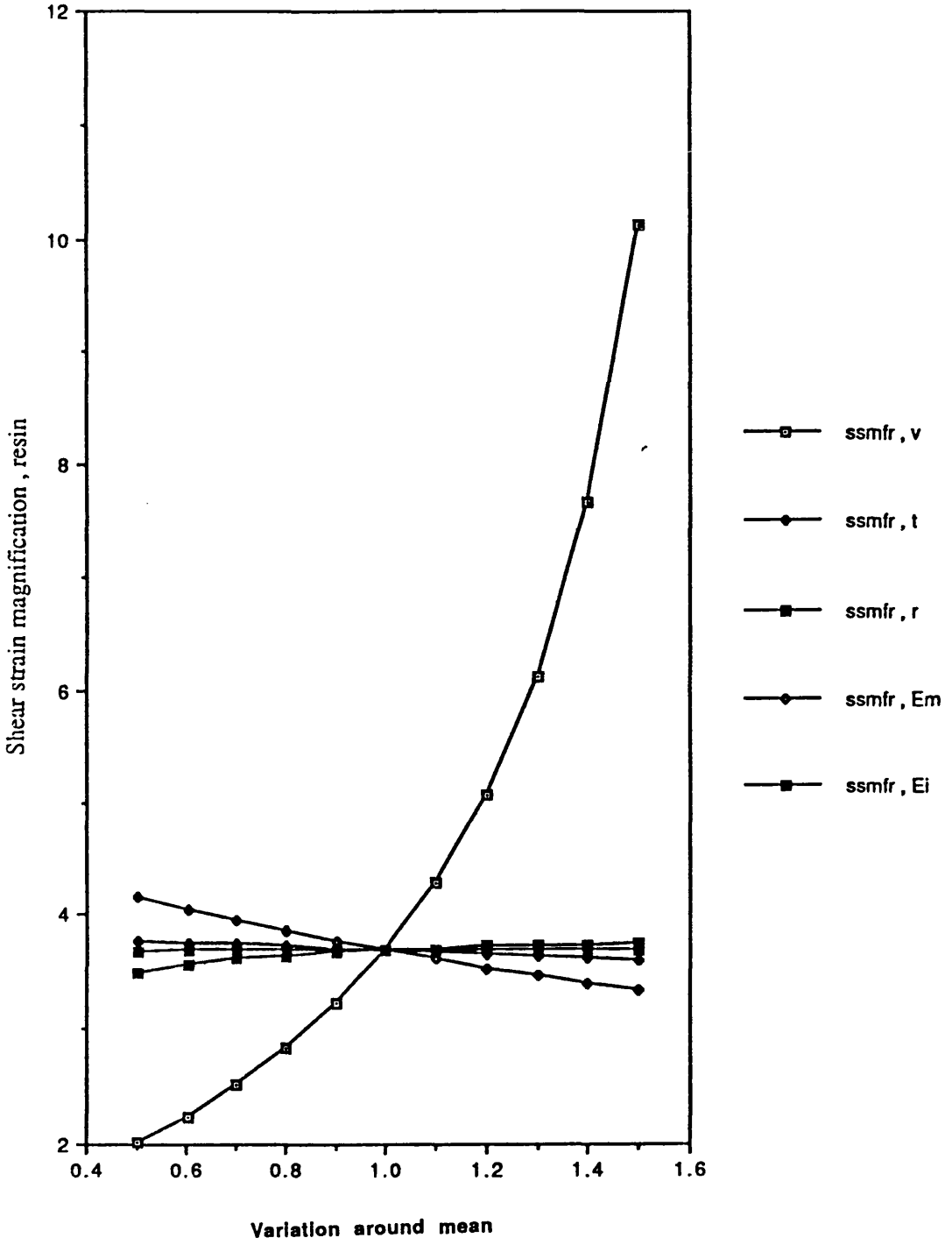


Figure 20. Variations in the shear strain magnification factor , resin

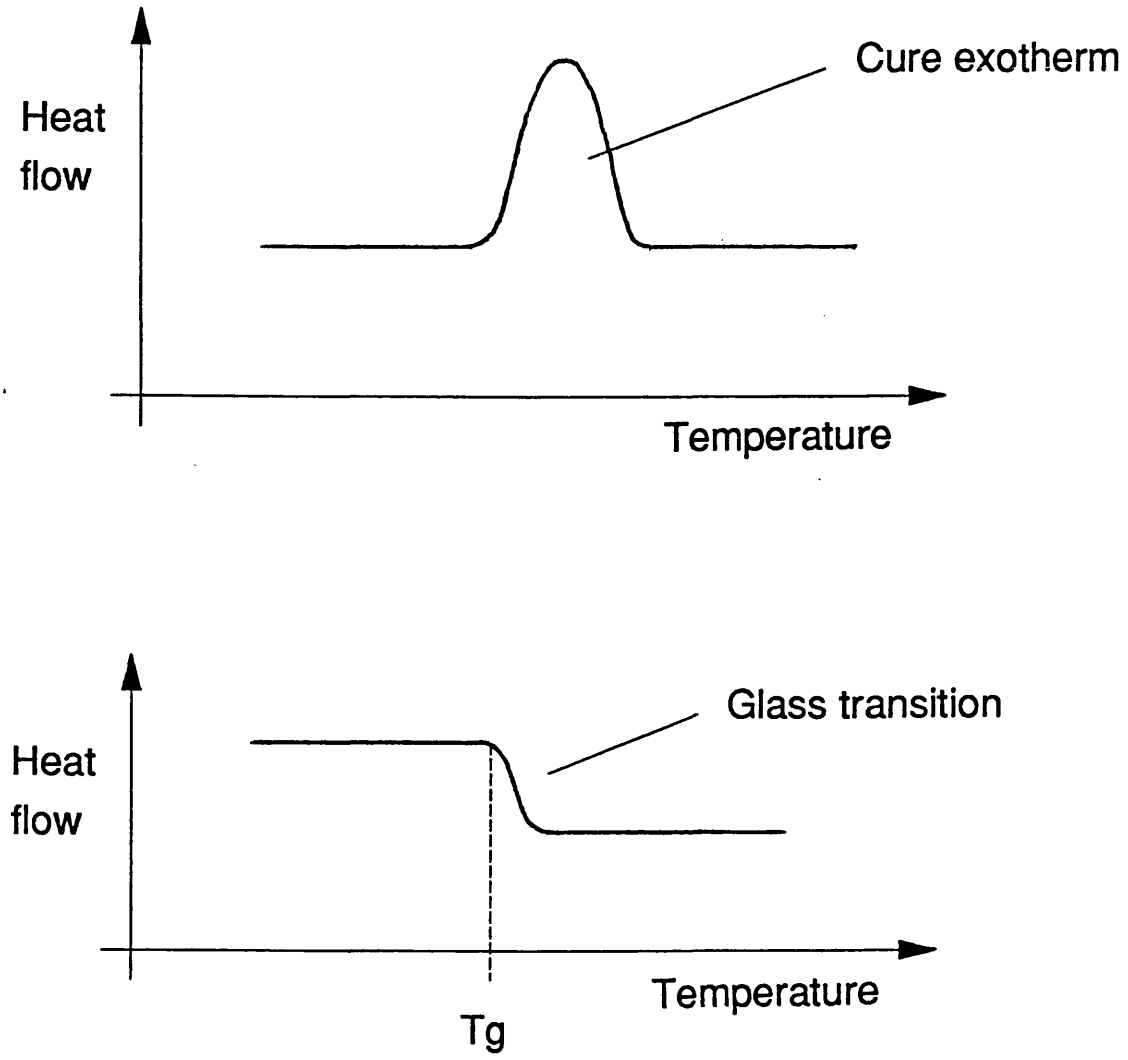


Figure 21. Cure exotherm and glass transition temperature

Figure 22. Differential scanning calorimetry curve for vinyl ester post cured for 10 minutes at 100 °C

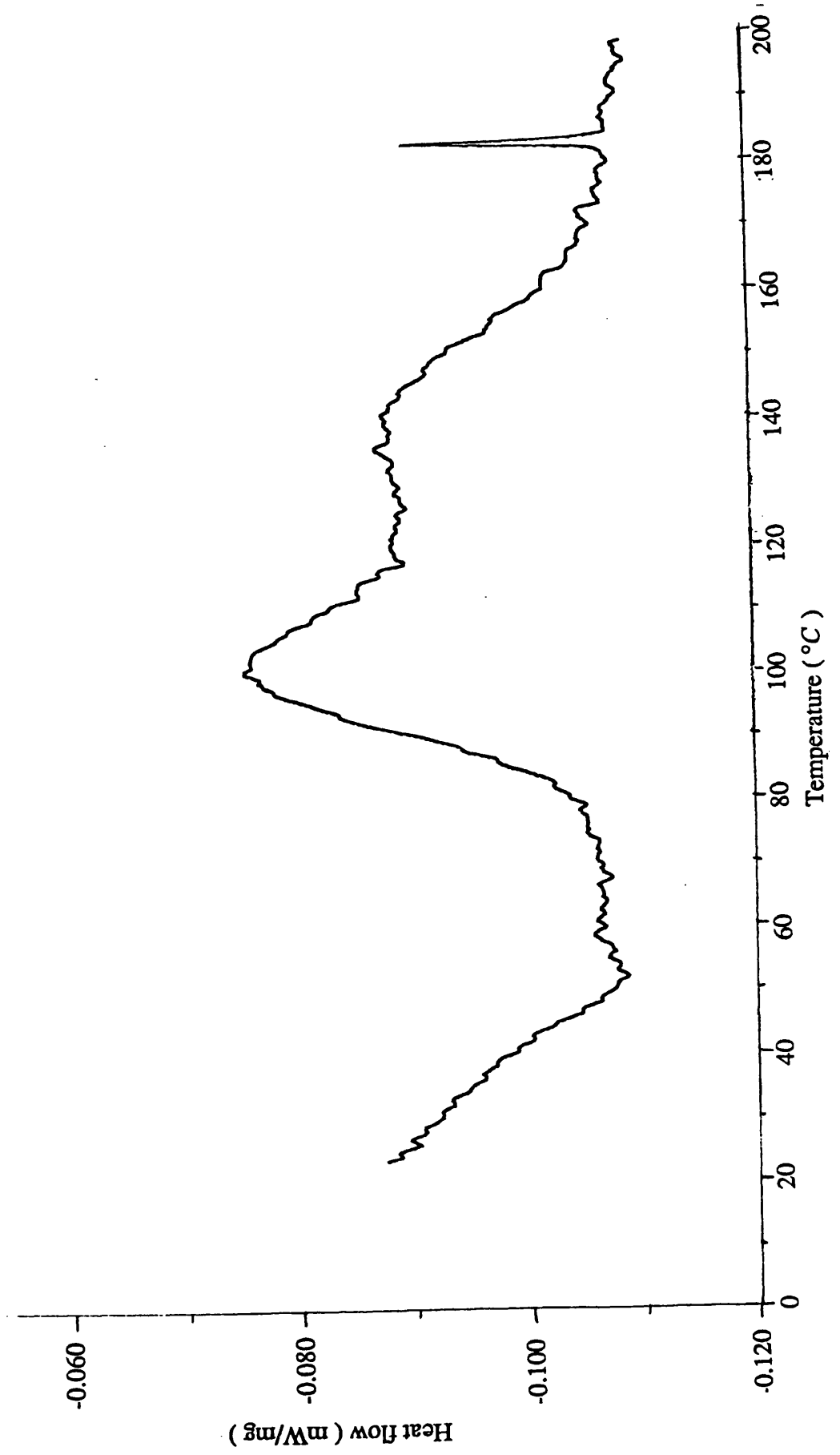

Figure 23. Differential scanning calorimetry curve for inhibited vinyl ester subject to various post cure treatments

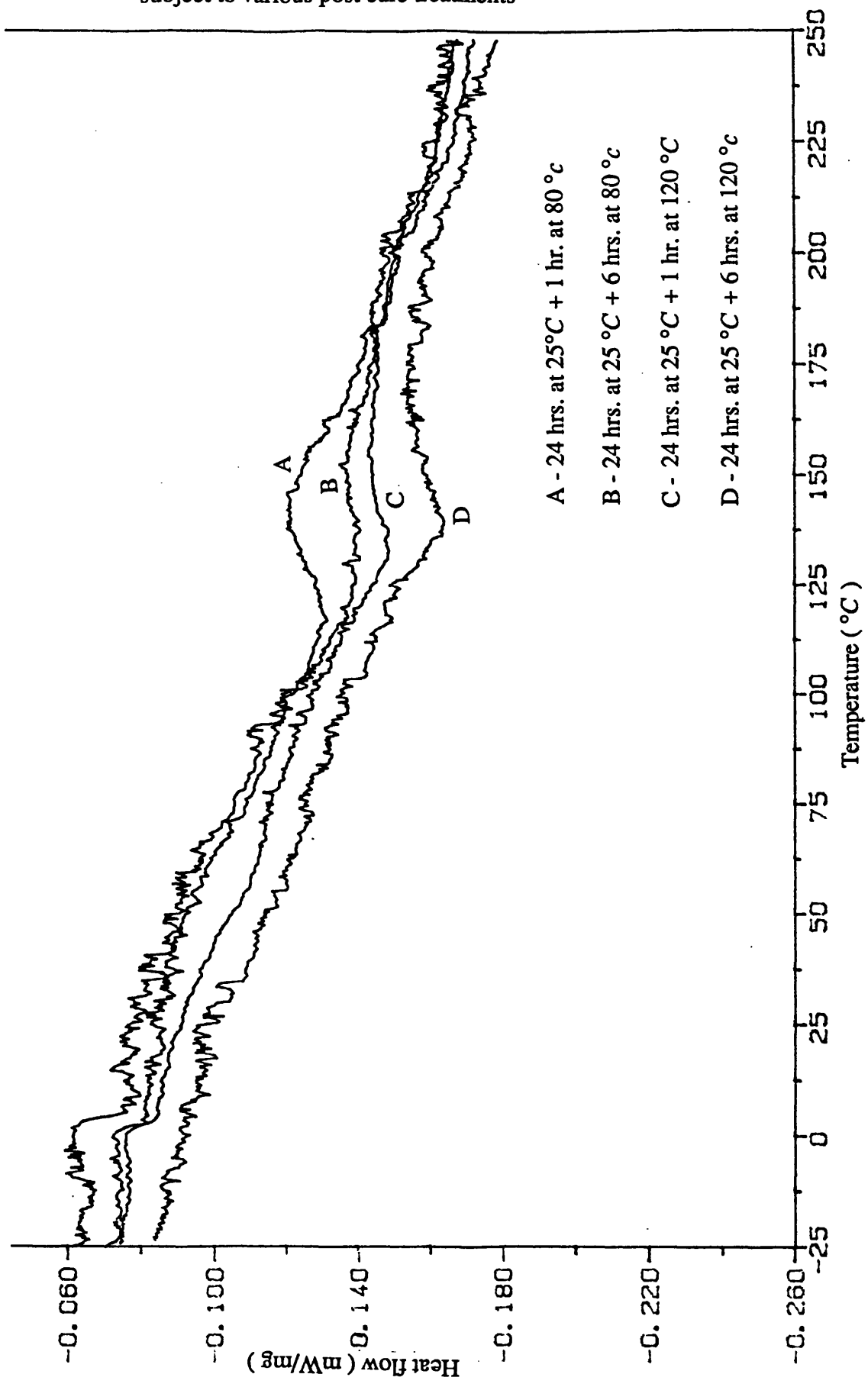

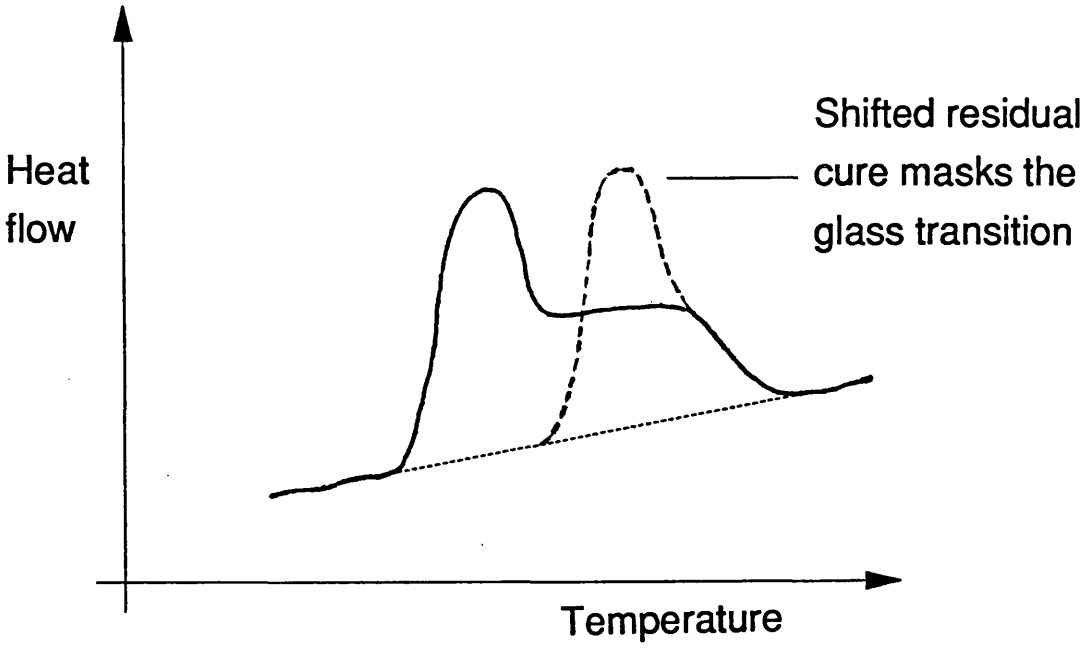


Figure 24. Shifted residual cure exotherm

Figure 25. Differential scanning calorimetry curve for acrylic dried and post cured for 3 hours at 80 °C

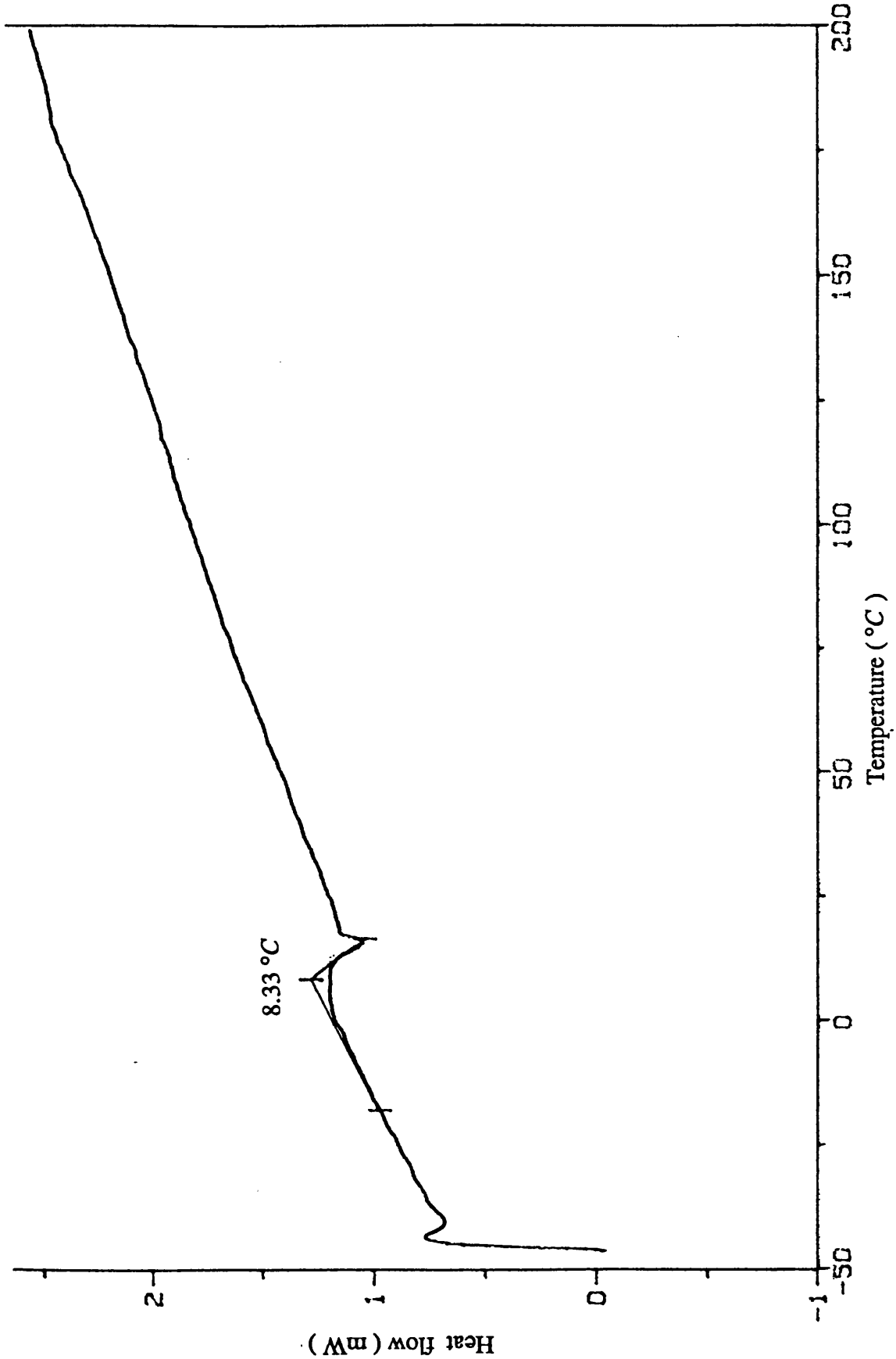

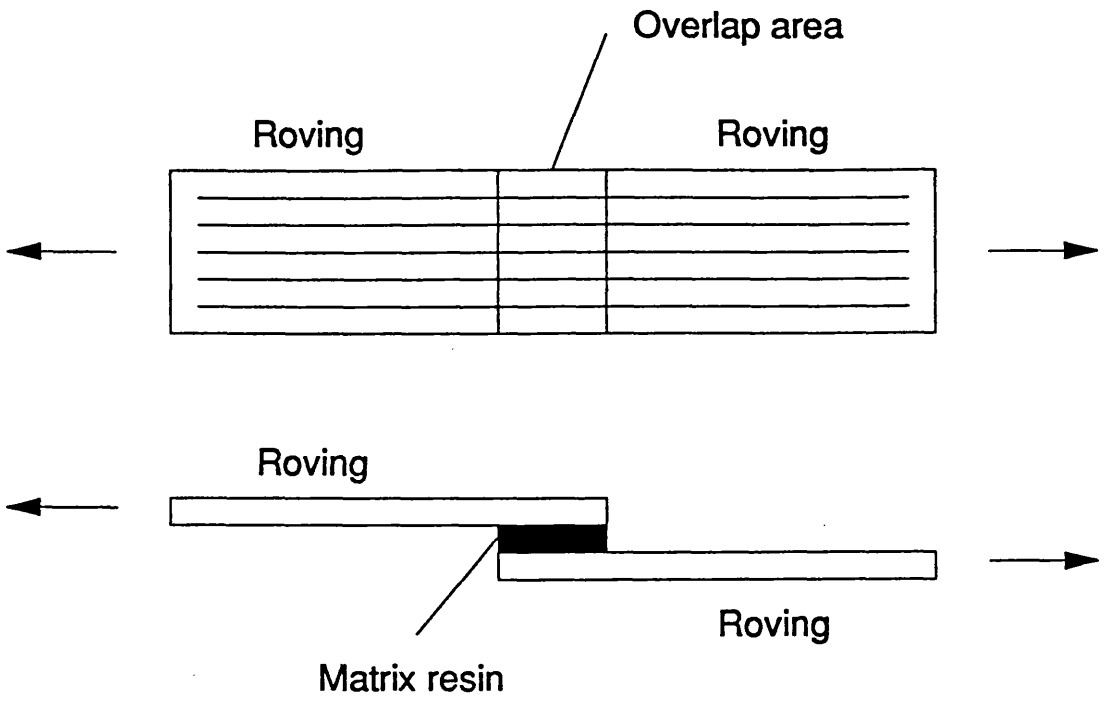


Figure 26. Schematic of adhesion tests

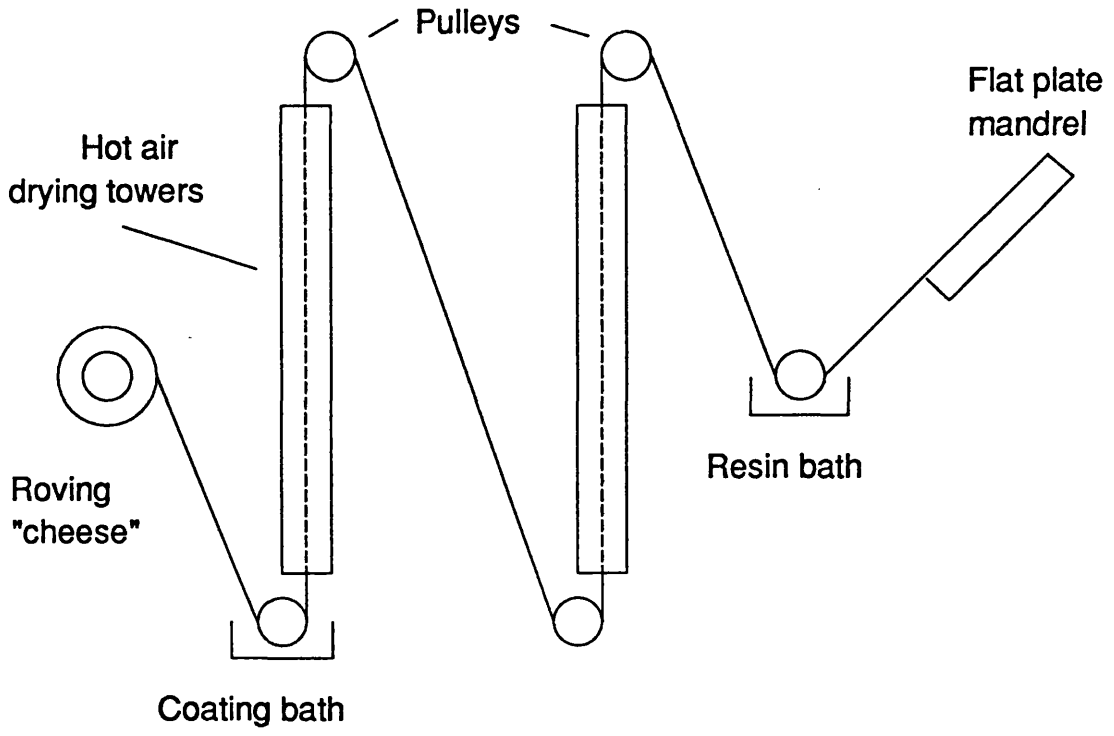


Figure 27. Schematic of initial production apparatus

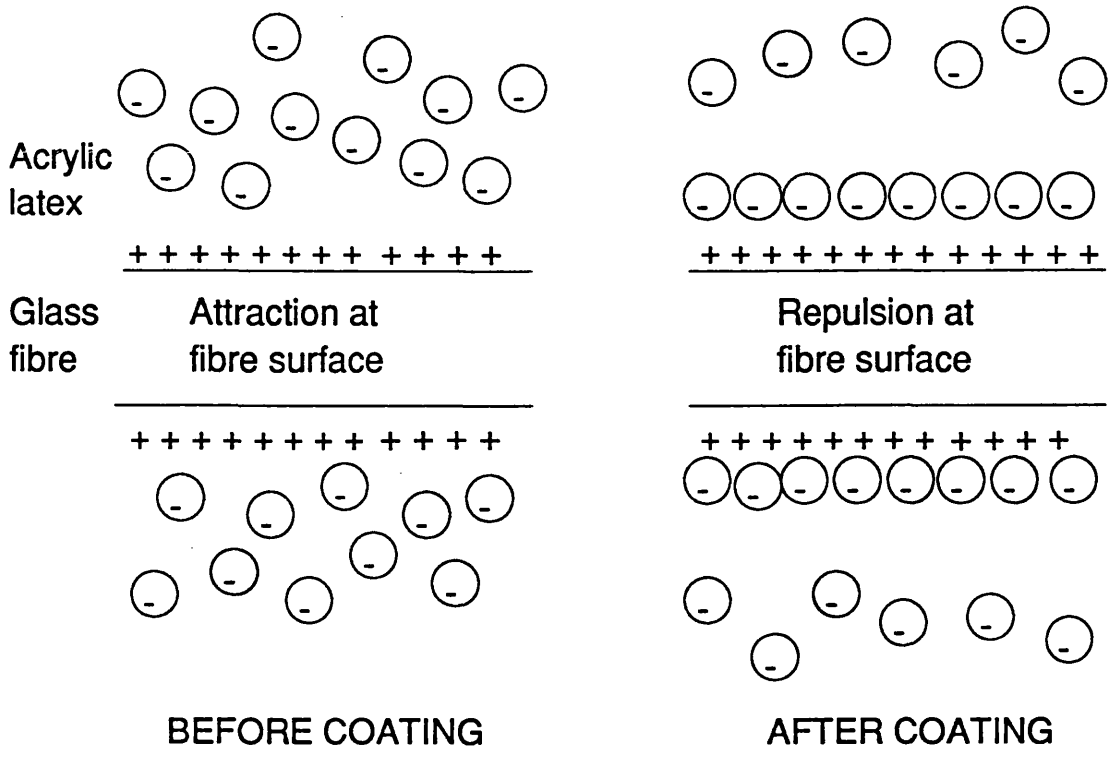


Figure 28. Electrostatic control of coating thickness

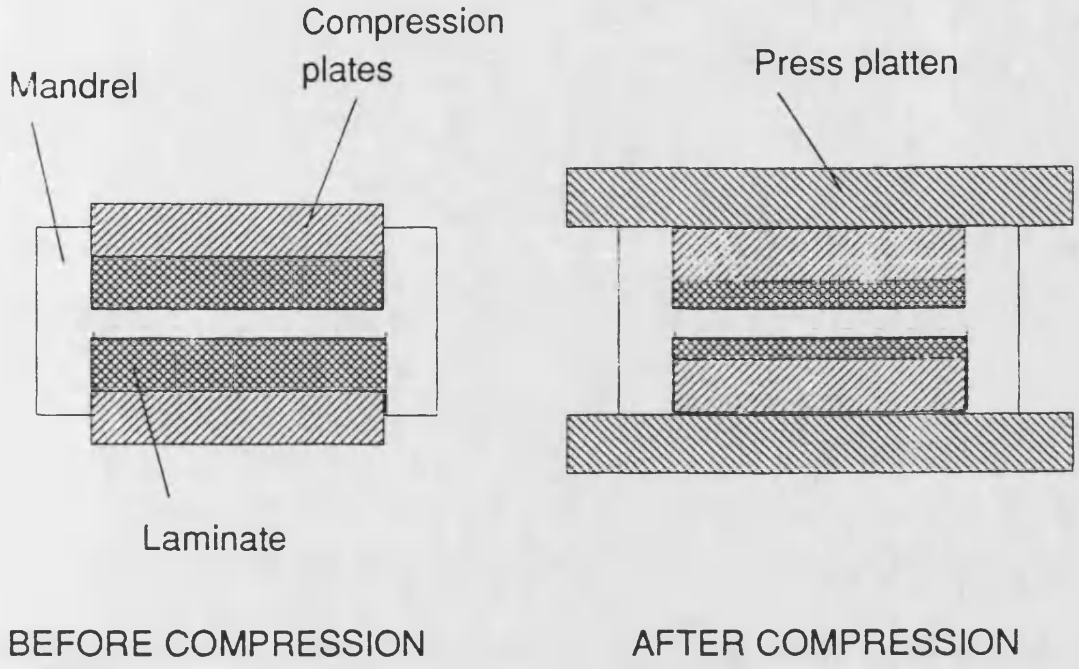


Figure 29. Compression moulding apparatus

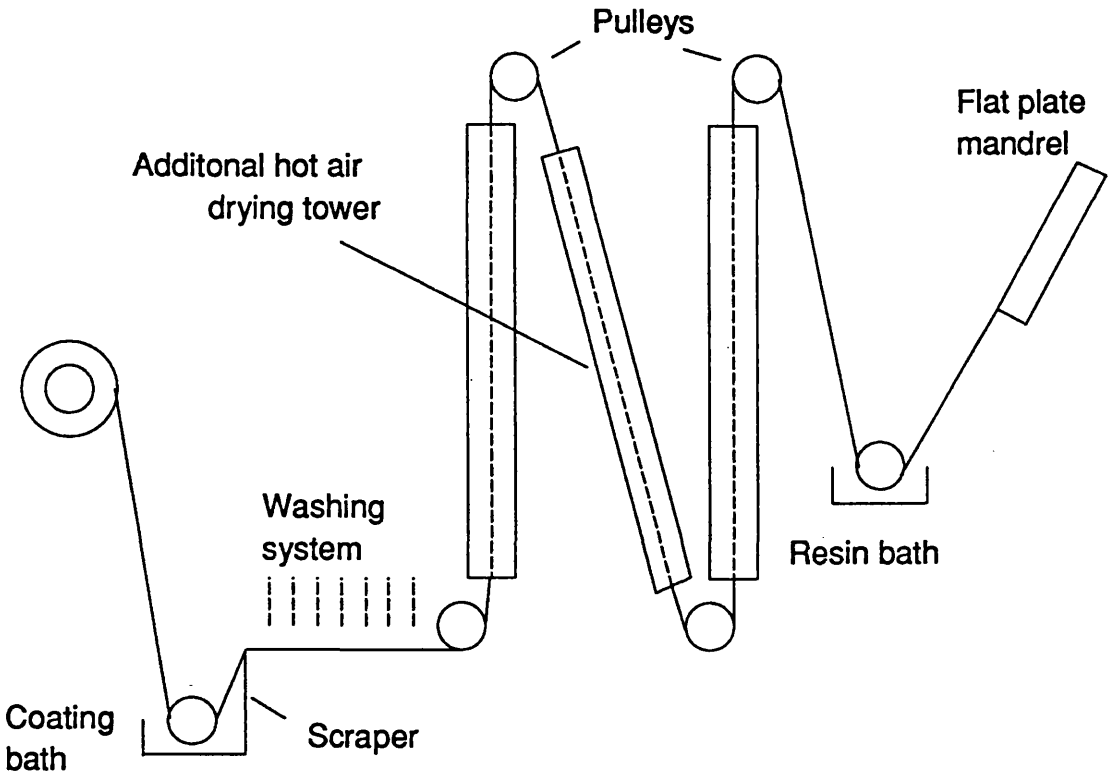


Figure 30. Schematic of final production apparatus

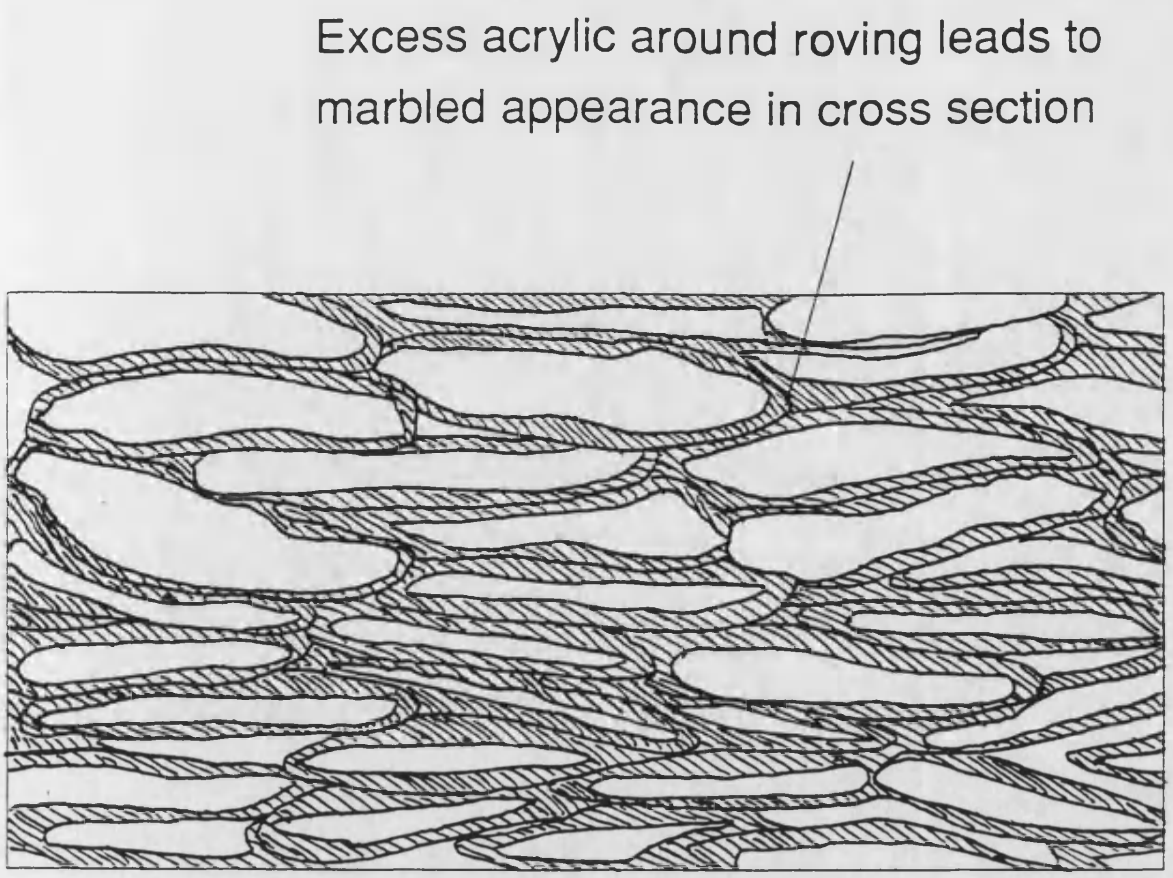


Figure 31. Schematic of marbling in coated fibre composite

Figure 32. Marbling in coated fibre composite ( X 40 )

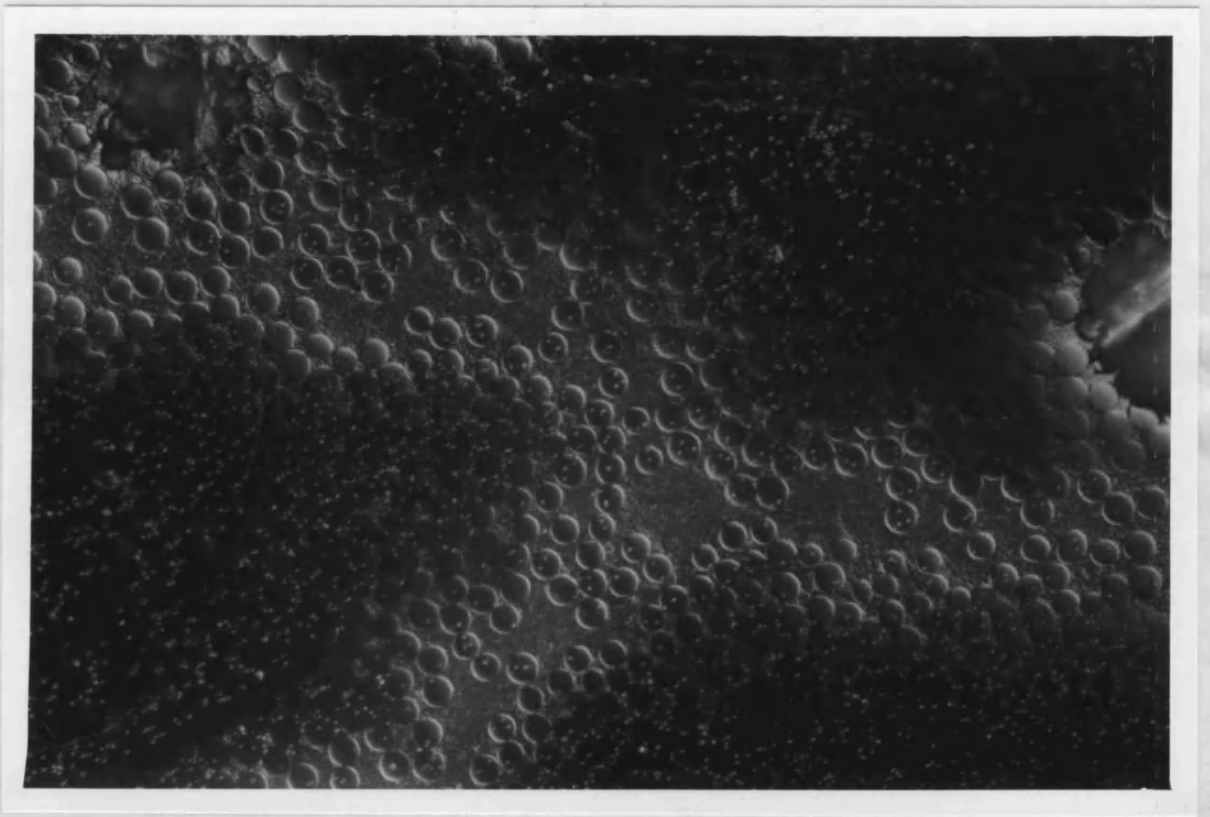

Figure 33. Close up of marbling ( X 160 )

Figure 34. Final apparatus

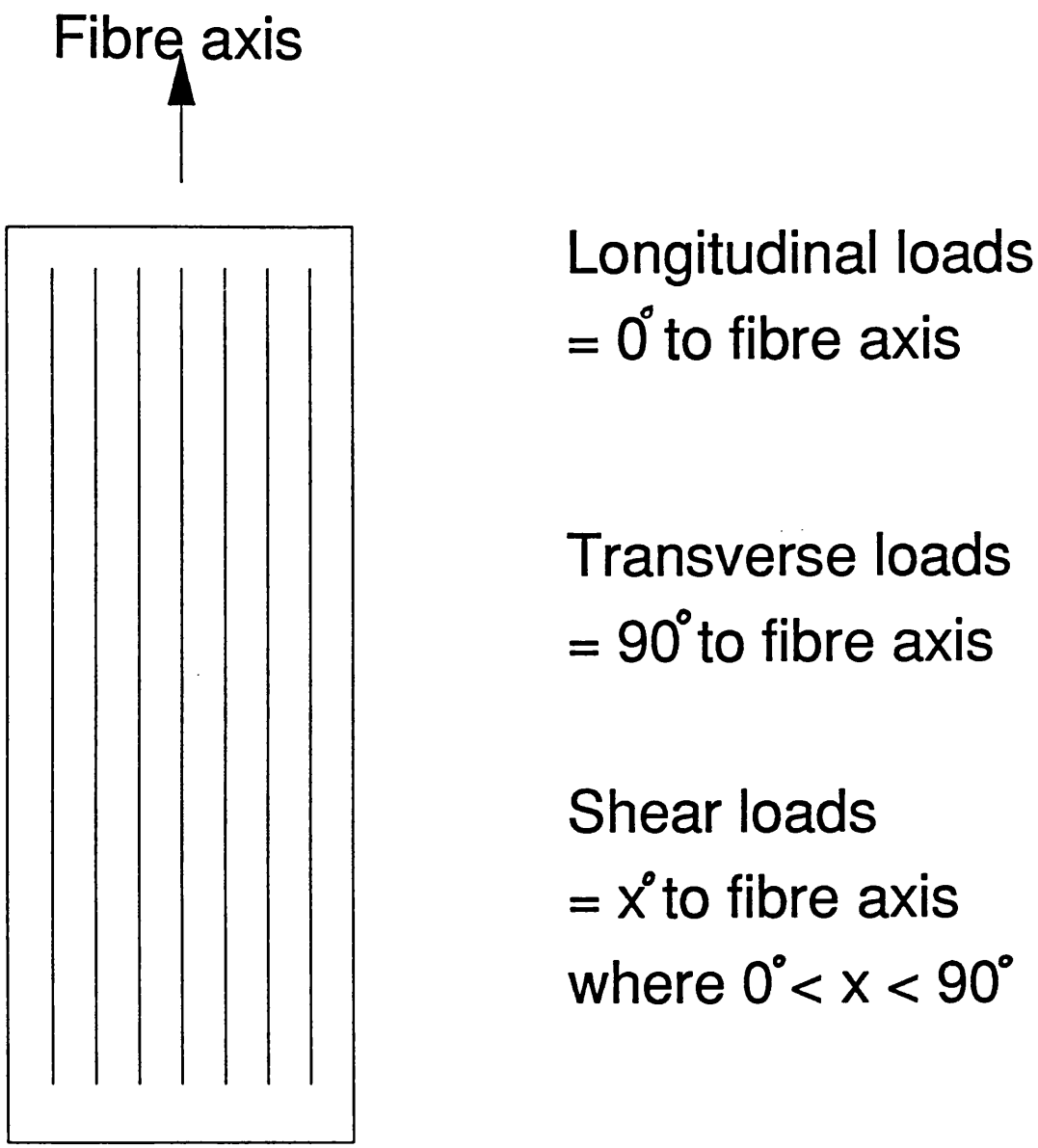


Figure 35. Unidirectional fibre composite

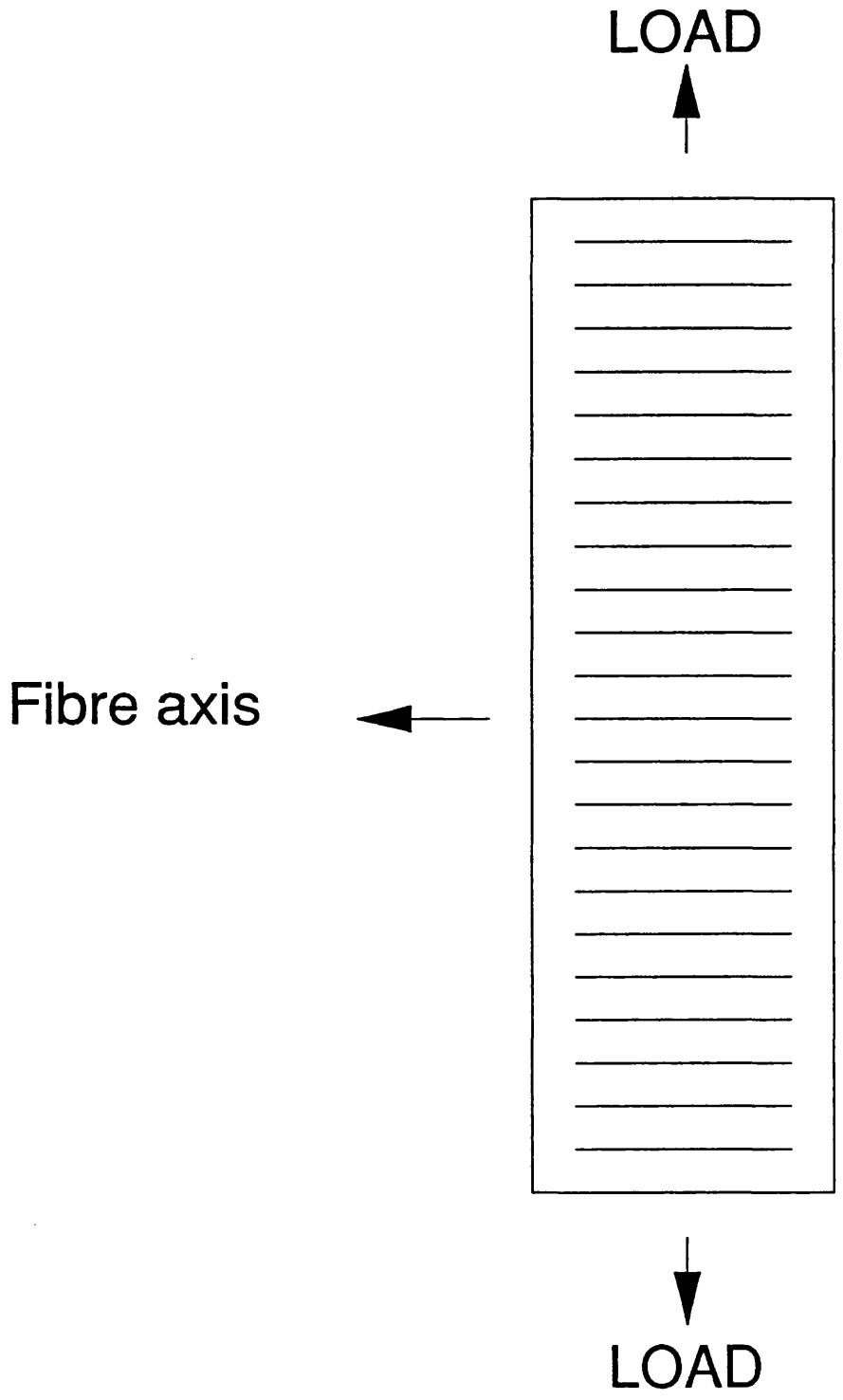


Figure 36. Transverse tensile testing

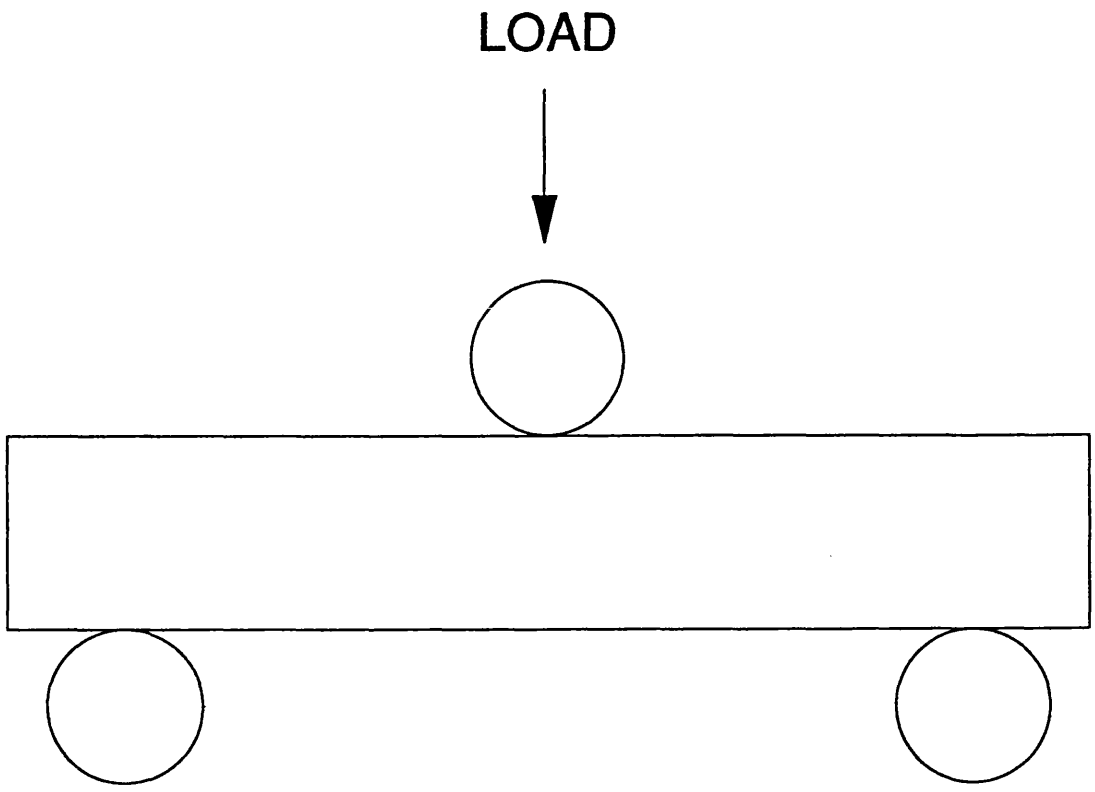


Figure 37. Transverse bend testing

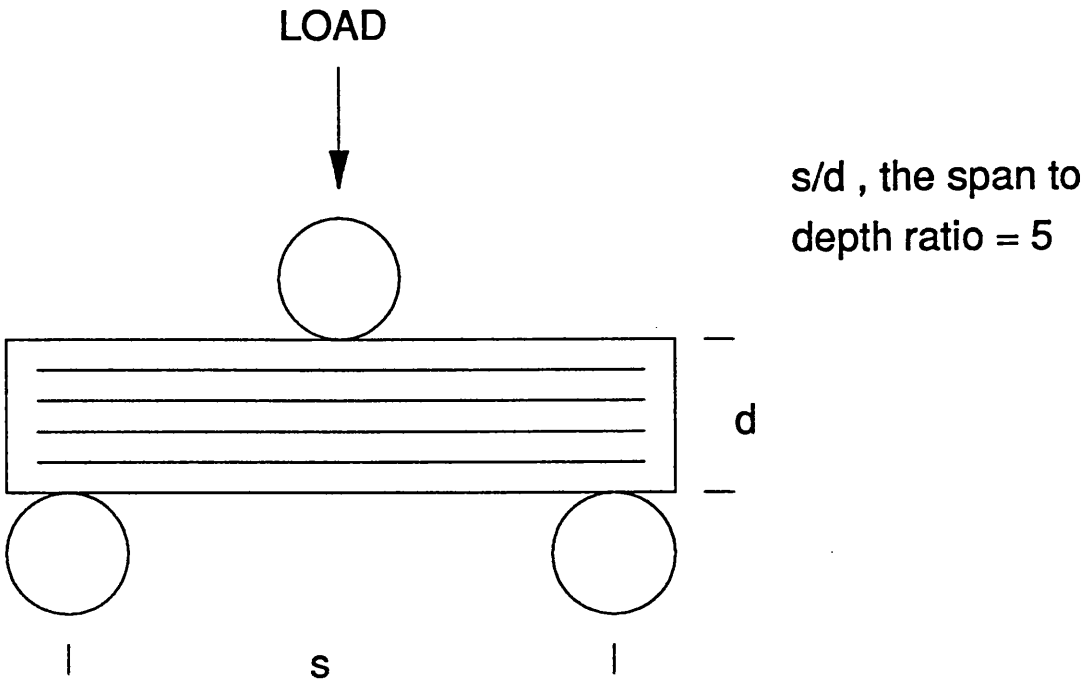


Figure 38. Short beam shear test

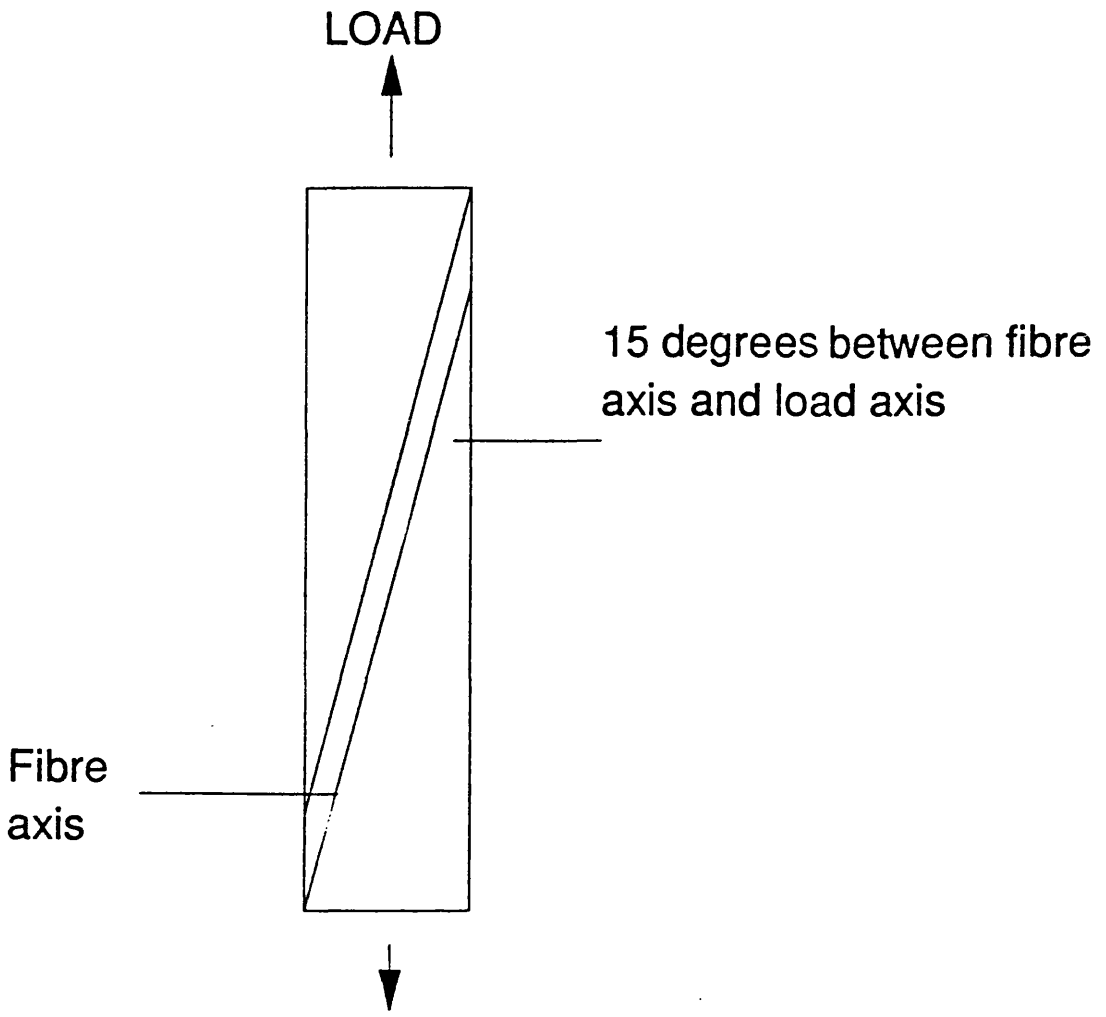


Figure 39. 15° off axis test

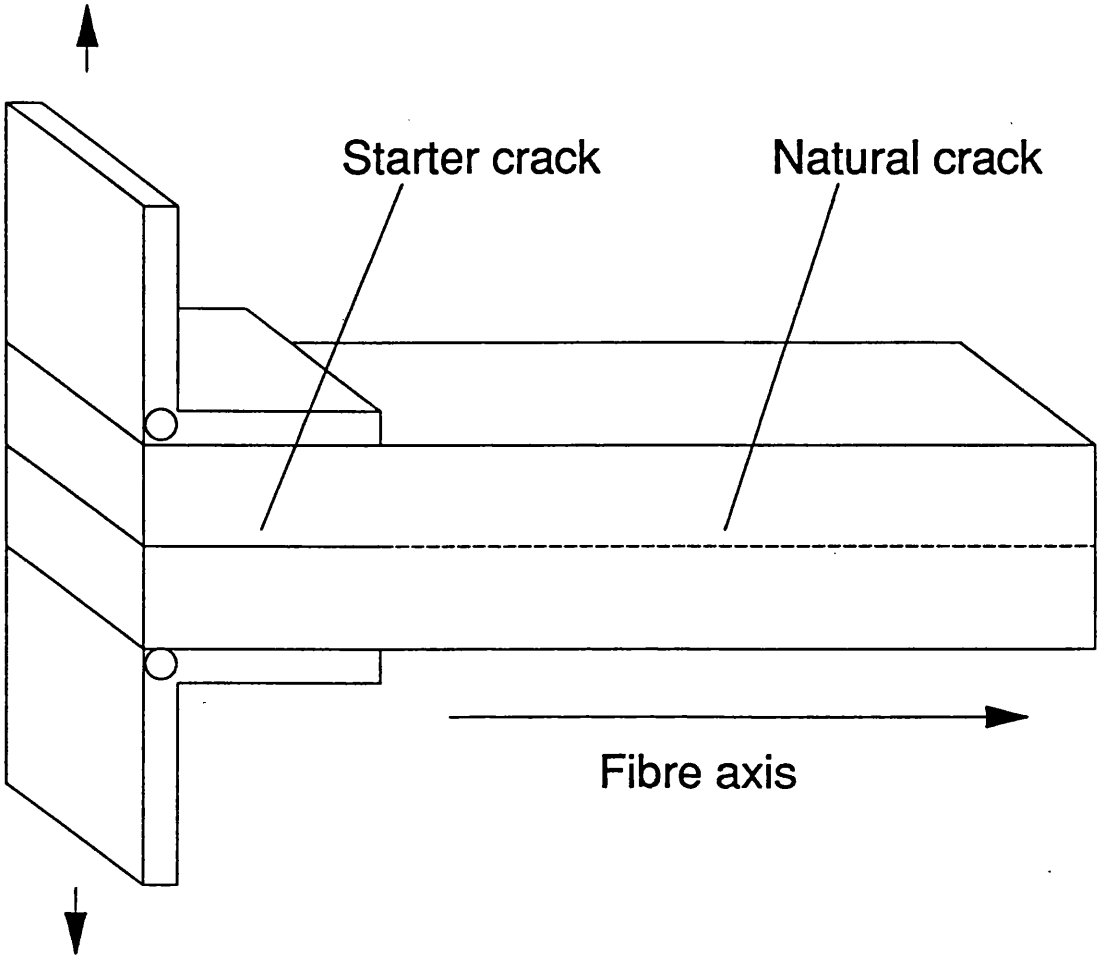


Figure 40. Interlaminar double cantilever beam test

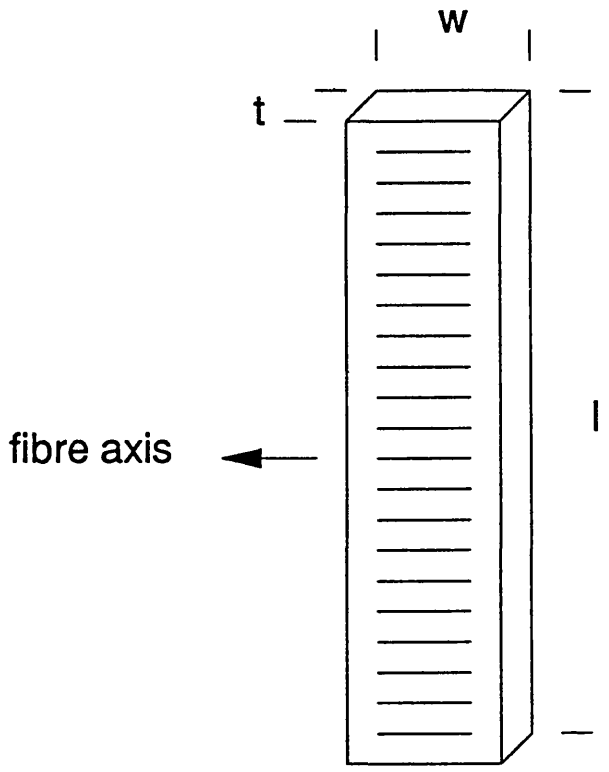


TENSION
l = 90 mm
w = 20 mm
t = 2.5 mm

BENDING
l = 90 mm
w = 10 mm
t = 2.5 mm

Figure 41. Dimensions of transverse test sample

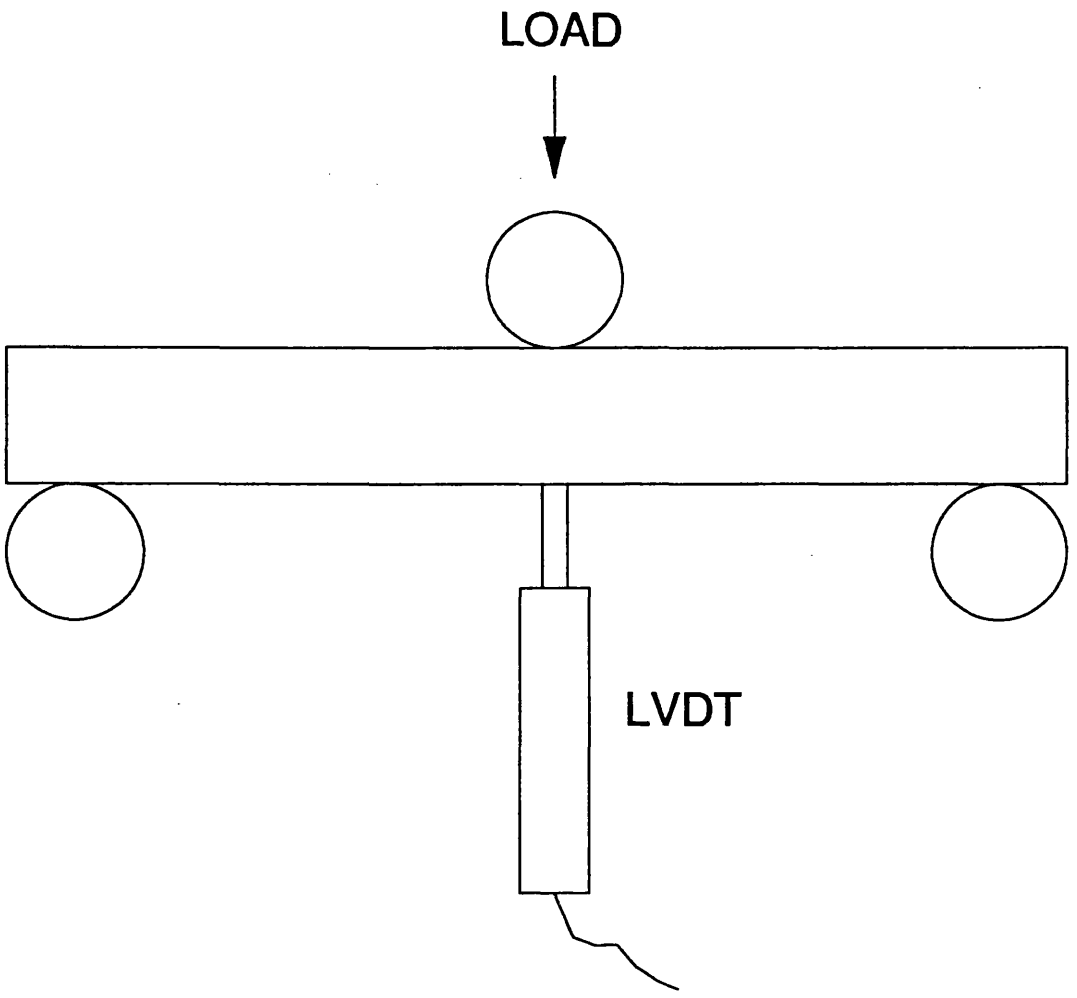


Figure 42. Position of LVDT in bend testing

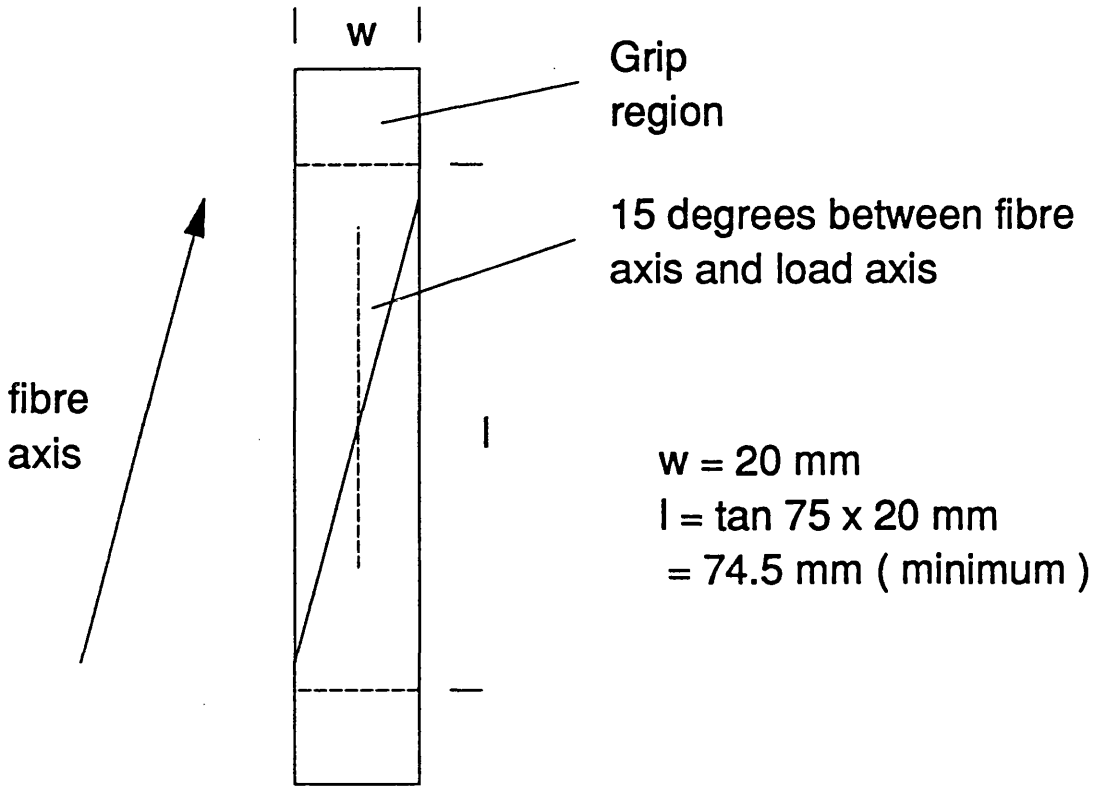


Figure 43. Dimensions of 15° off axis test sample

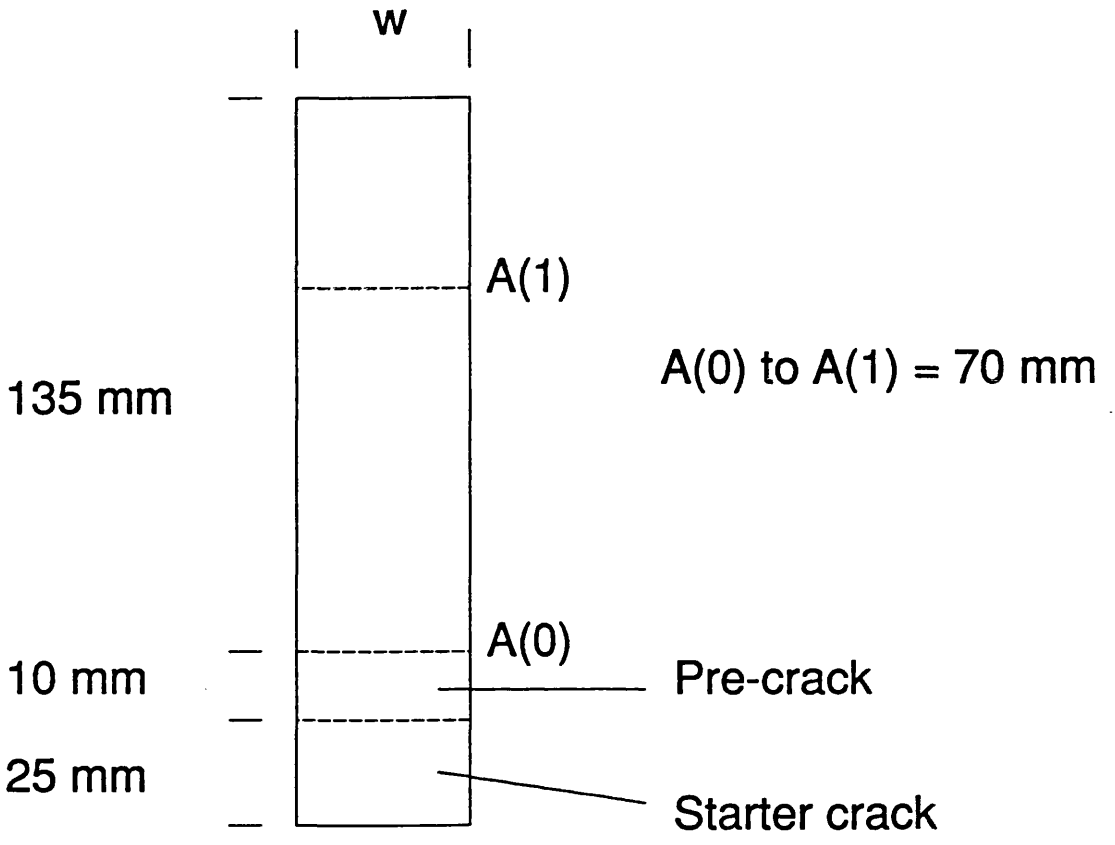


Figure 44. Dimensions of DCB test sample

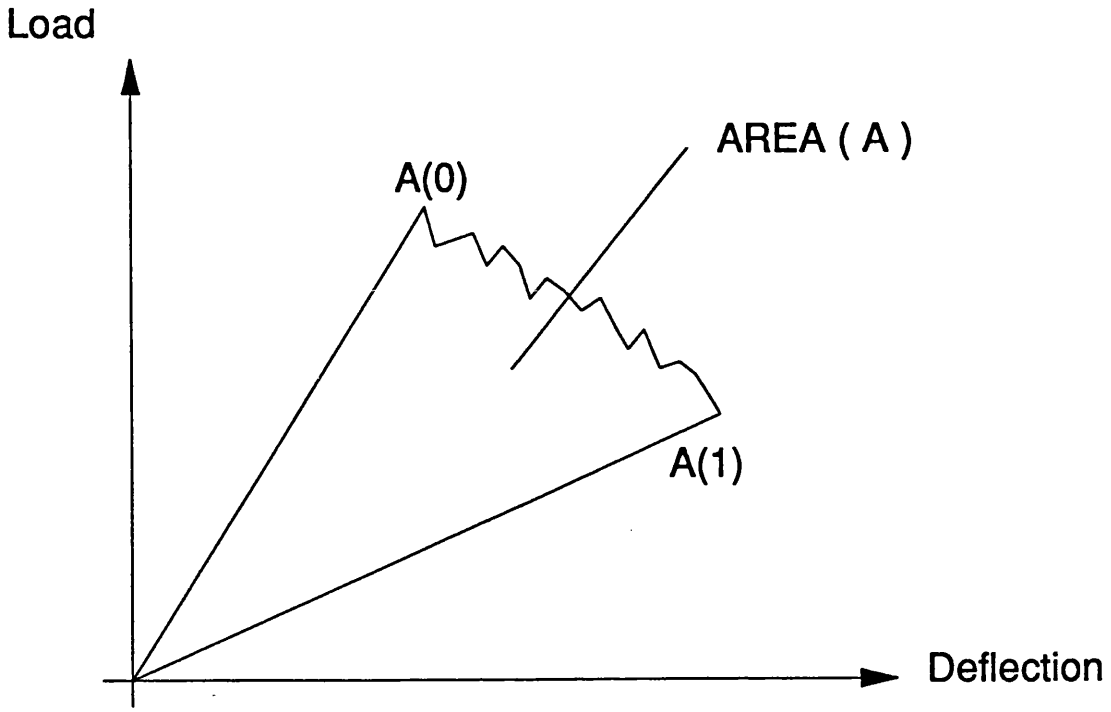


Figure 45. Typical plot from DCB test

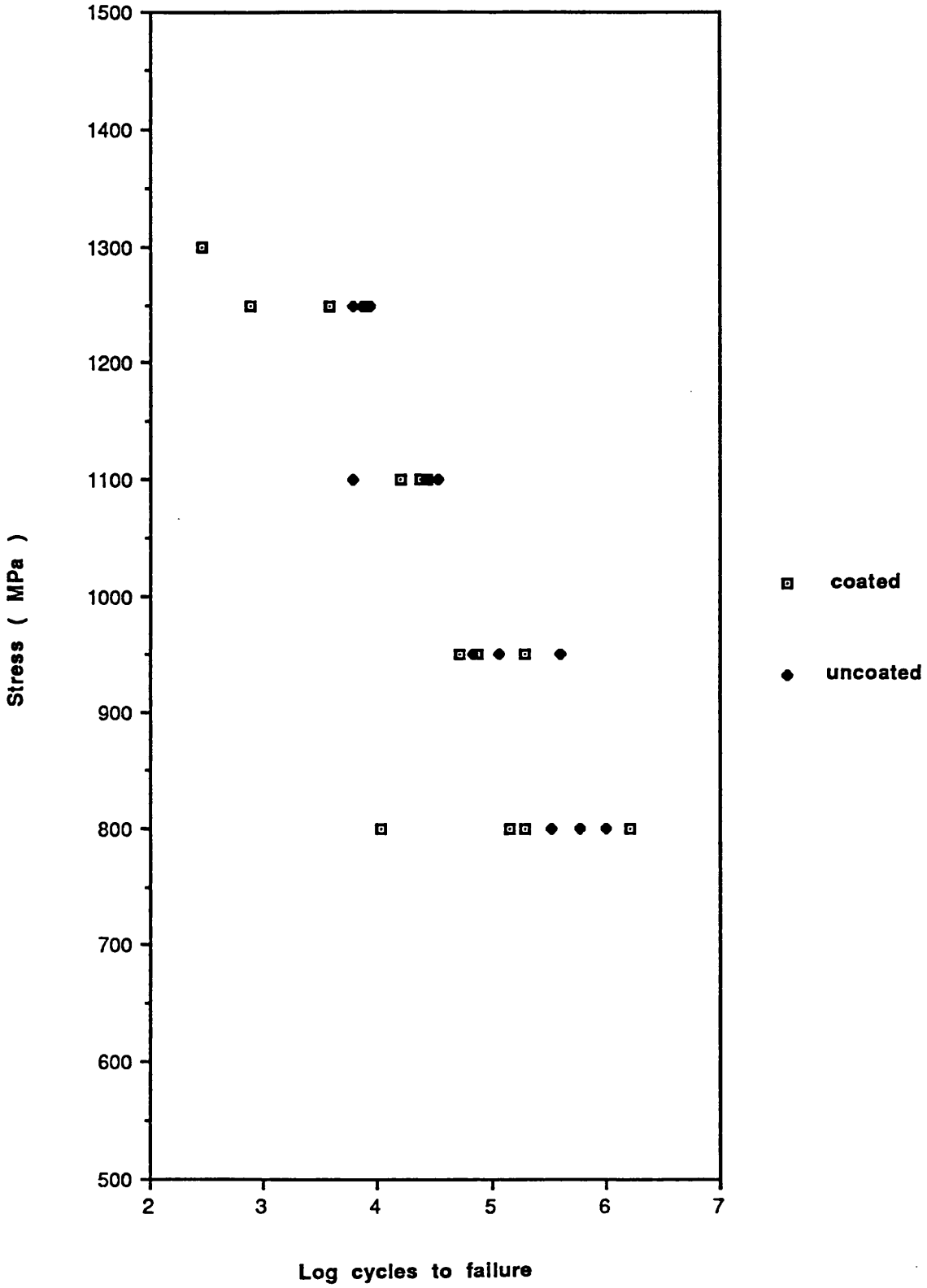


Figure 46. S-n curve from longitudinal fatigue testing

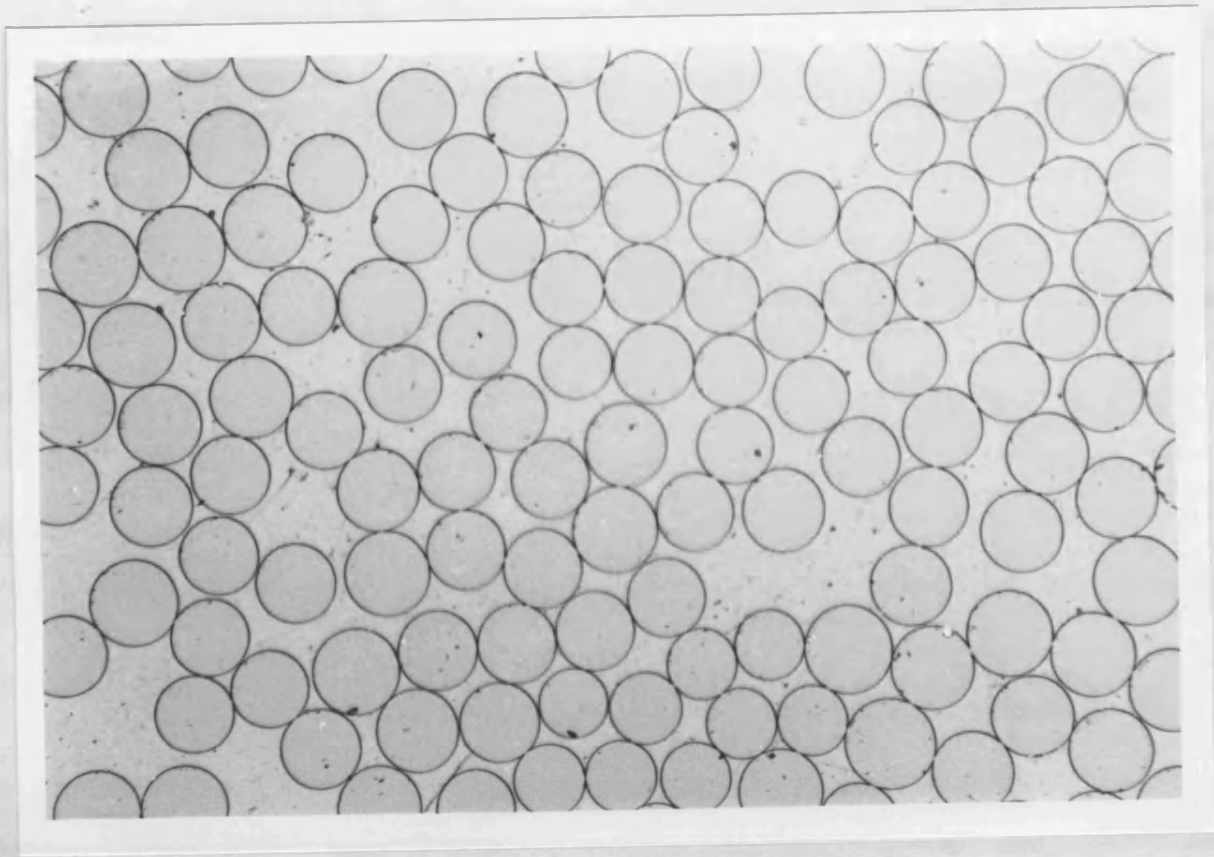

Figure 47. Cross section through uncoated fibre composite ( X 400 )

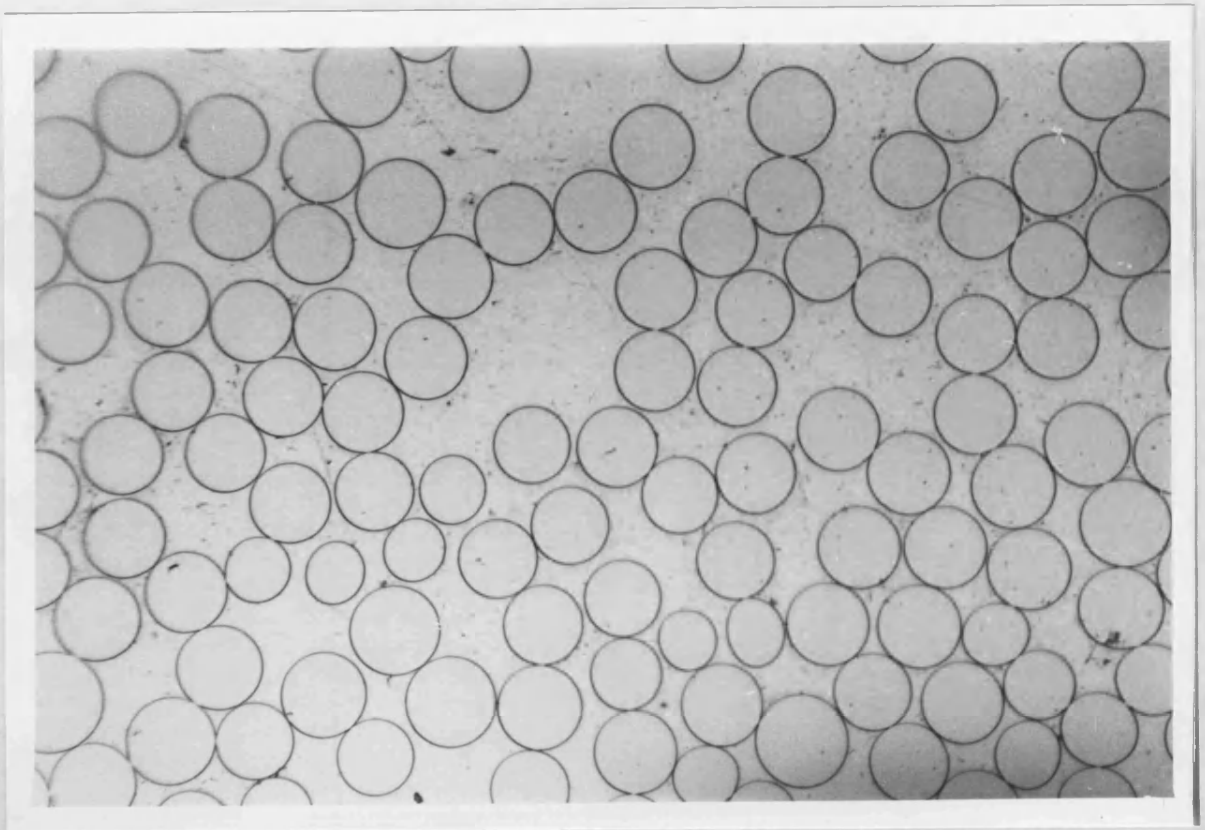

Figure 48. Cross section through coated fibre composite ( X400 )

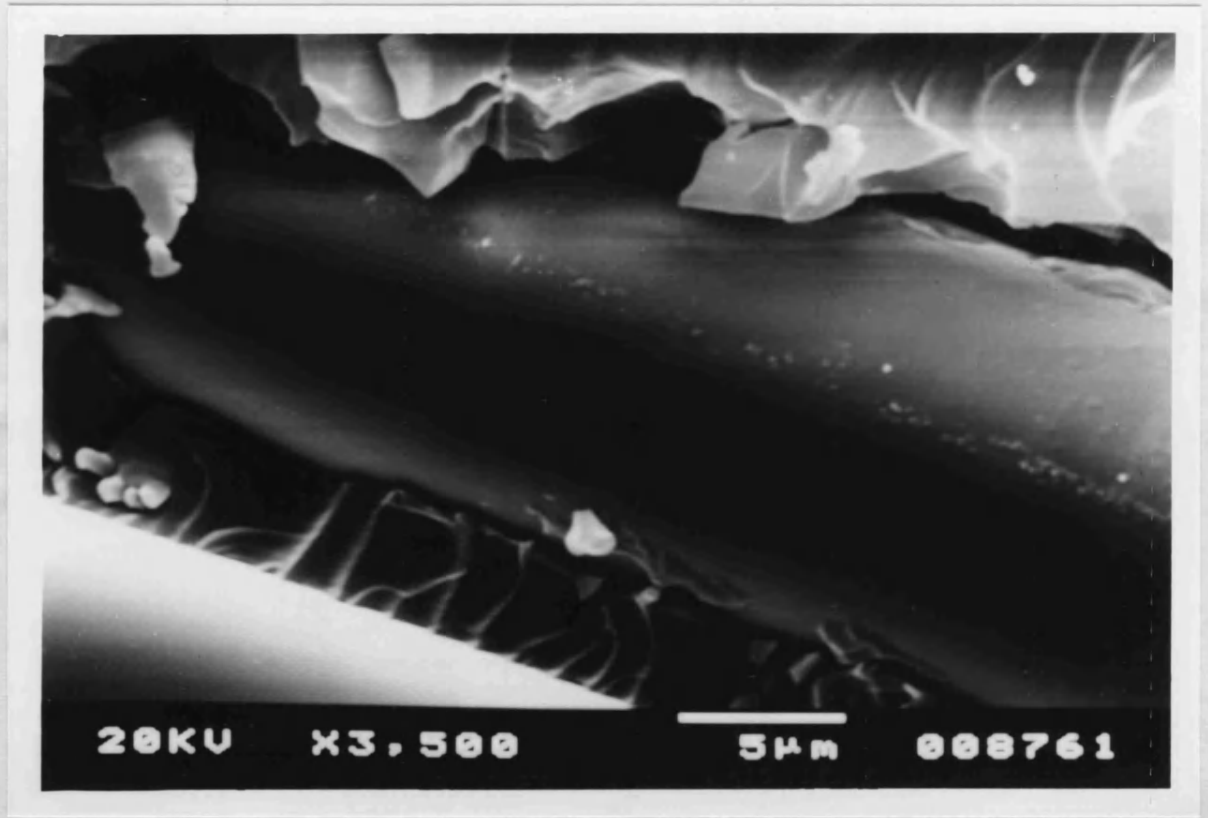


Figure 49. Transverse tensile fracture surface for the uncoated fibre composite


Figure 50. Transverse tensile fracture surface for the coated fibre composite

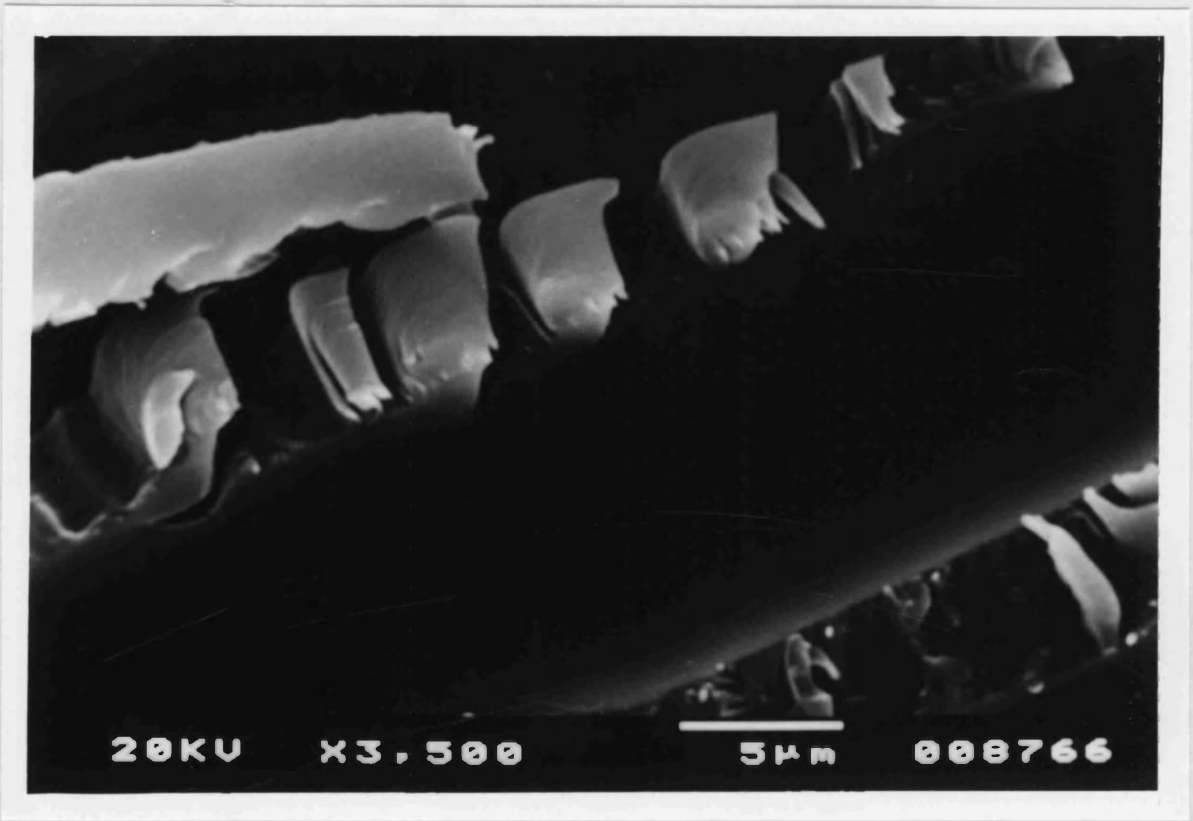


Figure 51. 15° off axis fracture surface for the uncoated fibre composite

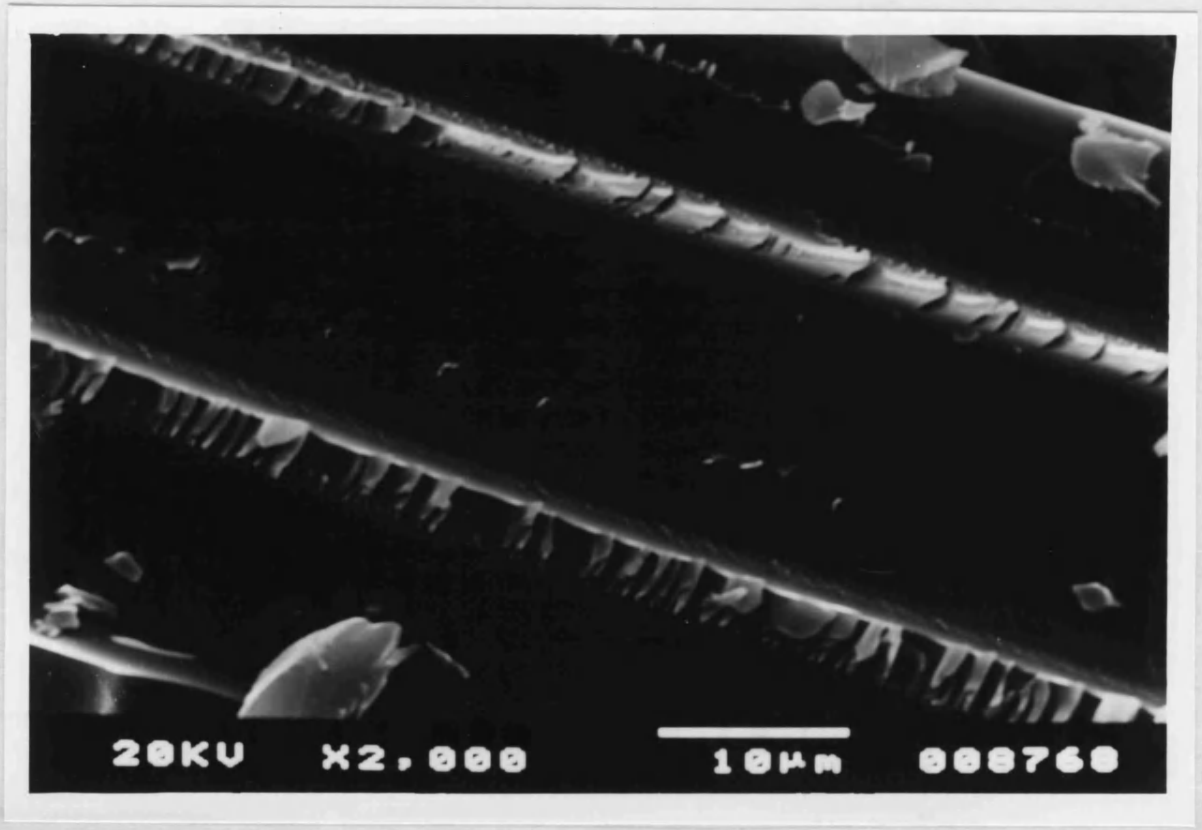


Figure 52. 15° off axis fracture surface for the coated fibre composite

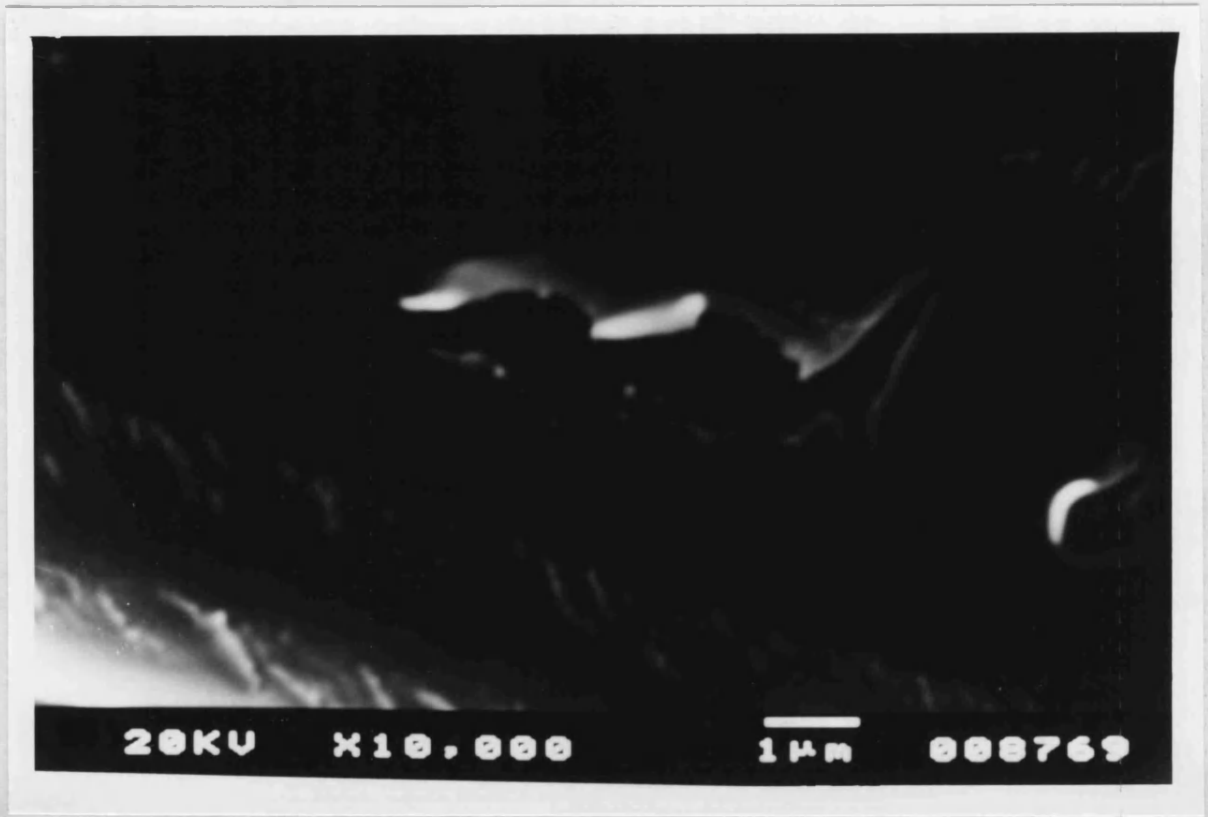


Figure 53. Close up of damaged area in figure 52

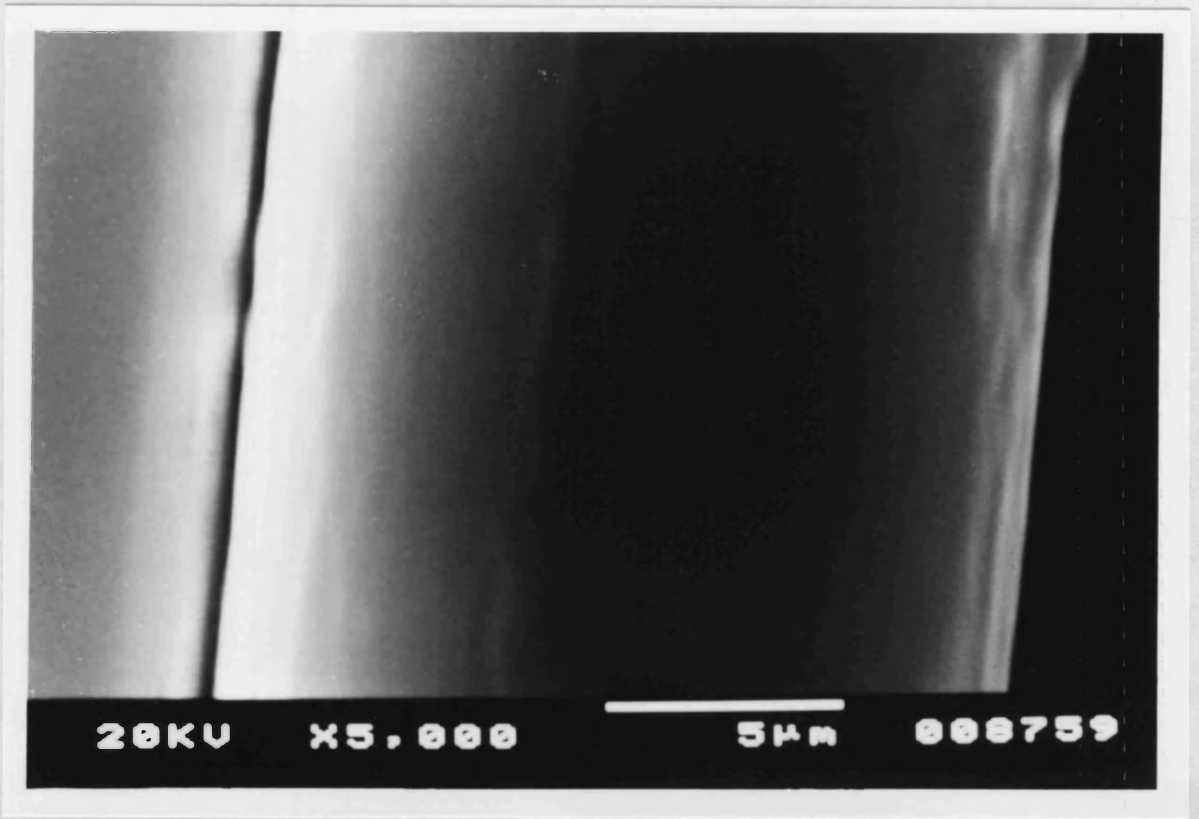


Figure 54. Coated single fibres

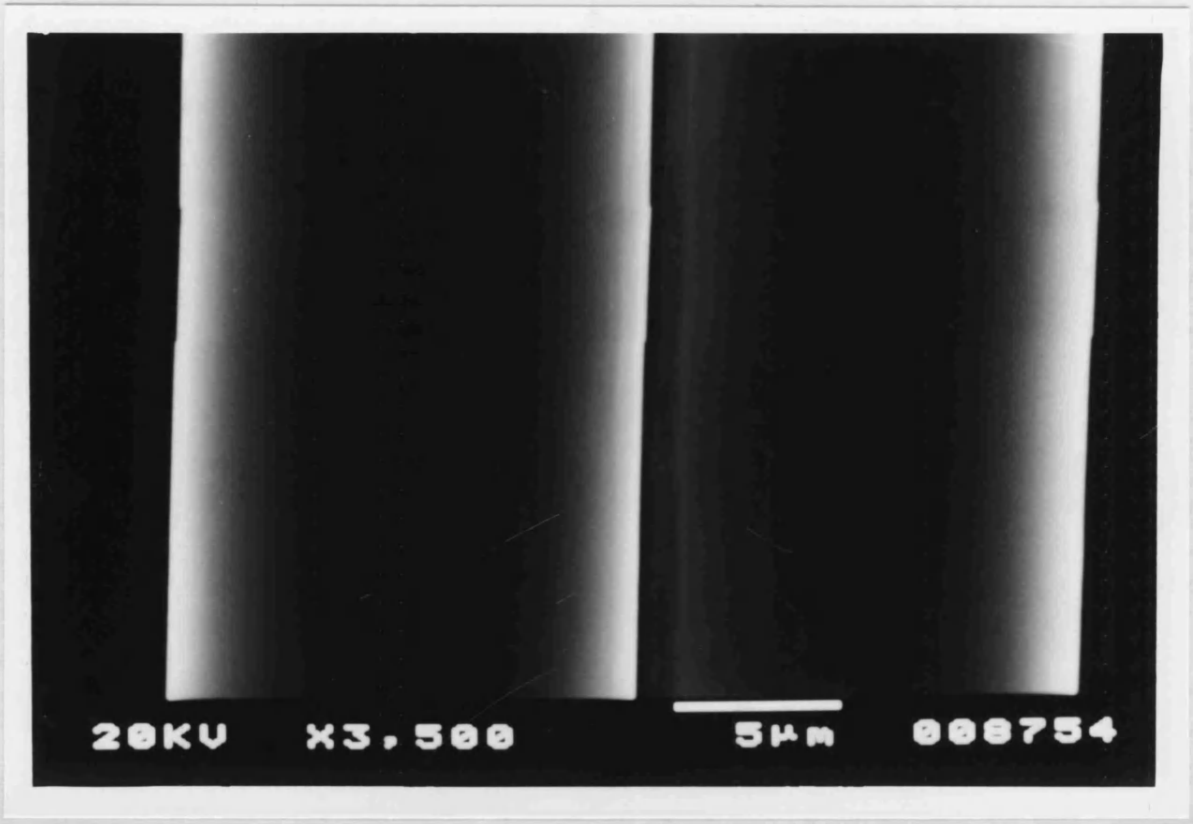


Figure 55. Uncoated single fibres

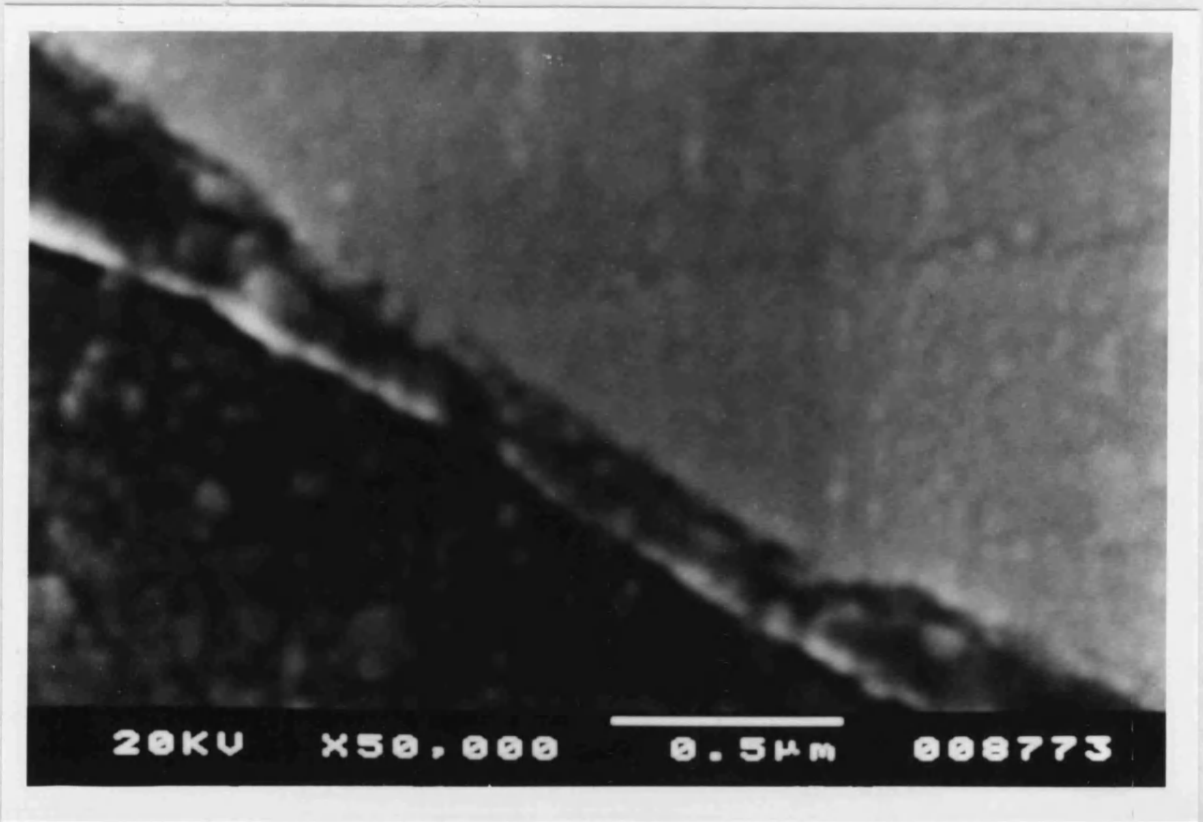


Figure 56. Cross section of coated fibre composite

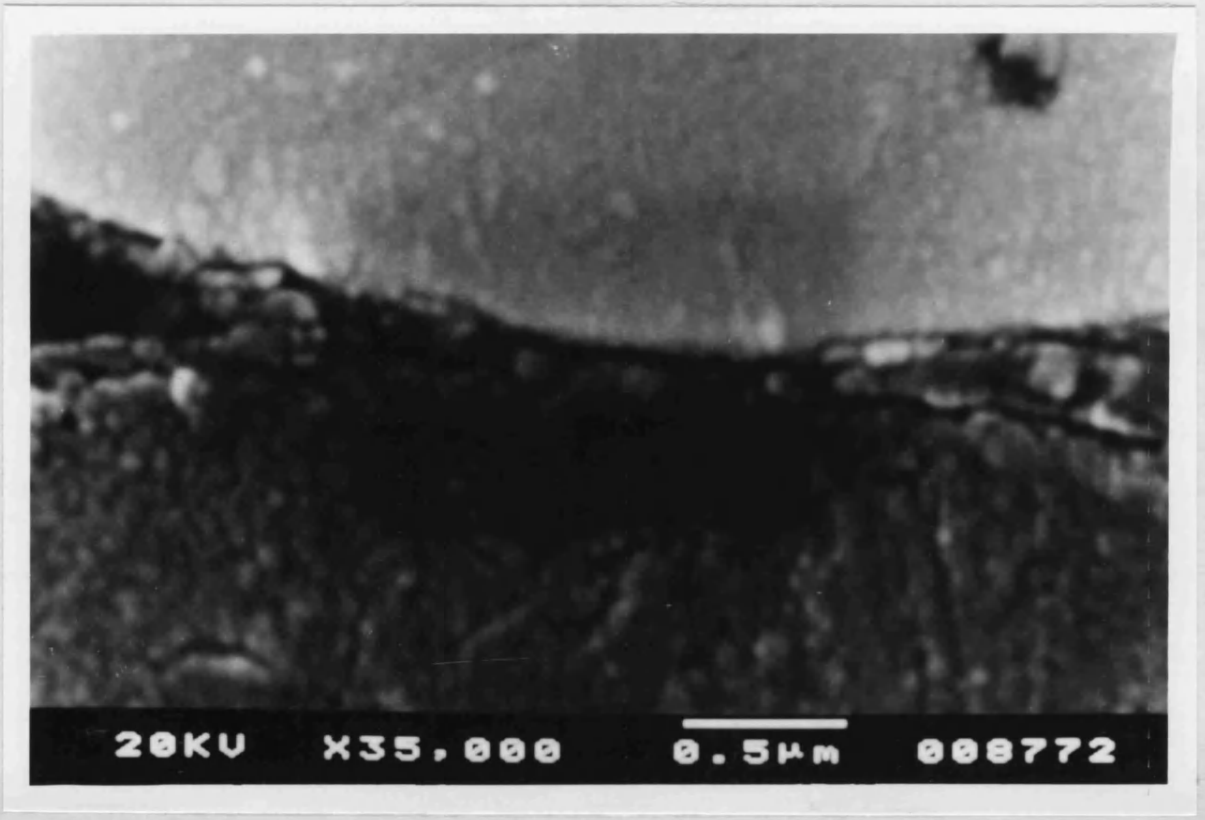


Figure 57. Cross section of uncoated fibre composite

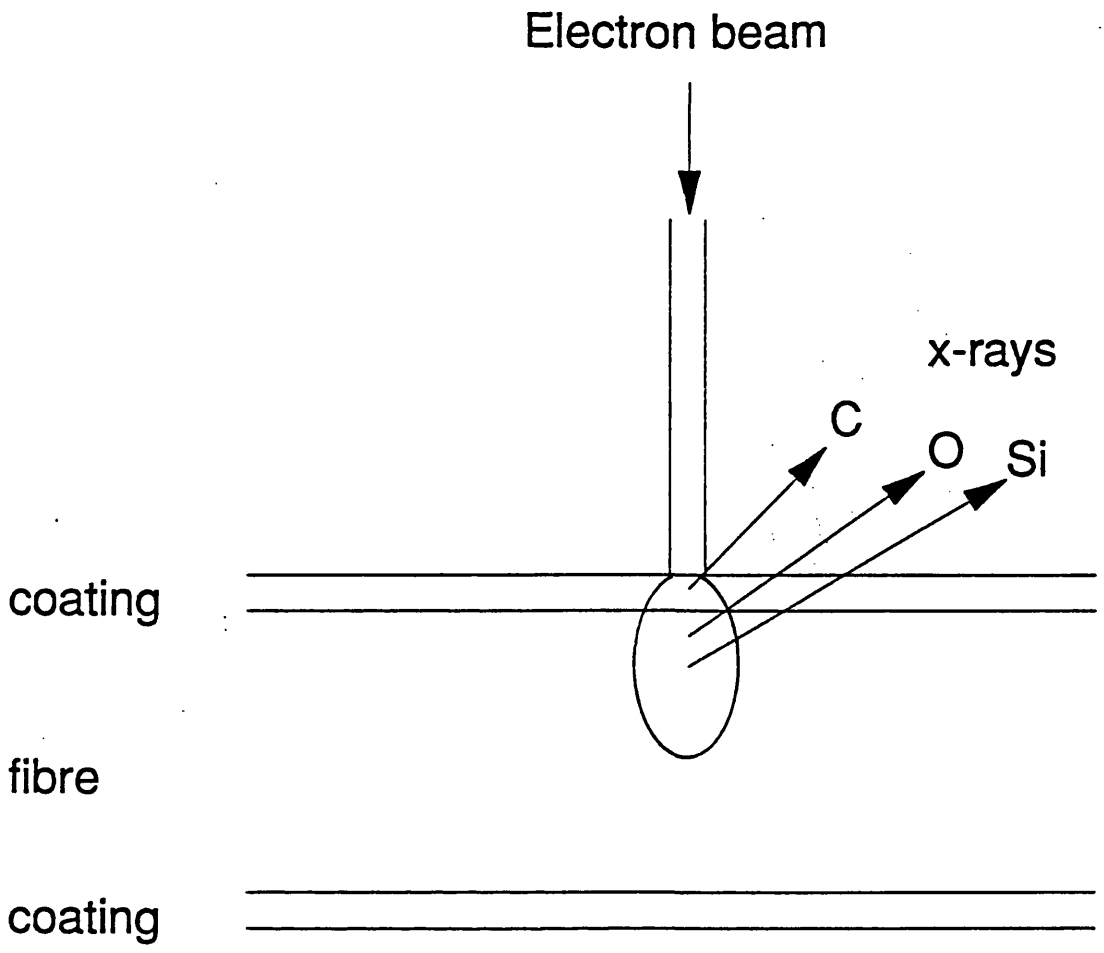


Figure 58. Electron beam producing x-rays

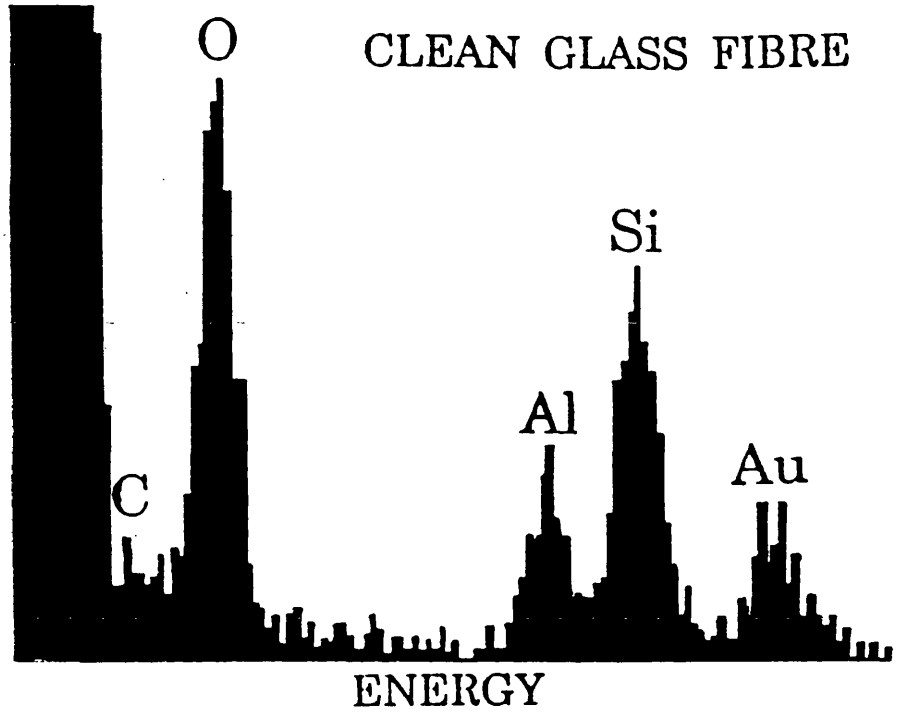


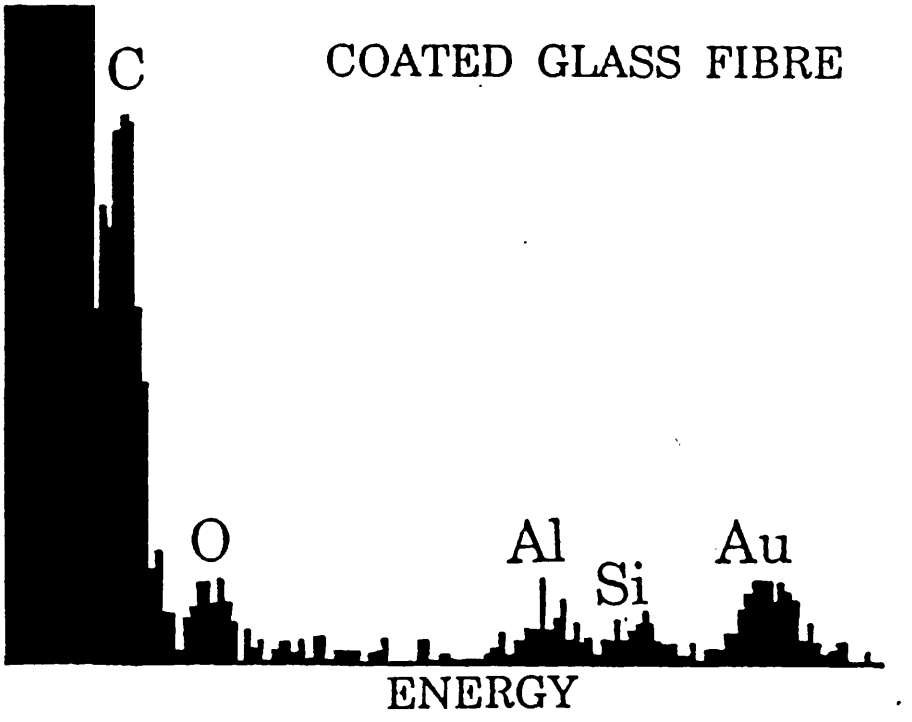


Figure 59. X-ray spectra from coated and uncoated fibres

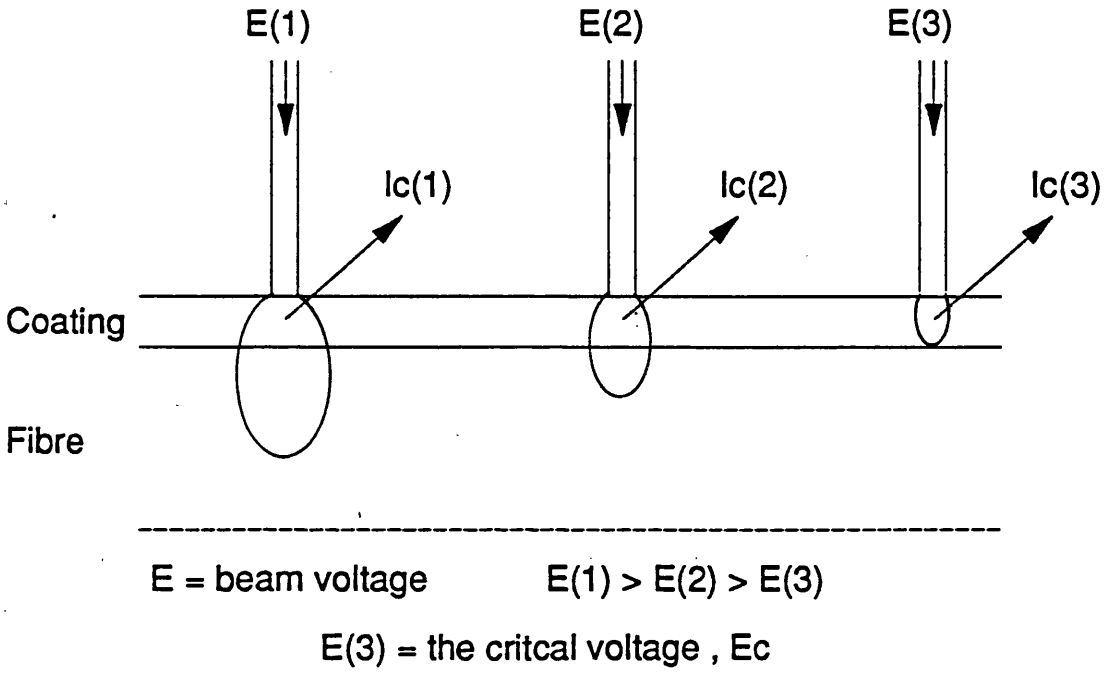


Figure 60. Variation of interaction volume with electron beam voltage

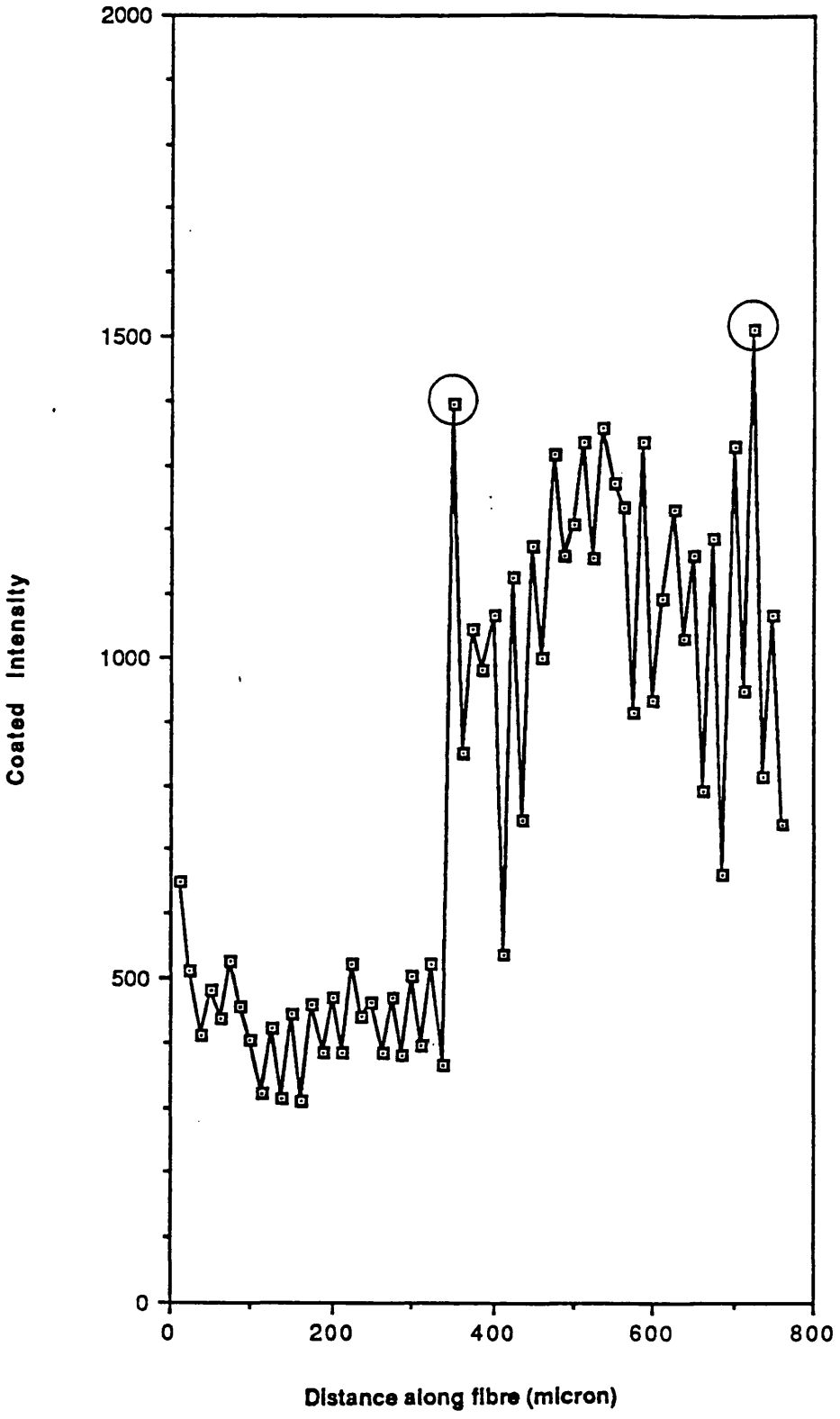


Figure 61. Carbon peak intensity versus position along coated fibre measured at 10 KeV beam voltage

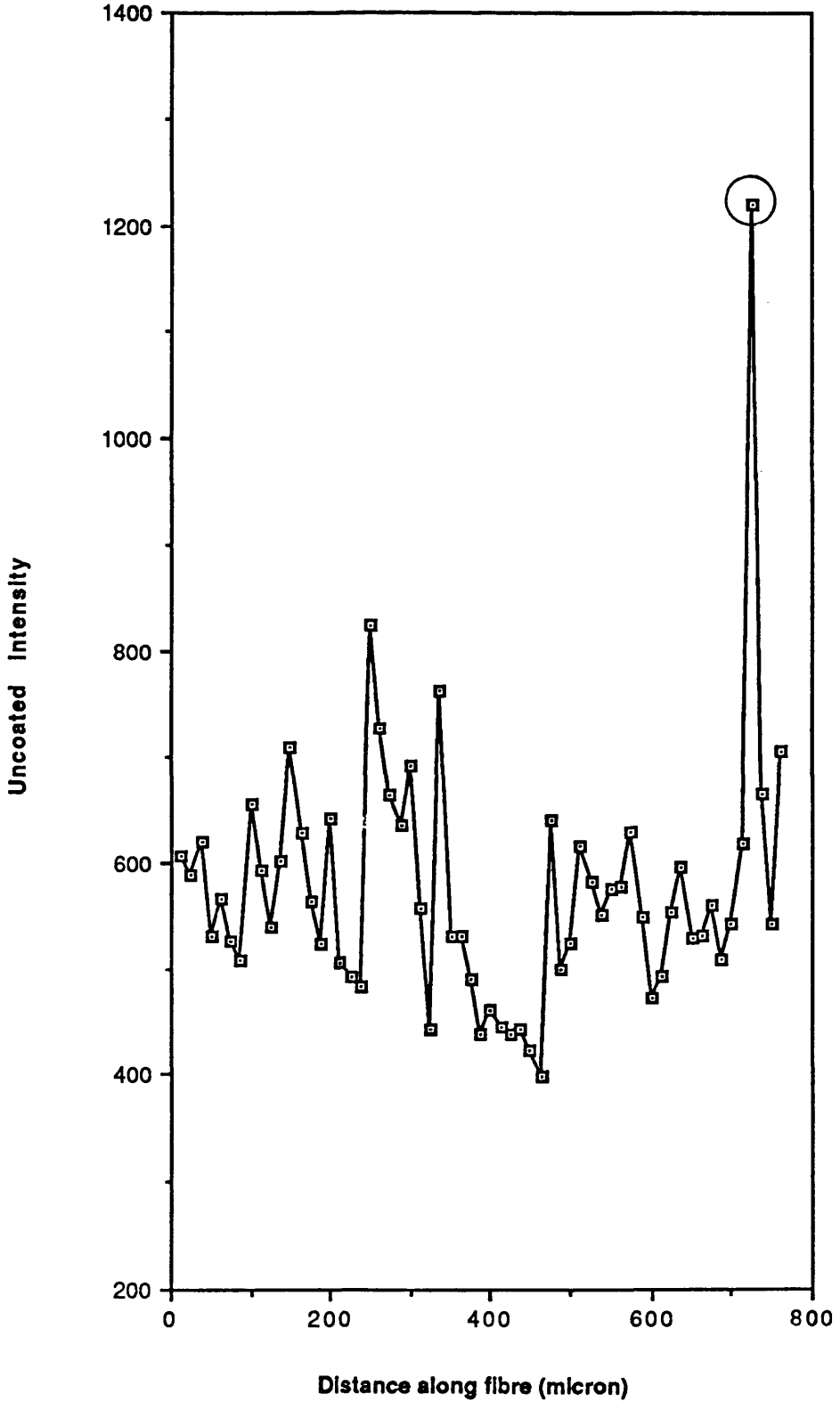


Figure 62. Carbon peak intensity versus position along uncoated fibre measured at 10 KeV beam voltage

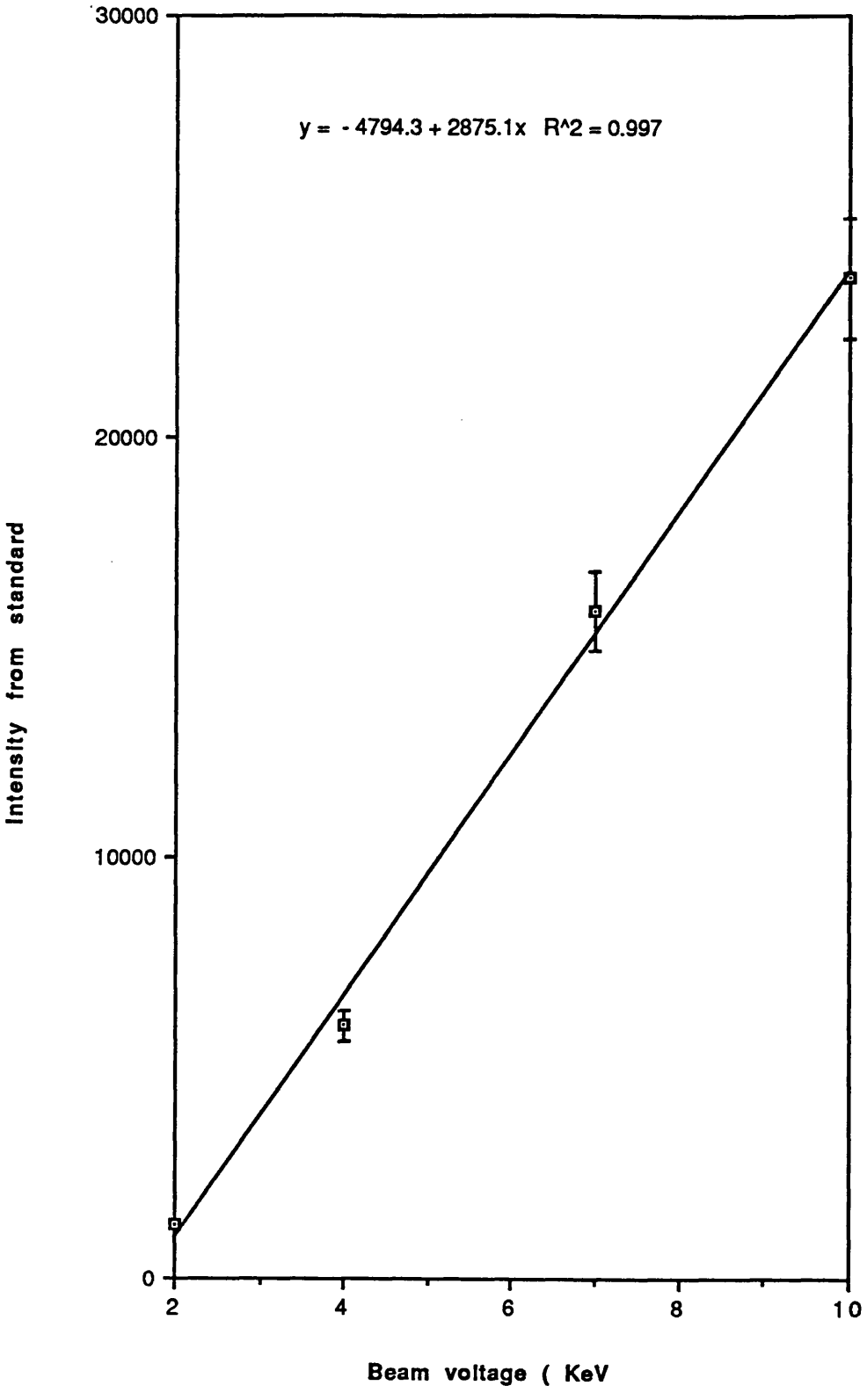


Figure 63. Carbon peak intensity from standard versus beam voltage

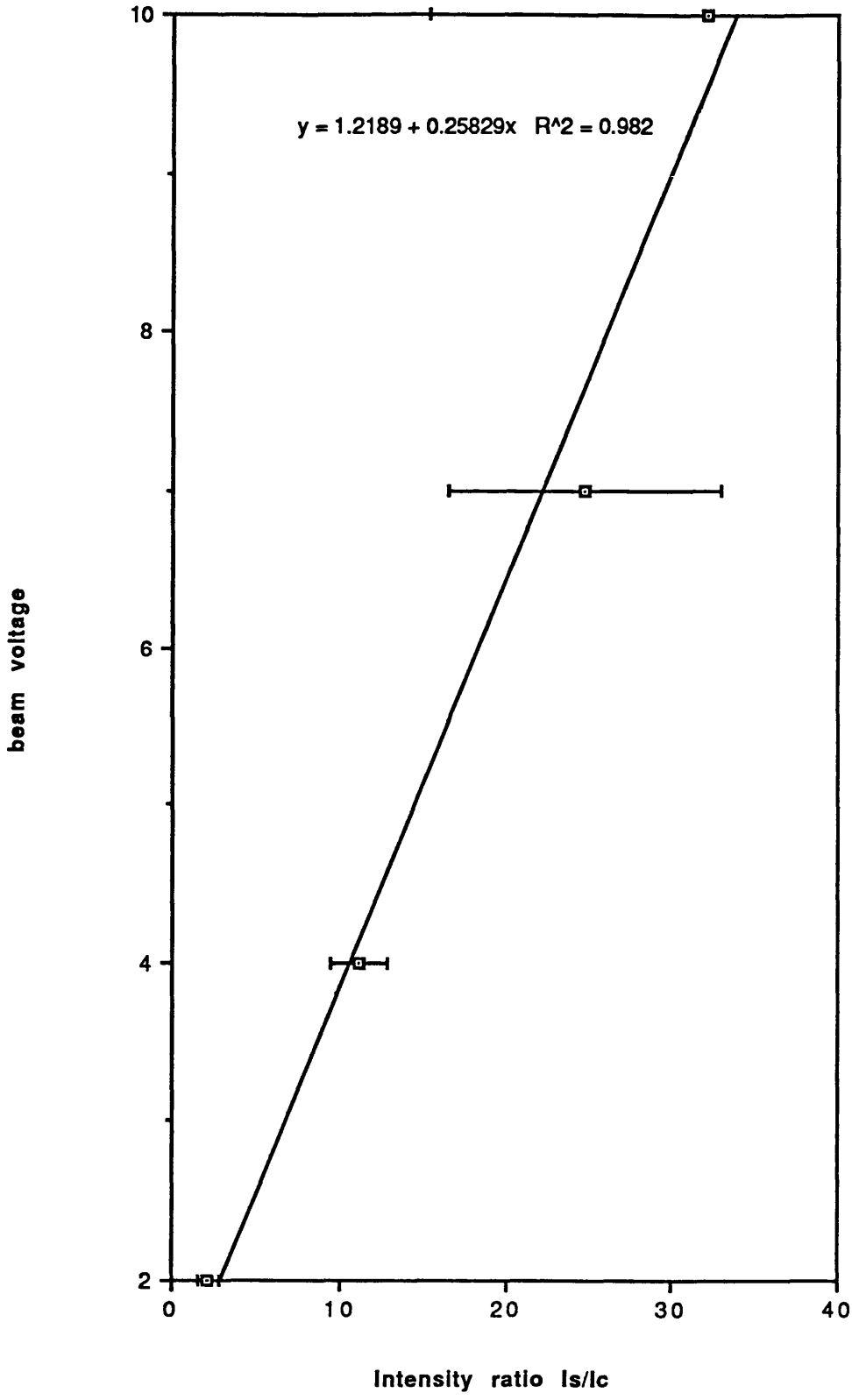


Figure 64. Standard to coating intensity ratio versus beam voltage

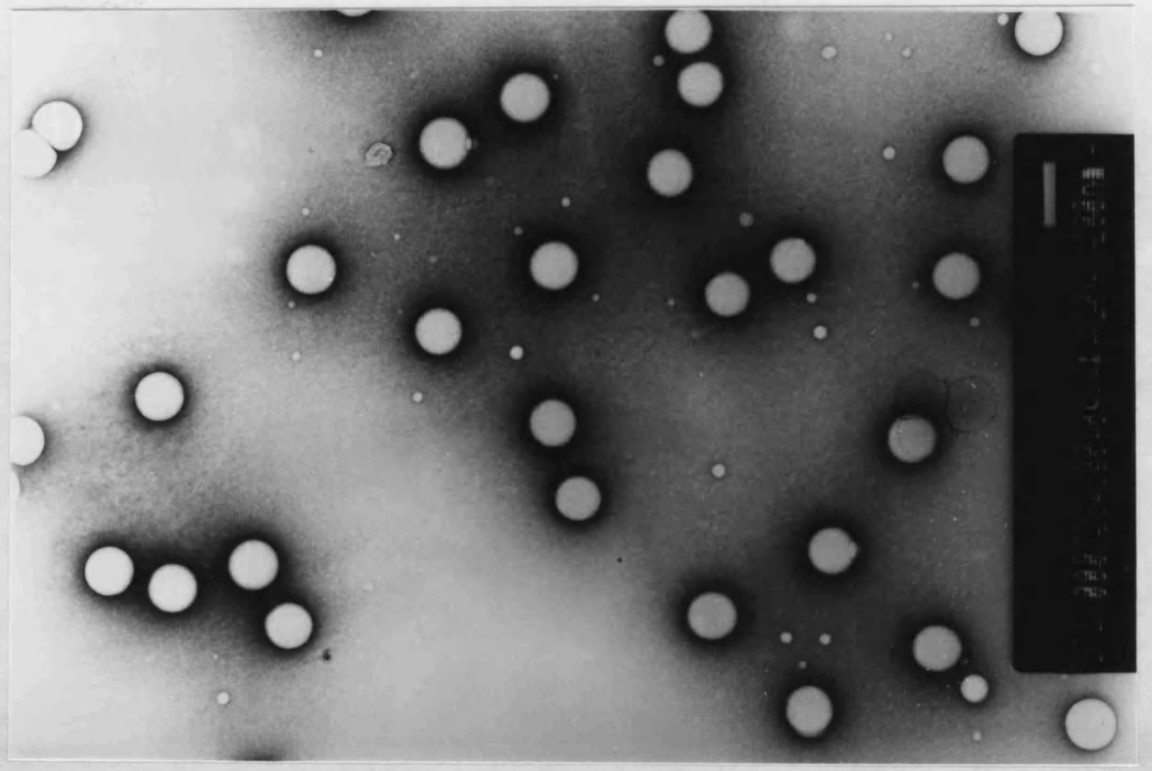

Figure 65. Transmission electron micrograph of latex particles

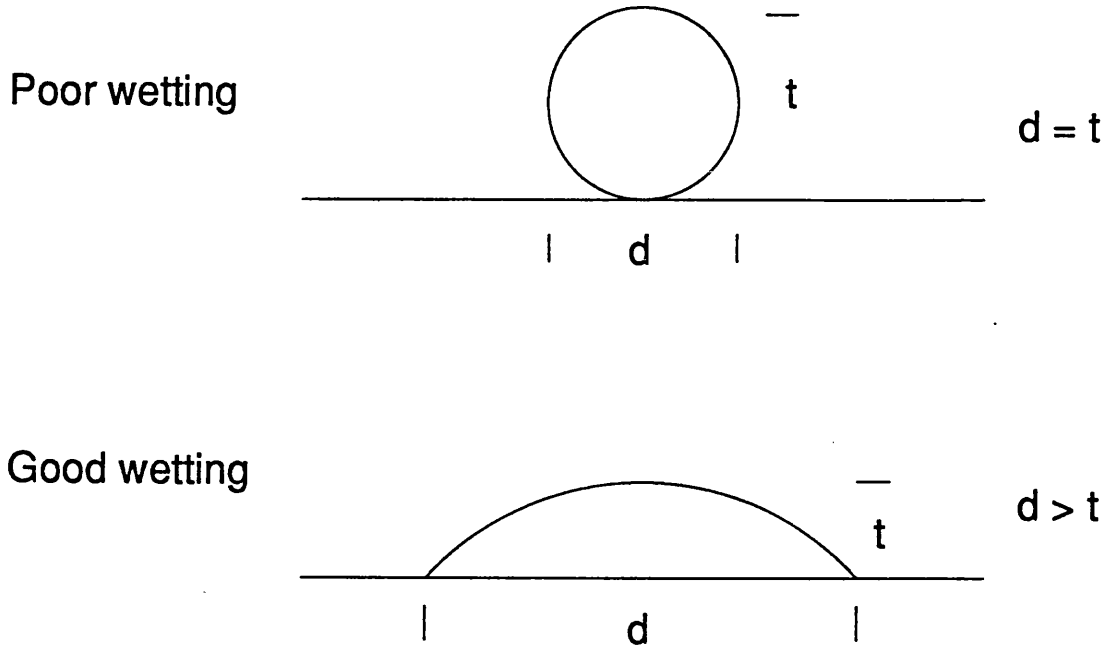


Figure 66. Schematic side view of latex particles

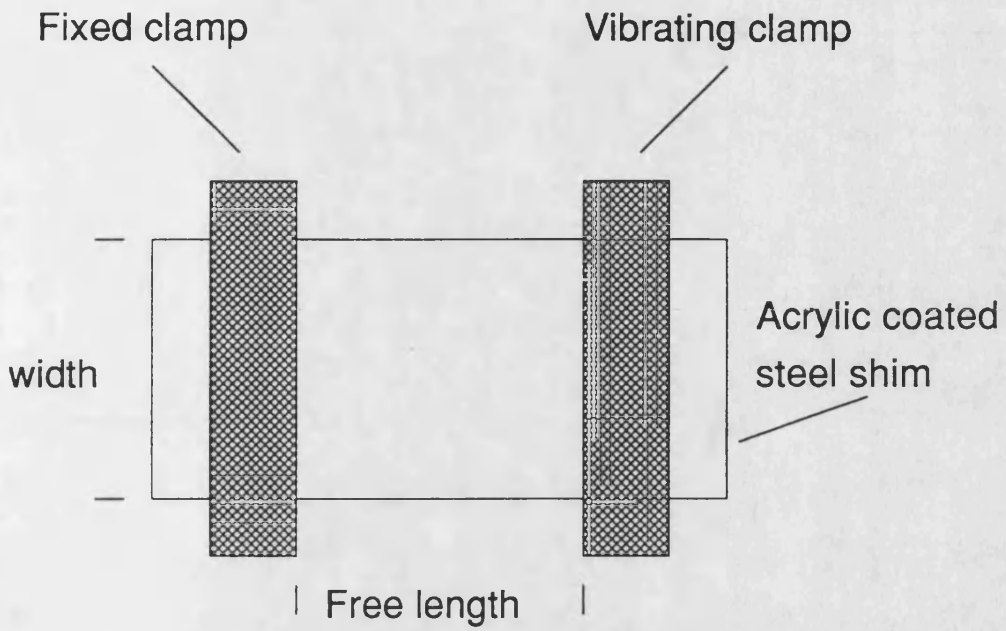


Figure 67. Arrangement for determining the coating tensile modulus

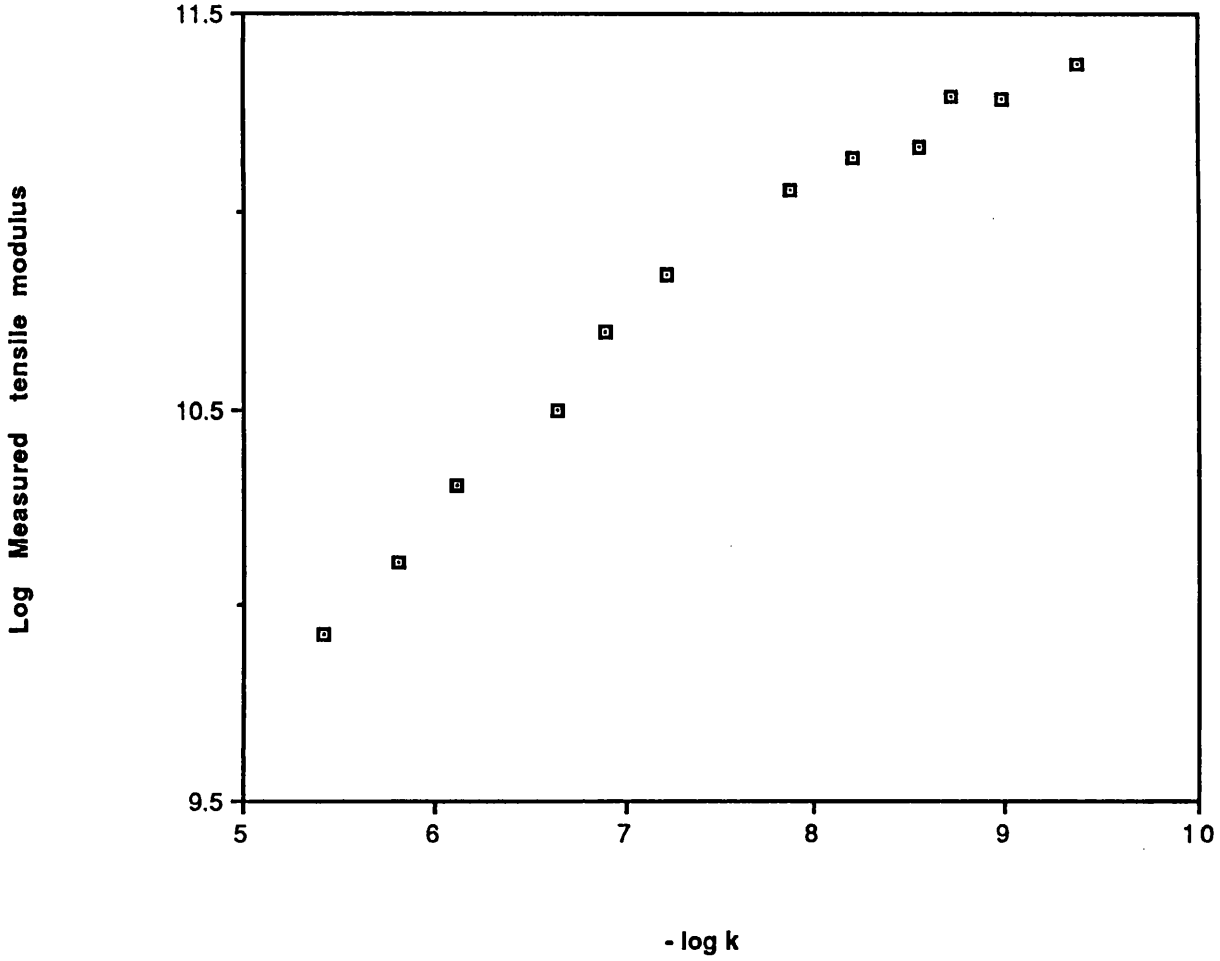


Figure 68. Steel substrate modulus versus variations in geometry

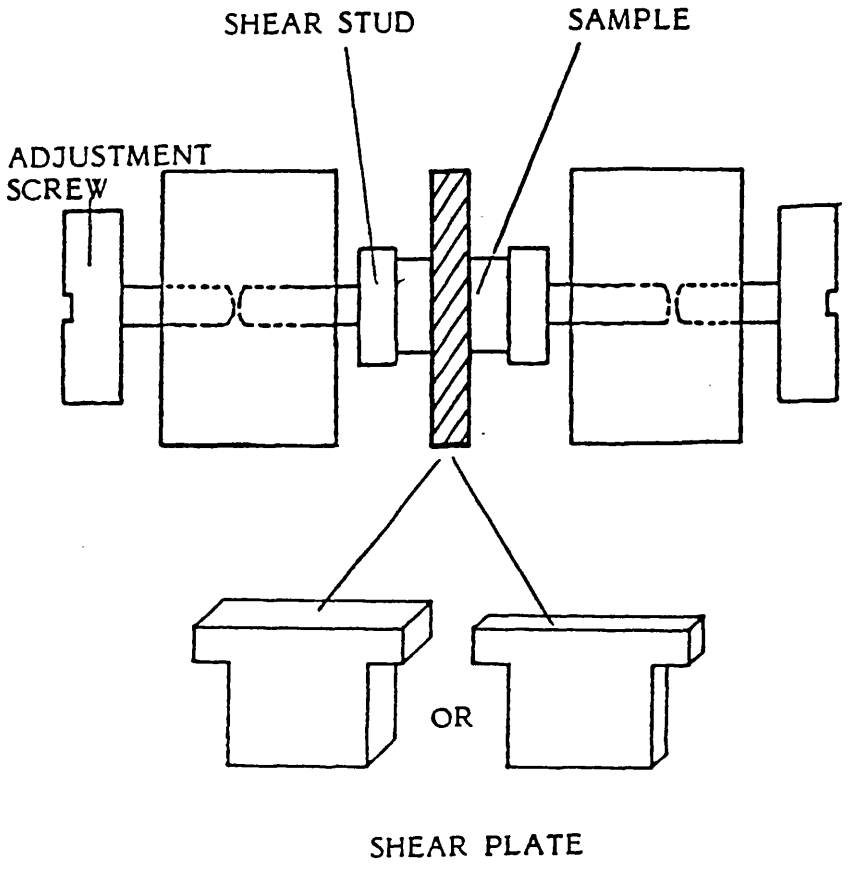


Figure 69. Arrangement for determining the acrylic shear modulus

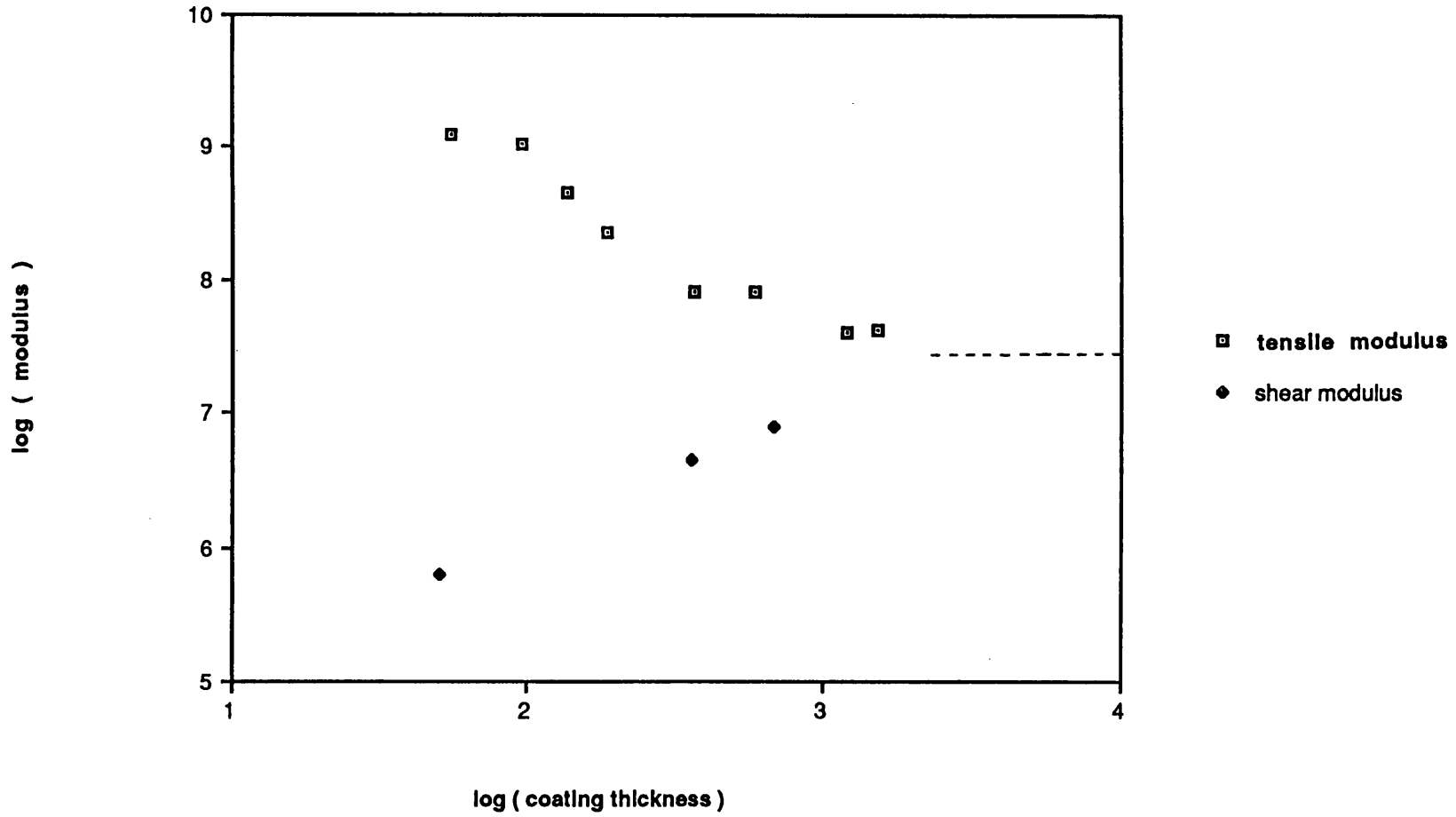


Figure 70. Coating moduli versus coating thickness

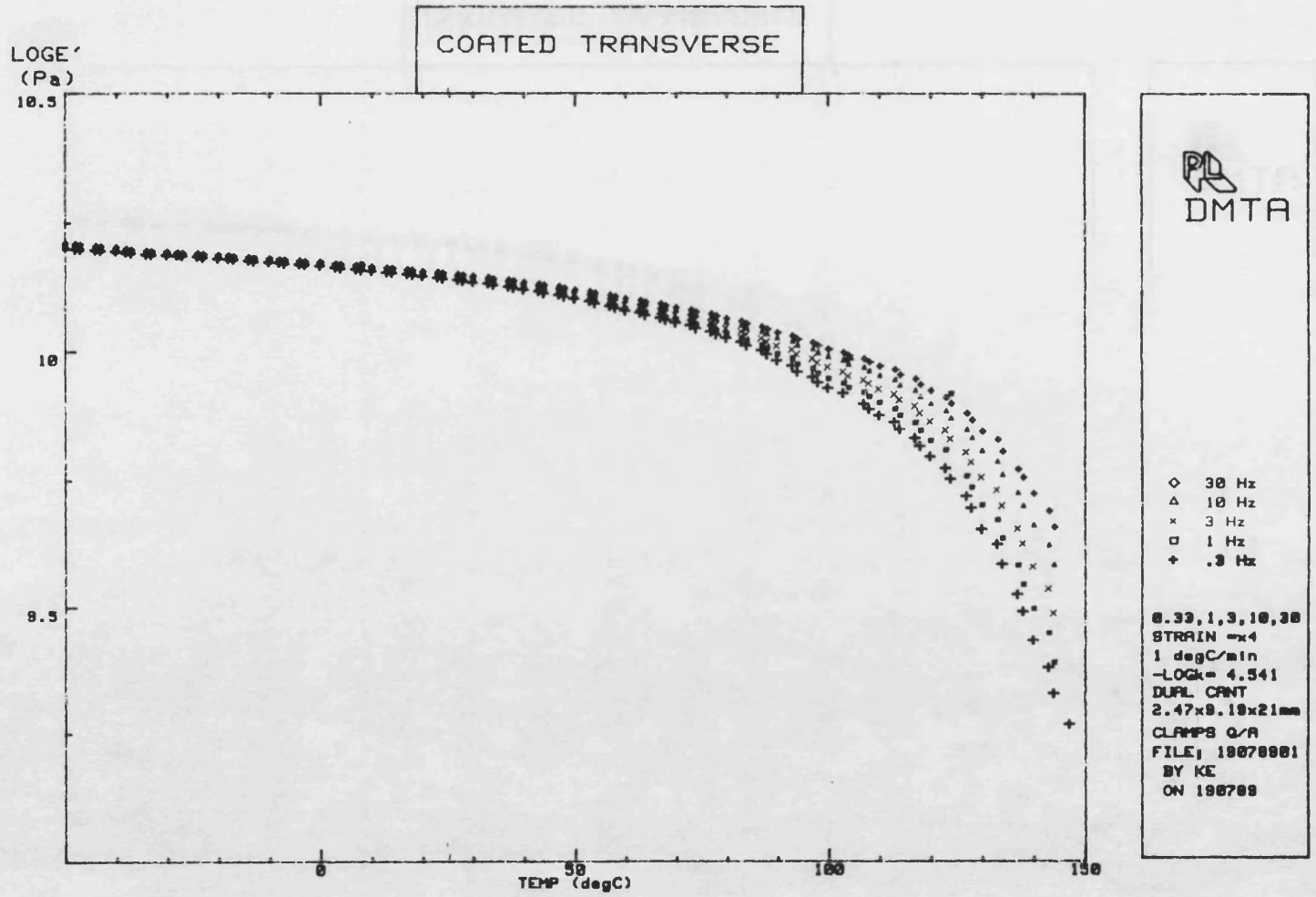


Figure 71. Storage modulus versus temperature for coated fibre composite in transverse bending

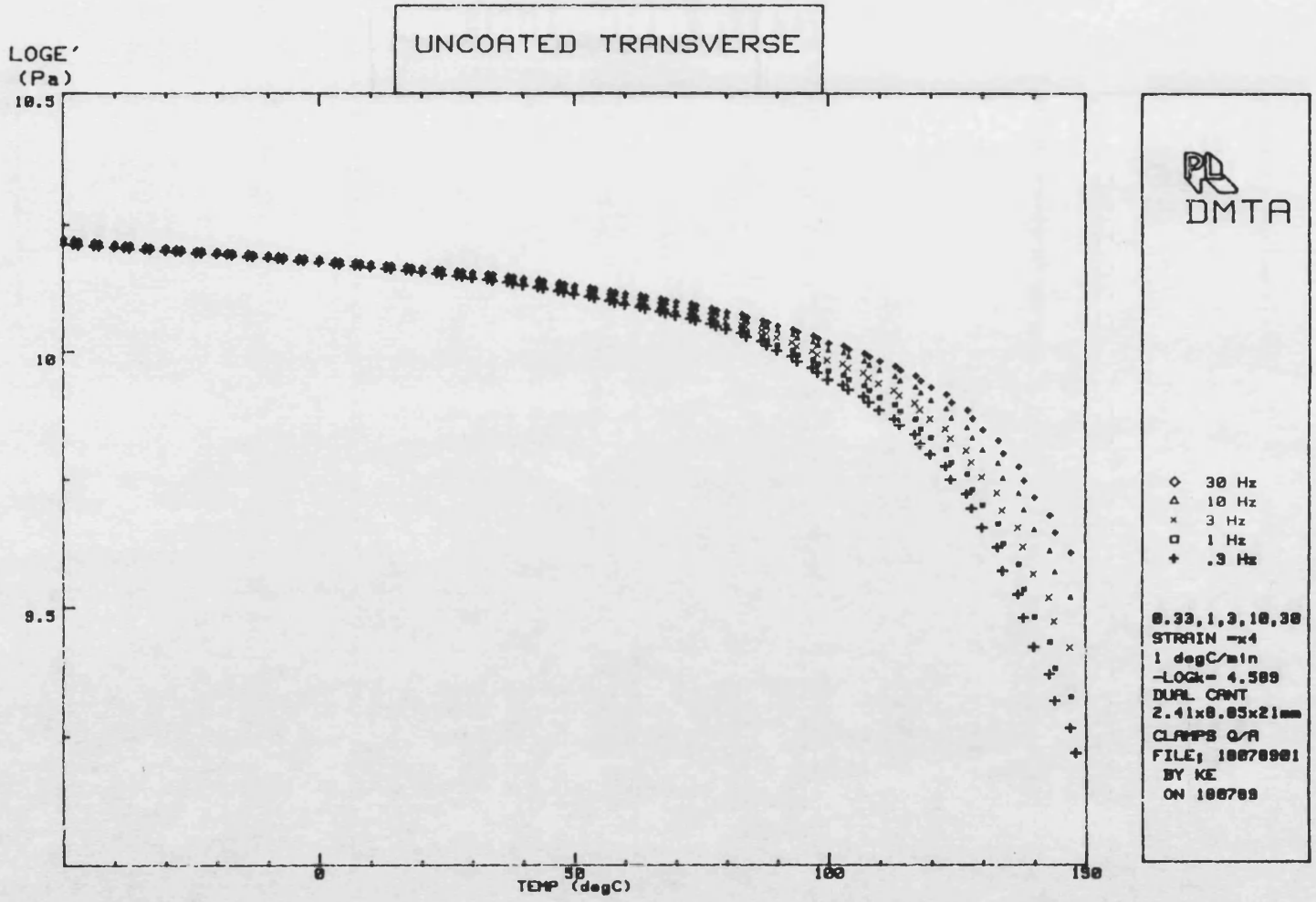


Figure 72. Storage modulus versus temperature for uncoated fibre composite in transverse bending

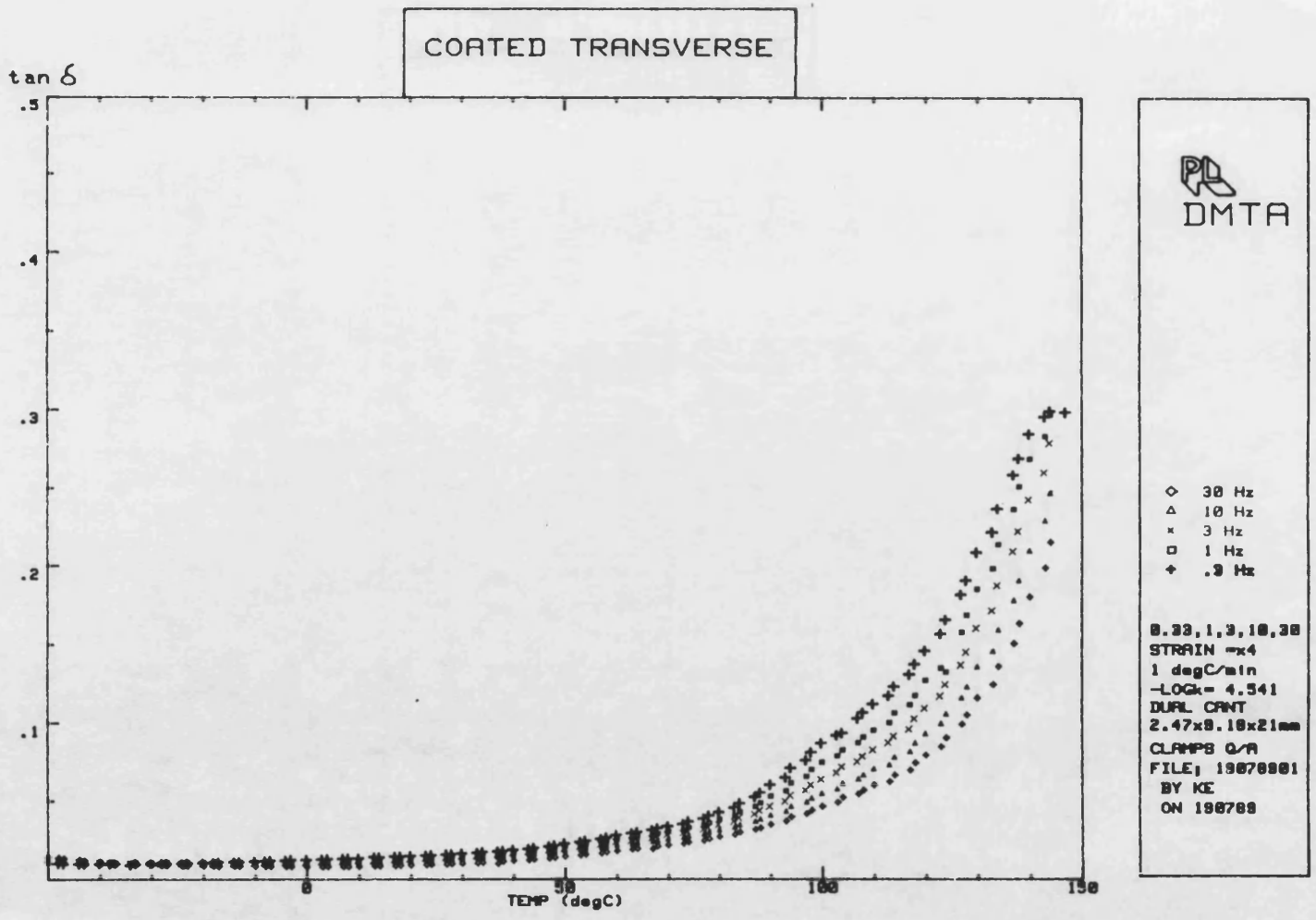


Figure 73. Damping versus temperature for coated fibre composite in transverse bending

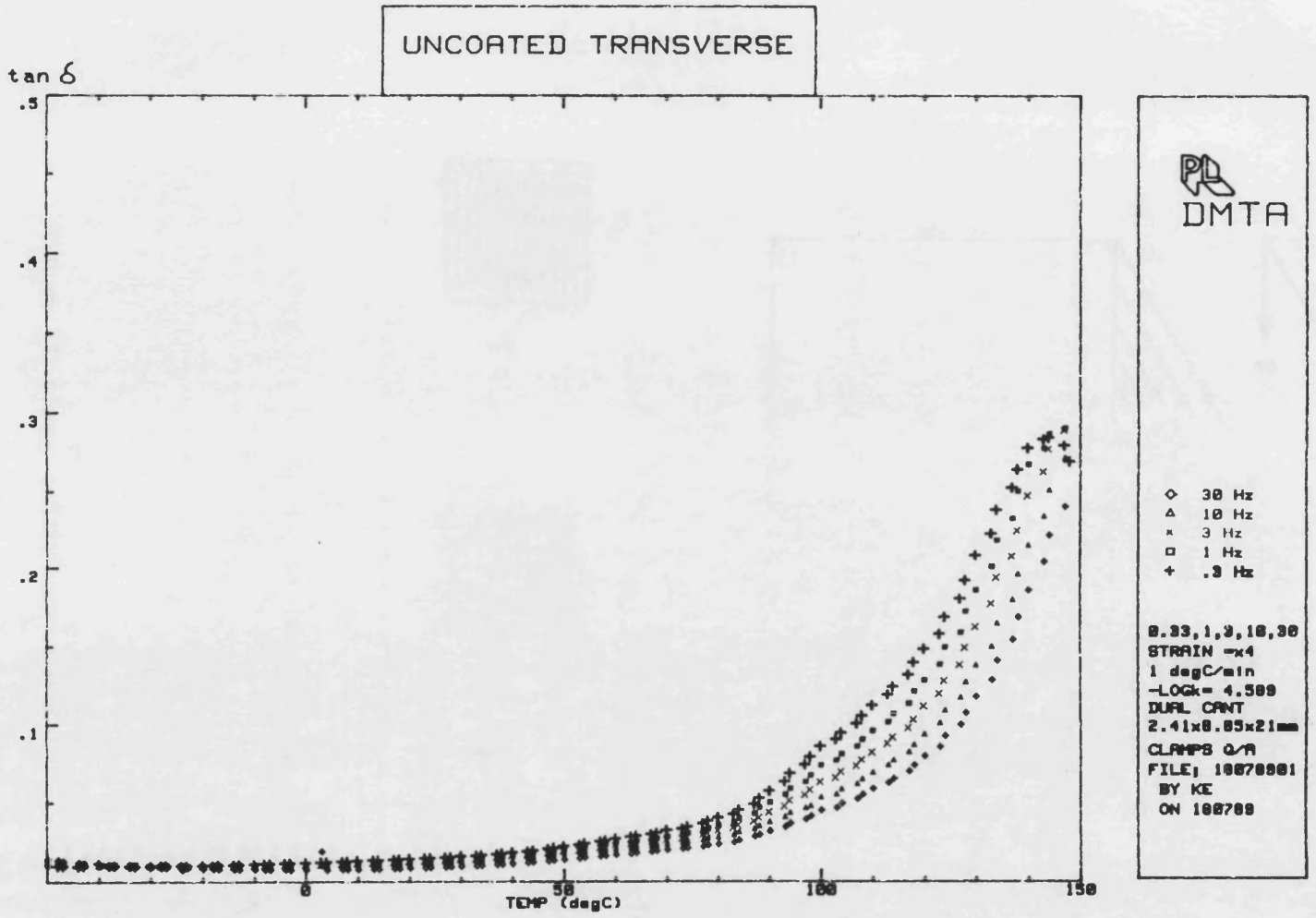


Figure 74. Damping versus temperature for uncoated fibre composite in transverse bending

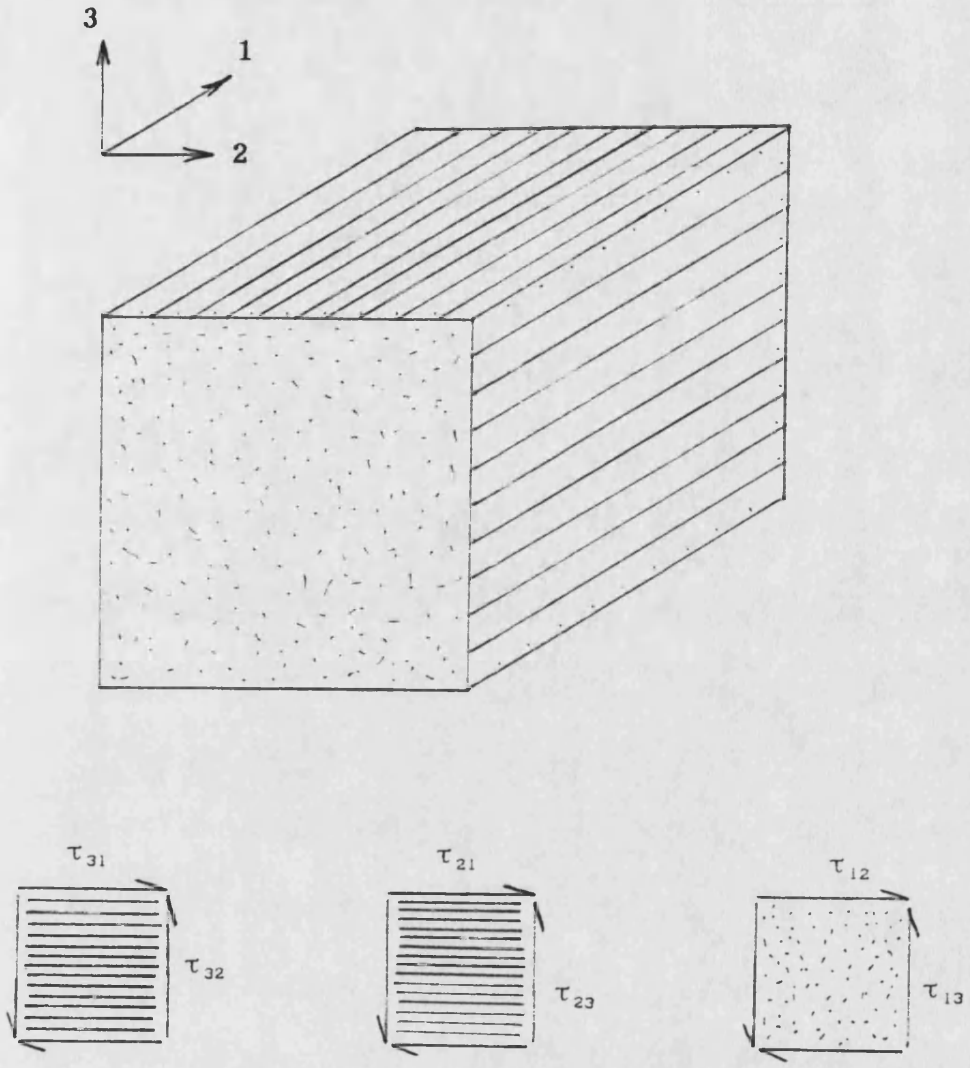


**Figure 75. Shear planes and directions**

| Property | Vinyl ester resin | Acrylic interphase |
|---|---|---|
| Strength ( MPa ) | 63.4 ( 17.3 ) | 4.34 |
| Faiure strain ( % ) | 2.4 ( 1.34 ) | 1600 |
| Young's modulus ( GPa) | 3.75 ( 0.18 ) | 0.004 |

TABLE 1. Bulk material properties

| Fibre treatment | Failure stress (MPa) (standard deviation) | Number of specimens |
|---|---|---|
| 1. Untreated | 1.98 ( 1.39 ) | 6 |
| 2. Treated with A174 silane | 15.70 ( 7.2 ) | 9 |
| 3. Untreated , acrylic coated | 5.68 ( 2.08 ) | 7 |
| 4. A174 , acrylic coated | 8.04 ( 1.08 ) | 7 |

TABLE 2. Roving lap shear test results

| Acrylic concentration / roving treatment | Short beam shear strength ( MPa ) ( s ) | Marbling condition |
|---|---|---|
| First attempt | 65.7 ( 2.4 ) | Heavy |
| 5% / scraped | 62.6 ( 2.5 ) | Medium |
| 5% / scraped and washed | 70.9 ( 2.7 ) | Light |
| 1% / scraped and washed | 76.2 ( 2.2 ) | No longer visible |

TABLE 3. Screening test for optimisation of production process

| Specimen | Modulus (GPa) | Strength (MPa) | Failure strain (%) | Fibre volume fraction |
|---|---|---|---|---|
| Coated fibre dog bone | 17.22 (2.21) | 25.57 (5.71) | 0.174 (0.045) | 59.5 % |
| Uncoated fibre dog bone | 17.31 (2.58) | 26.81 (3.20) | 0.171 (0.035) | 59.5 % |

TABLE 4. Transverse tensile results

| Specimen | Modulus (GPa) | Strength (MPa) | Failure strain (%) | Fibre volume fraction |
|---|---|---|---|---|
| Coated | 15.21 (1.01) | 74.05 (13.85) | 0.97 (0.17) | 60.0 % |
| Uncoated | 14.96 (0.85) | 61.31 (5.64) | 0.81 (0.09) | 60.5 % |

TABLE 5. Transverse bending results

| Composite | Intralaminar shear strength (MPa) | Fibre volume fraction (%) | Short beam shear strength (MPa) | fibre volume fraction (%) |
|---|---|---|---|---|
| Coated fibre | 44.80 (4.96) | 60 | 72.41 (3.84) | 60.5 |
| Uncoated fibre | 38.33 (3.17) | 60 | 68.80 (3.00) | 63.5 |

TABLE 6. Shear results

| Composite | Strength at 1 mm/min (MPa) | Longitudinal splitting threshold (MPa) | Fibre volume fraction (%) |
|---|---|---|---|
| Coated | 1532 (26) | 800 (210) | 58 |
| Uncoated | 1544 (46) | 593 (134) | 58 |

TABLE 7. Longitudinal bending results

| Composite | $G_{1C}$ ( KJ/$m^2$ ) | Fibre volume fraction (%) |
|---|---|---|
| Coated | 0.77 | 60 |
| Uncoated | 0.74 | 60.5 |

TABLE 8. Composite fracture energy

| Maximum stress (MPa) | Fatigue life (log cycles) coated fibre composite | Fatigue life (log cycles) uncoated fibre composite |
|---|---|---|
| 800 | 5.16 | 6.01 |
| 800 | 5.29 | 5.77 |
| 800 | 4.04 | 5.53 |
| 800 | 6.22 | - |
| 950 | 5.29 | 5.07 |
| 950 | 4.72 | 5.61 |
| 950 | 4.88 | 4.83 |
| 1100 | 4.43 | 3.78 |
| 1100 | 4.21 | 4.53 |
| 1100 | 4.37 | 4.46 |
| 1250 | 3.57 | 3.93 |
| 1250 | 3.89 | 3.86 |
| 1250 | 2.89 | 3.78 |
| 1300 | 2.46 | - |

TABLE 9. Fatigue test results

| Property | Improvement |
|---|---|
| Transverse bending stength | 21 % |
| Intralaminar shear strength | 17 % |
| Short beam shear strength | 5 % |
| Longitudinal splitting threshold | 35 % |

TABLE 10. Summary of property improvements

| | uc/10kv | c/10kv | uc/7kv | c/7kv |
|---|---|---|---|---|
| 1 | 607.000 | 650.000 | 750.000 | 608.000 |
| 2 | 589.000 | 512.000 | 662.000 | 550.000 |
| 3 | 620.000 | 411.000 | 697.000 | 624.000 |
| 4 | 531.000 | 482.000 | 611.000 | 617.000 |
| 5 | 565.000 | 438.000 | 665.000 | 2673.000 |
| 6 | 525.000 | 527.000 | 637.000 | 819.000 |
| 7 | 508.000 | 454.000 | 516.000 | 900.000 |
| 8 | 654.000 | 404.000 | 678.000 | 617.000 |
| 9 | 593.000 | 320.000 | 518.000 | 634.000 |
| 10 | 539.000 | 421.000 | 580.000 | 623.000 |
| 11 | 601.000 | 314.000 | 550.000 | 510.000 |
| 12 | 708.000 | 445.000 | 566.000 | 621.000 |
| 13 | 629.000 | 309.000 | 687.000 | 693.000 |
| 14 | 564.000 | 458.000 | 568.000 | 577.000 |
| 15 | 523.000 | 386.000 | 684.000 | 536.000 |
| 16 | 642.000 | 469.000 | 578.000 | 539.000 |
| 17 | 506.000 | 384.000 | 595.000 | 514.000 |
| 18 | 493.000 | 522.000 | 794.000 | 495.000 |
| 19 | 484.000 | 439.000 | 758.000 | 635.000 |
| 20 | 825.000 | 464.000 | 763.000 | 600.000 |
| 21 | 727.000 | 386.000 | 1014.000 | 550.000 |
| 22 | 663.000 | 469.000 | 731.000 | 554.000 |
| 23 | 636.000 | 382.000 | 667.000 | 3105.000 |
| 24 | 691.000 | 505.000 | 938.000 | 3426.000 |
| 25 | 556.000 | 395.000 | 783.000 | 1313.000 |
| 26 | 444.000 | 524.000 | 548.000 | 1556.000 |
| 27 | 763.000 | 366.000 | 522.000 | 831.000 |
| 28 | 530.000 | 1396.000 | 615.000 | 1029.000 |
| 29 | 529.000 | 851.000 | 571.000 | 651.000 |
| 30 | 490.000 | 1045.000 | 697.000 | 786.000 |
| 31 | 439.000 | 981.000 | 655.000 | 540.000 |
| 32 | 460.000 | 1068.000 | 933.000 | 587.000 |
| 33 | 445.000 | 537.000 | 1122.000 | 506.000 |
| 34 | 439.000 | 1128.000 | 931.000 | 646.000 |
| 35 | 443.000 | 745.000 | 789.000 | 588.000 |
| 36 | 422.000 | 1176.000 | 727.000 | 725.000 |
| 37 | 399.000 | 1001.000 | 641.000 | 597.000 |
| 38 | 639.000 | 1317.000 | 666.000 | 808.000 |
| 39 | 499.000 | 1159.000 | 710.000 | 1004.000 |
| 40 | 524.000 | 1209.000 | 586.000 | 816.000 |
| 41 | 614.000 | 1336.000 | 557.000 | 1872.000 |
| 42 | 582.000 | 1155.000 | 745.000 | 2050.000 |
| 43 | 550.000 | 1357.000 | 725.000 | 1227.000 |
| 44 | 574.000 | 1271.000 | 1095.000 | 782.000 |
| 45 | 578.000 | 1234.000 | 702.000 | 771.000 |
| 46 | 628.000 | 914.000 | 730.000 | 960.000 |
| 47 | 548.000 | 1336.000 | 939.000 | 628.000 |
| 48 | 473.000 | 931.000 | 709.000 | 544.000 |
| 49 | 492.000 | 1095.000 | 1387.000 | 993.000 |
| 50 | 552.000 | 1230.000 | 1677.000 | 569.000 |
| 51 | 594.000 | 1028.000 | 744.000 | 939.000 |
| 52 | 527.000 | 1162.000 | 1258.000 | 770.000 |
| 53 | 529.000 | 790.000 | 986.000 | 668.000 |
| 54 | 560.000 | 1188.000 | 2013.000 | 983.000 |
| 55 | 508.000 | 662.000 | 745.000 | 1218.000 |
| 56 | 542.000 | 1328.000 | 990.000 | 688.000 |
| 57 | 617.000 | 948.000 | 575.000 | 1009.000 |
| 58 | 1220.000 | 1513.000 | 492.000 | 687.000 |
| 59 | 664.000 | 815.000 | 521.000 | 1109.000 |
| 60 | 541.000 | 1068.000 | 609.000 | 1554.000 |
| 61 | 705.000 | 737.000 | 575.000 | 1048.000 |

TABLE 11. X-ray intensity measurements

| | uc/4kv | c/4kv | uc/2kv | c/2kv |
|---|---|---|---|---|
| 1 | 2680.000 | 1264.000 | 466.000 | 309.000 |
| 2 | 2441.000 | 1064.000 | 479.000 | 330.000 |
| 3 | 2302.000 | 1243.000 | 507.000 | 290.000 |
| 4 | 2233.000 | 1142.000 | 492.000 | 299.000 |
| 5 | 2336.000 | 1540.000 | 508.000 | 334.000 |
| 6 | 2271.000 | 1178.000 | 471.000 | 288.000 |
| 7 | 2211.000 | 891.000 | 506.000 | 316.000 |
| 8 | 900.000 | 1119.000 | 444.000 | 302.000 |
| 9 | 783.000 | 990.000 | 254.000 | 278.000 |
| 10 | 800.000 | 1040.000 | 346.000 | 231.000 |
| 11 | 967.000 | 990.000 | 329.000 | 273.000 |
| 12 | 826.000 | 1028.000 | 318.000 | 379.000 |
| 13 | 883.000 | 1065.000 | 278.000 | 298.000 |
| 14 | 620.000 | 1310.000 | 308.000 | 299.000 |
| 15 | 569.000 | 960.000 | 285.000 | 288.000 |
| 16 | 612.000 | 1092.000 | 279.000 | 247.000 |
| 17 | 618.000 | 1021.000 | 223.000 | 286.000 |
| 18 | 517.000 | 1106.000 | 198.000 | 247.000 |
| 19 | 571.000 | 973.000 | 220.000 | 240.000 |
| 20 | 738.000 | 1062.000 | 392.000 | 322.000 |
| 21 | 535.000 | 1028.000 | 333.000 | 215.000 |
| 22 | 565.000 | 967.000 | 372.000 | 248.000 |
| 23 | 621.000 | 981.000 | 428.000 | 273.000 |
| 24 | 601.000 | 1076.000 | 457.000 | 232.000 |
| 25 | 704.000 | 1006.000 | 370.000 | 279.000 |
| 26 | 536.000 | 1142.000 | 451.000 | 367.000 |
| 27 | 666.000 | 1003.000 | 374.000 | 210.000 |
| 28 | 557.000 | 1518.000 | 375.000 | 200.000 |
| 29 | 488.000 | 1040.000 | 381.000 | 295.000 |
| 30 | 478.000 | 1188.000 | 318.000 | 199.000 |
| 31 | 456.000 | 1054.000 | 317.000 | 197.000 |
| 32 | 457.000 | 1439.000 | 371.000 | 238.000 |
| 33 | 455.000 | 1108.000 | 397.000 | 232.000 |
| 34 | 478.000 | 1271.000 | 402.000 | 262.000 |
| 35 | 450.000 | 1172.000 | 365.000 | 246.000 |
| 36 | 408.000 | 1314.000 | 363.000 | 209.000 |
| 37 | 451.000 | 1171.000 | 249.000 | 194.000 |
| 38 | 482.000 | 1249.000 | 270.000 | 215.000 |
| 39 | 398.000 | 1018.000 | 174.000 | 157.000 |
| 40 | 421.000 | 1129.000 | 208.000 | 170.000 |
| 41 | 467.000 | 990.000 | 217.000 | 192.000 |
| 42 | 409.000 | 1240.000 | 249.000 | 173.000 |
| 43 | 416.000 | 1076.000 | 174.000 | 169.000 |
| 44 | 512.000 | 1291.000 | 212.000 | 218.000 |
| 45 | 525.000 | 1435.000 | 194.000 | 142.000 |
| 46 | 436.000 | 1546.000 | 304.000 | 182.000 |
| 47 | 488.000 | 1303.000 | 226.000 | 147.000 |
| 48 | 472.000 | 1094.000 | 192.000 | 216.000 |
| 49 | 453.000 | 1257.000 | 212.000 | 180.000 |
| 50 | 582.000 | 1131.000 | 255.000 | 217.000 |
| 51 | 549.000 | 1060.000 | 201.000 | 159.000 |
| 52 | 668.000 | 1131.000 | 171.000 | 171.000 |
| 53 | 608.000 | 1203.000 | 171.000 | 227.000 |
| 54 | 526.000 | 1095.000 | 191.000 | 186.000 |
| 55 | 1081.000 | 1075.000 | 229.000 | 164.000 |
| 56 | 611.000 | 1291.000 | 218.000 | 223.000 |
| 57 | 486.000 | 1179.000 | 200.000 | 162.000 |
| 58 | 444.000 | 2299.000 | 388.000 | 170.000 |
| 59 | 1300.000 | 1139.000 | 292.000 | 236.000 |
| 60 | 448.000 | 1221.000 | 314.000 | 227.000 |
| 61 | 480.000 | 1269.000 | 222.000 | 227.000 |

TABLE 11. X-ray intensity measurements ( Continued )

| Beam voltage (KeV) | Intensity standard | Intensity uncoated fibre | Intensity coated fibre | Beam current standard ($\times 10^{-8}$ A) | Beam current uncoated fibre ($\times 10^{-8} A$) | Beam current coated fibre ($\times 10^{-8} A$) |
|---|---|---|---|---|---|---|
| 10 | 25567 (1619) | 564 (87) | 796 (367) | 3.225 (0.001) | 3.233 (0.003) | 3.259 (0.026) |
| 7 | 18348 (604) | 725 (187) | 742 (223) | 3.465 (0.001) | 3.457 (0.004) | 3.465 (0.002) |
| 4 | 12803 (246) | 561 (136) | 1150 (148) | 6.387 (0.003) | 6.341 (0.006) | 6.369 (0.0150 |
| 2 | 511 (30) | 313 (101) | 233 (52) | 1.210 (0.001) | 1.203 (0.026) | 1.223 (0.034) |

TABLE 12. X-ray intensity results

| Beam voltage (KeV) | Normalised intensity standard | Normalised intensity coated fibre | Normalised intensity uncoated fibre |
|---|---|---|---|
| 10 | 23783 | 523 | 733 |
| 7 | 15886 | 629 | 642 |
| 4 | 6014 | 265 | 542 |
| 2 | 1267 | 781 | 572 |

TABLE 13. Intensities normalised to $3.0 \times 10^{-8} A$ beam current

| Beam voltage (KeV) | Ratio $\frac{I_c}{I_s}$ | Ratio $\frac{I_s}{I_c}$ |
|---|---|---|
| 10 | 0.031 | 32.26 |
| 7 | 0.040 | 25.00 |
| 4 | 0.090 | 11.11 |
| 2 | 0.451 | 2.22 |

TABLE 14. Intensity ratios versus beam voltage

| Free length (l) | Width (W) | Ratio l/W | - log k | log E (Pa) | E (GPa) |
|---|---|---|---|---|---|
| 1 | 2 | 0.5 | 6.110 | 10.31 | 20.4 |
| 1 | 5 | 0.2 | 5.801 | 10.11 | 12.9 |
| 1 | 10 | 0.1 | 5.415 | 9.928 | 8.5 |
| 2 | 2 | 1.0 | 7.221 | 10.84 | 69.2 |
| 2 | 5 | 0.4 | 6.900 | 10.70 | 50.1 |
| 2 | 10 | 0.2 | 6.640 | 10.50 | 31.6 |
| 5 | 2 | 2.5 | 8.556 | 11.16 | 144 |
| 5 | 5 | 1.0 | 8.200 | 11.13 | 135 |
| 5 | 10 | 0.5 | 7.875 | 11.05 | 122 |
| 9 | 2 | 4.5 | 9.377 | 11.37 | 234 |
| 9 | 5 | 1.8 | 8.988 | 11.28 | 191 |
| 9 | 10 | 0.9 | 8.723 | 11.29 | 195 |

TABLE 15. Modulus of steel substrate versus measurement geometry

| Sample ( No.layers : Run no. ) | Free length (mm) | Beam width (mm) | Beam thickness (mm) | log Ek (stiffness) |
|---|---|---|---|---|
| 1:1 | 8.81 | 10.01 | 0.16 | 2.532 |
| 1:2 | 8.88 | 10.01 | 0.16 | 2.555 |
| 1:3 | 8.89 | 10.01 | 0.16 | 2.616 |
| 2:1 | 8.92 | 9.81 | 0.24 | 2.648 |
| 2:2 | 8.89 | 9.81 | 0.24 | 2.734 |
| 2:3 | 8.87 | 9.81 | 0.24 | 2.718 |
| 4:1 | 8.92 | 9.81 | 0.32 | 2.667 |
| 4:2 | 8.75 | 9.81 | 0.32 | 2.694 |
| 4:3 | 8.72 | 9.81 | 0.32 | 2.749 |
| 5:1 | 8.73 | 10.04 | 0.42 | 2.694 |
| 5:2 | 8,75 | 10.04 | 0.42 | 2.781 |
| 10:1 | 8.80 | 10.28 | 0.78 | 2.940 |
| 10:2 | 8.72 | 10.28 | 0.78 | 2.986 |
| 10:3 | 8.88 | 10.28 | 0.78 | 2.909 |
| 20:1 | 8.96 | 10.28 | 1.24 | 3.446 |
| 20:2 | 8.72 | 10.28 | 1.24 | 3.376 |
| 20:3 | 8.92 | 10.28 | 1.24 | 3.396 |
| 35:1 | 9.05 | 10.70 | 2.45 | 3.945 |
| 35:2 | 9.00 | 10.70 | 2.45 | 3.994 |
| 35:3 | 9.11 | 10.70 | 2.45 | 3.917 |
| 50:1 | 8.80 | 10.75 | 3.15 | 4.335 |
| 50:2 | 8.89 | 10.75 | 3.15 | 4.305 |
| 50:3 | 8.80 | 10.75 | 3.15 | 4.299 |

TABLE 16. Coating tensile modulus versus coating thickness

| Coating thickness (micron) | Coating modulus and one standard deviation (MPa) | Log coating thickness | Log coating modulus |
|---|---|---|---|
| 55 | 1267 (674) | 1.74 | 9.103 |
| 95 | 1067 (262) | 1.98 | 9.028 |
| 135 | 440.7 (91.9) | 2.13 | 8.644 |
| 185 | 225.5 (71.4) | 2.27 | 8.353 |
| 365 | 81.5 (8.9) | 2.56 | 7.911 |
| 595 | 80.4 (10.6) | 2.77 | 7.905 |
| 1200 | 40.8 (3.2) | 3.08 | 7.611 |
| 1550 | 41.6 (1.8) | 3.19 | 7.619 |

TABLE 17. Summary coating thickness versus coating tensile modulus

| Thickness (micron) | Shear modulus (MPa) | Log thickness | Log modulus |
|---|---|---|---|
| 680 | 7.82 | 2.833 | 6.893 |
| 360 | 4.40 | 2.556 | 6.643 |
| 50 | 0.63 | 1.699 | 5.800 |

TABLE 18. Shear modulus versus acrylic thickness